AD NUMBER

AD863664

LIMITATION CHANGES

TO:

Approved for public release; distribution is unlimited.

FROM:

**Distribution authorized to U.S. Gov't. agencies and their contractors;
Administrative/Operational Use; SEP 1969. Other requests shall be referred to Army Aviation Materiel Labs., Fort Eustis, VA.**

AUTHORITY

USAAMRDL ltr 18 Jun 1971

AD

USAAVLABS TECHNICAL REPORT 69-74

ANALYSIS AND COMPARISON OF AERODYNAMIC DATA OBTAINED IN A LARGE WIND TUNNEL AND A MOVING-MODEL/TRACK FACILITY FOR A GENERAL RESEARCH TILT-WING/PROPELLER VTOL CONFIGURATION

By

Joseph James Traybar

September 1969

U. S. ARMY AVIATION MATERIEL LABORATORIES
FORT EUSTIS, VIRGINIA

CONTRACT DAAJ02-67-C-0025

PRINCETON UNIVERSITY
PRINCETON, NEW JERSEY

Disclaimers

The findings in this report are not to be construed as an official Department of the Army position unless so designated by other authorized documents.

When Government drawings, specifications, or other data are used for any purpose other than in connection with a definitely related Government procurement operation, the United States Government thereby incurs no responsibility nor any obligation whatsoever; and the fact that the Government may have formulated, furnished, or in any way supplied the said drawings, specifications, or other data is not to be regarded by implication or otherwise as in any manner licensing the holder or any other person or corporation, or conveying any rights or permission, to manufacture, use, or sell any patented invention that may in any way be related thereto.

Disposition Instructions

Destroy this report when no longer needed. Do not return it to the originator.

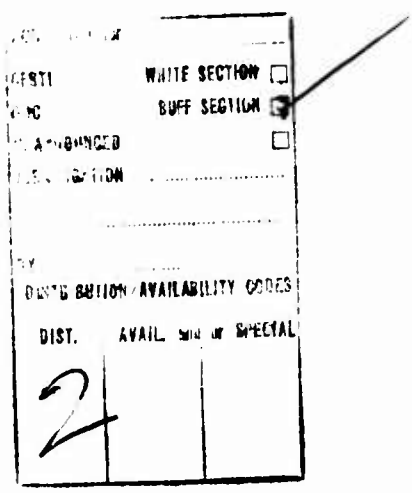

DEPARTMENT OF THE ARMY
HEADQUARTERS US ARMY AVIATION MATERIEL LABORATORIES
FORT EUSTIS, VIRGINIA 23604

IN REPLY REFER TO:

This report has been reviewed by the U. S. Army Aviation Materiel Laboratories, the Naval Air Systems Command, and the Air Force Flight Dynamics Laboratories. It is considered to be technically sound.

This report is published for the exchange of information and the stimulation of ideas.

Task 1F162204A14233
Contract DAAJ02-67-C-0025
USAAVLABS Technical Report 69-74
September 1969

ANALYSIS AND COMPARISON OF AERODYNAMIC DATA OBTAINED IN A LARGE WIND TUNNEL AND A MOVING-MODEL/TRACK FACILITY FOR A GENERAL RESEARCH TILT-WING/PROPELLER VTOL CONFIGURATION

Report 872

by

Joseph James Traybar

Prepared by

Department of Aerospace and Mechanical Sciences
Princeton University
Princeton, New Jersey

for

U. S. ARMY AVIATION MATERIEL LABORATORIES
FORT EUSTIS, VIRGINIA

SUMMARY

A comparison and analysis was conducted of the aerodynamic characteristic data obtained in a large wind tunnel and a moving-model/track facility for a general research tilt-wing/propeller VTOL configuration. The two facilities were the Langley 30-by-60 Full-Scale Wind Tunnel and the Princeton Dynamic Model Track. The experiments included test conditions corresponding to free-stream velocities from transition flight to hovering and wing angles of attack up to 90 degrees. The experimental data obtained from both facilities are compared in several ways in a series of graphs plotted in coefficient form for the range of slipstream thrust coefficients of 0.80 to 0.95. The comparisons and analyses first are made on the basis of wind-axes force and moment coefficients and drag polars. An additional comparison is made of the wing forces by using body-axes force coefficients and polars.

FOREWORD

This research was performed by the Department of Aerospace and Mechanical Sciences, Princeton University, under the direction of Professor H. C. Curtiss, Jr., and the sponsorship of the United States Army Aviation Materiel Laboratories Contract DAAJ02-67-C-0025 (Task 1F162204A14233) with guidance and financial support from the United States Air Force Flight Dynamics Laboratory of the Research and Technology Division and the United States Navy, Naval Air Systems Command. The research was monitored by Mr. Robert P. Smith of the United States Army Aviation Materiel Laboratories.

BLANK PAGE

TABLE OF CONTENTS

LIST OF ILLUSTRATIONS

LIST OF SYMBOLS

A	total propeller disc area, square feet
b	propeller blade chord, feet
c	chord length, wing, feet
c/4	quarter chord position, wing
C_D	drag coefficient based on free-stream q and wing area (wind axes)
C_L	lift coefficient based on free-stream q and wing area (wind axes)
$C_{T,S}$	slipstream thrust coefficient, $\frac{T}{q_{SS}S}$, as defined in Reference 1 and identical to the notation CT,SS,S in Reference 2
$C_{X_{BODY}}$	axial force coefficient based on free-stream q and wing area; oriented parallel to the wing chord line and thrust axis (body-axis system)
$C_{Z_{BODY}}$	normal force coefficient based on free-stream q and wing area; oriented normal to the wing chord line (body-axis system)
CL,FS,S	lift coefficient based on free-stream q and wing area $\frac{L}{q_{FS}S}$
CM,FS,S	pitching moment coefficient based on free-stream q and wing area (about quarter chord) $\frac{M_Y}{q_{FS}S\ c}$
CT,FS,S	free-stream thrust coefficient based on free-stream q and wing area $\frac{T}{q_{FS}\ S}$

CT,SS,S — slipstream thrust coefficient based on slipstream q and wing area

$$\frac{T}{q_{ss} \quad S}$$

CT,TS,A — tip-speed thrust coefficient based on propeller tip speed and total propeller disc area

$$\frac{T}{\rho \; A \; (\Omega R)^2}$$

CX,FS,S — horizontal force coefficient based on free-stream q and wing area

$$\frac{F_X}{q_{fs} \quad S}$$

d — propeller diameter, feet

fps — feet per second

F_X — horizontal force, pounds

h' — propeller blade thickness, feet

L — lift, pounds

M_Y — pitching moment, about quarter chord point, foot-pounds

q — dynamic pressure based on some referenced velocity, pounds per square foot

q_{fs} — free-stream dynamic pressure, $\frac{1}{2} \rho V^2$, pounds per square foot

q_{ss} — slipstream dynamic pressure, $q_{fs} + \frac{T}{A}$, pounds per square foot

r/R — ratio of propeller blade span station to total span

rpm — propeller rotational speed, revolutions per minute

R — propeller radius, feet

S — total wing area, square feet

T — propeller total thrust, pounds

T_c''	slipstream thrust coefficient, $\frac{T}{q_{ss} A}$ as defined in Reference 3
V	free-stream velocity, feet per second
X_{BODY}	longitudinal body fixed axis; aligned with wing chord line or propeller thrust line (body-axis system)
X_{WIND}	longitudinal wind axis; aligned into and parallel to the free-stream velocity (wind-axis system)
Z_{BODY}	vertical body fixed axis; oriented perpendicular to the wing chord line (body-axis system)
Z_{WIND}	vertical wind axis; oriented perpendicular to the free-stream velocity (wind-axis system)
α	angle of attack relative to free-stream velocity, degrees
δ_f	flap deflection, degrees
μ_x	propeller advance ratio, $\frac{V}{\Omega R}$
ρ	mass density of air, slugs per cubic foot
Ω	propeller rotational speed, radians per second
$_{TRIM}$	subscript denoting trim condition where drag is equal to zero
$*$	superscript as used in Wing* Force where force is equal to resultant force minus propeller thrust force

BLANK PAGE

INTRODUCTION

General interest in VTOL aircraft has reached the point where considerable amounts of model testing have resulted in a significant compilation of aerodynamic characteristic data for a variety of configurations. One of the proposed concepts that has been tested in wind tunnels and of which a prototype has been built involves the use of a tilt-wing/propeller vehicle where the wing is either fully or partially immersed in the propeller slipstream. The propellers are used as "lifting rotors" similar to a helicopter for the takeoff, transition, and landing maneuvers. For cruising flight the propellers and wing are rotated to a configuration similar to an airplane where the propeller provides the thrust for forward flight. Typically, the thrust-to-weight ratios of VTOL aircraft are much greater than those of conventional airplanes.

One of the most vital areas of model testing of the tilt-wing/propeller configuration centers on the need for aerodynamic data in the speed regime from transition to hover. Unfortunately, this speed range includes flight conditions where the slipstream or wake angles are large (up to 90°) with respect to the free-stream direction and the velocity of the slipstream is much greater than the free stream. When wind tunnels are used to obtain data under these conditions, an understanding of the validity or limitations of the measured quantities is necessary with reference to the application or need for wall corrections. Frequently, use is made of facilities with large test sections where the ratio of the model size to test section size is small so that "wall-effect" corrections may be negligible. However, an additional requirement of precise tunnel speed measurement in the slow forward velocity range may be necessary. Also, attention may need to be paid to test section flow profiles and turbulence for testing highly powered models in this slow-speed range.

Results are presented of experimental data obtained in two different types of facilities with large test sections. One is a large wind tunnel and the other is a moving-model/track type test facility. The investigations included test conditions corresponding to free-stream velocities from transition to hovering. Identical models representing a general research tilt-wing/propeller vehicle were tested. Comparisons of the data are shown in a series of graphs, and the analysis of the data is discussed.

DESCRIPTION OF MODEL AND TEST APPARATUS

The general research tilt-wing model utilized in this investigation is shown installed on a sting-type mount in the Princeton Dynamic Model Track Facility (Figure 1). A drawing of the model is presented in Figure 2 and shows the layout, pertinent dimensions, and characteristics. The wing has an aspect ratio of 2.82, and the airfoil section is an NACA 0015. The propellers, spinners, motor-nacelle-strain gauge assemblies, and main six-component balance were borrowed from NASA, Langley Field. The propeller blade form characteristics are plotted in Figure 3. The model had two propeller-and-nacelle assemblies but no fuselage. The sting balance mount entry was provided by a 5-by-2.7-inch tunnel located at mid-span of the wing from maximum thickness aft to the trailing edge. Also, a 1/8-inch-wide roughness or transition strip (using number 60 Carborundum of 0.012 inch mean grain diameter) was affixed along the span at the wing leading edge at 8 percent chord.

The wing was fabricated using fiberglass vacuum molding techniques. The master molds were made from the model used in Reference 1 and were exact replicas of the NASA wing. The NASA wing (constructed of aluminum plate and wood) was too heavy for the current structure used on the moving model testing technique; therefore, a lighter weight wing was made utilizing a fiberglass skin with an aluminum spar. Using the various components borrowed from NASA and the items fabricated by Princeton, a new model was assembled identical to the one tested in Reference 1.

Also, the model was made with small flap bracket attachments so that some flaps-on test runs could be made. The flap airfoil section was a 30-percent chord, Clark Y with a total flap area of 1.69 square feet. The flap chord was 0.45 foot, and the total span (with the center tunnel cut-out for the mount excluded) was 3.75 feet. The mounting and deflection characteristics of the flap make it a typical "external airfoil flap" type high-lift device (Reference 4).

The same nacelle strain gauge instrumentation (measuring propeller thrust) was utilized and a NASA six-component, internal strain gauge was installed to measure the total (wing plus propeller) forces and moments on the system. Wing angle was varied about a pitch center attachment (referenced to the quarter chord) on the moving carriage so that no variations of the model pitch center with respect to wall clearance occurred. The model was positioned in the center of the 30-by-30-foot test section of the facility.

The two facilities used to obtain the aerodynamic data for the comparisons made in this report are the 30-by-60 Full-Scale Wind tunnel located at Langley Field, Virginia, and the 30-by-30 Dynamic Model Track located at Princeton, New Jersey. The 30-by-60 wind tunnel is a facility designed and built in the early 1930's and has been utilized for a wide range of aeronautical investigations and test techniques (Reference 5). The tunnel has a double-return flow and an elliptic throat with two 35-foot-diameter propellers mounted downstream of the test section. The test section is open throat. The Princeton Dynamic Model Track Facility is a facility specially designed for the study of the dynamic and static stability and control of helicopters and V/STOL-type configurations for the speed regime ranging from hover through transition (Reference 6). Basic components of the facility include a test section building with a cross section of 30-by-30 feet; an automated, servo-controlled, powered carriage that moves on a 760-foot-long track; a carriage-model computer; and various model mounts, measuring transducers, and data conditioning and recording equipment. The various mounts permit methods of attaching the models to the carriage so that the longitudinal and lateral/directional degrees of dynamic motion may be studied. Also, special mounts may be used for transition experiments, static tests, and "ground effect" research.

Although the track facility was designed primarily to conduct dynamic testing, certain features make it especially well suited for static testing. The moving-model/track technique provides some unique advantages for particular experiments (such as ground effect studies or transition flight experiments) that are difficult to accomplish in wind tunnels. Numerous research programs measuring static parameters on helicopters and V/STOL-type configurations for the hover and transition speed range, in and out of ground effect, have been conducted on this apparatus. Though this form of testing is somewhat more complex compared to wind tunnel testing, it does appear to have some advantages needed for this range of interest; namely, precise airspeed measurement under all flight conditions, uniform velocity profile free from turbulence (still air), and a relatively large test section.

A scale drawing of the model and two facilities is shown in Figure 4 to display the relative size of the model and the two facility test sections, blockage and wall proximity. For the size model used and for the purpose of this report, both test sections are considered to be large enough to assume that corrections to the data due to wall proximity are negligible.

EXPERIMENTAL DATA AND PROCEDURES

LARGE WIND TUNNEL DATA (REFERENCE 1)

The analysis covered in this report deals with the comparison of results from References 1 and 2. As stated in Reference 1, power-on tests were made for nearly constant slipstream thrust coefficients for a range of angles of attack from 0° to 90°. The tests were conducted in three test sections at the NASA Langley Field facility. First, the 7-by-10-foot test section of the 7-by-10 wind tunnel was used, and then the model was moved directly to the 30-by-60-foot full-scale tunnel in order to duplicate the test runs and conditions. Lastly, the model was placed in the 17-foot test section of the 7-by-10 wind tunnel, where the same runs (using the same instrumentation) were made again.

Attempts were made to hold propeller thrust constant during the course of a run. Propeller rotational speed was varied from 4,500 rpm to almost 6,000 rpm during the test program for the various thrust levels used. Blade angle was held constant at a pitch of 8 degrees measured at the three-quarter radius.

The basic power-on lift, horizontal force, and pitching moment data are presented for a number of nearly constant thrust coefficients in Appendix B of Reference 1. Lift-horizontal force polars are shown for various slipstream thrust coefficients. Also, the lift and horizontal force coefficients are plotted versus free-stream thrust coefficient for several angles of attack as shown in Figure 15 of Reference 1.

The principal purposes for conducting the research reported in Reference 1 were to determine the magnitude of the wind tunnel wall effects on the same tilt-wing type model configuration tested in three different sized test sections and to determine the validity of existing wall correction theory when applied to correct these data for wall effects.

It should be noted that little can be said about the aerodynamic characteristics of the propeller because of the methodology used for conducting the wind tunnel tests and the plotted results shown in Reference 1. Blade pitch remained fixed and propeller rpm was adjusted until a desired thrust was obtained on the propeller thrust force strain gauge. Then, rotational speed of the propellers was varied in order to hold thrust constant as angle of attack was changed during the course of a test run at each tunnel velocity. The propeller thrust force is always known (measured and set within the accuracy of the strain gauge readout) and held constant at the selected value. Therefore, the term CT,FS,S is used to denote a known vector (independent of angle of attack or tunnel q) that represents a given thrust force magnitude and direction and nothing more. The small variations of CT,FS,S shown in the various plots are caused by the difficulty in holding thrust constant at the time of the run.

MOVING-MODEL/TRACK DATA (REFERENCE 2)

In Reference 2, all data were presented in plots, in coefficient form, of lift, horizontal force, and pitching moment versus thrust for the various angles of attack. Much of the range of coefficients covered was governed by Reference 1. Within the capabilities of the Princeton Dynamic Model Track, efforts were made to cover the test points obtained in Reference 1. In all cases, only the 30-by-60 wind tunnel data of Reference 1 were used for the comparison purposes of the current analysis.

Thrust and free-stream velocity were varied over the widest ranges permissible in this facility so that the greatest coverage of coefficients would be obtained to match the ranges covered in Reference 1. Thrust coefficients based on slipstream dynamic pressure varied from approximately 0.5 (angle of attack equal to 30 degrees) to 1.0 at hovering (angle of attack equal to 90 degrees). Attempts were made to obtain the data about trim (horizontal force equal to zero) for all angles tested. Propeller rotational speed was varied between 4,500 rpm and 6,000 rpm using the same propellers and motors of Reference 1. Blade angle was held constant at a pitch of 8 degrees measured at the three-quarter radius.

The principal purpose for conducting the research in Reference 2 was to obtain additional aerodynamic data (on the same model using the moving-model/track testing technique) that could be analyzed and compared with the existing wind tunnel data reported in Reference 1. As mentioned, attempts were made to utilize precisely similar test points, models, and measuring transducers.

The test conditions from Reference 1 data were determined, and runs were made to duplicate dimensionally the same test points. On each run, propeller thrust was set and read, angle of attack was selected and locked, and velocity was programmed for the desired value by adjusting the carriage speed command controls. Model velocity (carriage speed) was determined by carriage tachometers and automatic electric timing clocks that are used to calculate speed to within a fraction of a foot per second. Angle of attack was set for each run with a protractor. Propeller thrust was measured by reading the output of the one-component strain gauge installed in the NASA motor nacelles. Six-component total forces and moments, measured by the NASA 711 balance, were recorded on digital tape. Approximately 300 runs were made during the course of the experiment. Both dimensional and nondimensional data were obtained for the propeller and wing.

Utilizing the data obtained, plots were made using digital printing equipment, and comparison data were selected for use with Reference 1.

COEFFICIENT FORMS

When a wing is immersed within the high slipstream velocities of propellers, large moments and forces may be produced even at the slower free-stream velocities. If an attempt is made to analyze the force and moment data, it is found that various forms of nondimensionalization are available depending on the type of information desired from the data. Since the method of nondimensionalization used in Reference 2 was selected to be similar to Reference 1 (so that results of the data could be compared easily to that work), certain well-known difficulties are encountered in attempting to utilize the different coefficient data based on free-stream or forward velocity (free-stream dynamic pressure).

Although there are certain advantages to nondimensionalization based on free-stream velocity for airplanes, disadvantages are noted when dealing with an aircraft whose airspeed tends toward zero. Since thrust remains finite as the forward speed tends toward zero, free-stream thrust coefficients become very large and approach infinite value as the vehicle comes to a hover (zero forward airspeed). Some forms of these nondimensional expressions used in this analysis are:

$$CL,FS,S = L/q_{FS}\,S \tag{1}$$

$$CX,FS,S = F_X/q_{FS}\,S \tag{2}$$

$$CM,FS,S = M_Y/q_{FS}\,Sc \tag{3}$$

$$CT,FS,S = T/q_{FS}\,S \tag{4}$$

$$CT,SS,S = T/q_{SS}\,S \tag{5}$$

$$CT,TS,A = T/\rho\,A\,(\Omega R)^2 \tag{6}$$

Note that the form CT,SS,S is similar in definition to $C_{T,S}$ and T_C'' used in References 1 and 3. Some attention must be paid to the characteristic area (wing area or total propeller disc area) used in the nondimensionalization. In Reference 1, wing area (S) was used for the thrust coefficients as well as for the coefficients of lift, horizontal force, and moment, so that all coefficients would have a common relationship based on one characteristic area. As it happens, for the model used in that analysis, the total propeller disc area (6.28 square feet) and the total wing area (6.34 square feet) are approximately equal ($S \approx A$), so that no great difference would be seen in this case. If the characteristic areas are different, area ratios will appear in the various relationships of the coefficients. It is known that definition and notation of all coefficients and especially thrust coefficients used in V/STOL or helicopter studies have been nondimensionalized and, on occasion, assigned symbols in an inconsistent and sometimes confusing

fashion. Care must be taken when comparing data from different sources to determine the precise definitions used for the coefficients and other parameters. The lengthy notation and form used herein are consistent with Reference 2 and resulted from the use of automated digital printing equipment in data reduction and presentation.

The difficulties encountered with the use of thrust coefficients based on free-stream velocities at the lower speeds for these types of configurations are well known. Similar awkward notation is encountered in the extremely large lift coefficients (based on free-stream velocity of the winged vehicle) at slow flight speeds (even, in reality, when the wing is providing practically no lift or force perpendicular to the free stream). At slow speeds, the lift is being provided primarily by the propeller (component of the thrust force), and the significant dynamic pressure or velocity in this situation is the tip speed.

In the data reduction for this type of vehicle and speed regime, another form of coefficient is usually calculated and is based on the slipstream velocity (slipstream q). A simple expression for slipstream dynamic pressure (developed in Reference 3) can be stated as:

$$q_{SS} = q_{FS} + \frac{T}{A} \tag{7}$$

The thrust coefficient, defined on the basis of slipstream q, can be written as defined in equation (5). An advantage of using the slipstream thrust coefficient (CT,SS,S), compared to the free-stream thrust coefficient for the range of speeds pertinent to slow flight, is that magnitudes are more reasonable and easier to utilize. As free-stream velocity is decreased from fast forward flight toward zero, the coefficient CT,FS,S increases from small values and approaches infinite value at hover. The coefficients become rather large and change radically in value particularly at slow speeds and around hover; whereas, when velocity is decreased from fast forward flight toward zero, the coefficient CT,SS,S tends to increase from a value of a few tenths in forward flight to a limiting value of 1.0 as the vehicle comes to a hover. One beneficial use of the slipstream thrust coefficient (and also the free-stream thrust coefficient when applied to higher speeds and normal airplane flight) is as an aid in defining or locating the flight conditions of interest. For example, for the purposes of studying slow flight regimes of VTOL's, when the parameter CT,SS,S is near 1.0, say, 0.95, it should be clear that the flight condition is one of slow forward speed near hover. Using the previous definitions of the coefficients, the following relationships can be derived:

$$CT,SS,S = \frac{(CT,FS,S)}{1+(CT,FS,S)} \tag{8}$$

$$CT,SS,S = \frac{2(CT,TS,A)}{\mu_x^2 + 2(CT,TS,A)} \tag{9}$$

$$CT,FS,S = \frac{2(CT,TS,A)}{\mu_x^2} \tag{10}$$

From equation (8), it can be seen that there is a unique relationship between the free-stream thrust coefficient (CT,FS,S) and the slipstream thrust coefficient (CT,SS,S). This relationship is shown in the plot in Figure 5.

Another useful thrust coefficient form normally utilized for helicopter and VTOL studies is the thrust coefficient based on propeller/rotor tip speed and disc area, equation (6). Figure 6 shows the relationships of typical plots (obtained from the experiments accomplished during the track tests) of free-stream thrust coefficient (CT,FS,S) and tip speed thrust coefficient (CT,TS,A) plotted versus advance ratio. The curves of thrust coefficient based on tip speed and disc area are typical of "helicopter" rotor data for a given blade pitch for two angles of attack of 40° and 90°. The curves of thrust coefficient based on free-stream velocity are typical of "airplane" propeller type data for a given blade pitch but for two non-axial flow angles of attack of 40° and 90°. The hovering flight condition is defined as α equal to 90 degrees. Note that in this type of plot the curve of CT,FS,S versus advance ratio becomes extremely sensitive to changes in μ_x (especially at the slower speeds) and results in large unwarranted changes due to the definition of the coefficient (the use of free-stream velocity as the nondimensionalization parameter). This definition tends to exaggerate the variation, making the actual nature or behavior of the propeller characteristics difficult to determine. It also makes it appear that there is little dependence on angle of attack at the slower advance ratios. Again, the usefulness of this method of nondimensionalization and plotting of the coefficient depends largely on the type of information desired from the data.

COMPARISON OF DATA

COMPARISON OF FORCE AND MOMENT COEFFICIENT DATA WITH FREE-STREAM THRUST COEFFICIENT

Utilizing the track data and the notation from Reference 2 as shown in Figure 7, curves were plotted showing lift, horizontal force, and pitching moment coefficient versus free-stream thrust coefficient for a number of angles of attack (Figure 8). Comparisons for the lift coefficient for the two data sources are shown in a series of separate graphs (because the curves tend to fall on top of one another) in Figure 9. Similarly, a comparison of horizontal force coefficient is shown in Figure 10. The data used from Reference 1 were the 30-by-60 tests points shown in Figure 15 of that report.

Although the curves are shown as plotted in Reference 1, the validity or usefulness of these graphs for comparison information is doubtful. For example, if an attempt is made to interpret the free-stream thrust coefficient in terms of free-stream velocity (at a given thrust level), it is evident that the scale is very non-linear. In Figure 10, CT,FS,S equal to 4,12,52, and 60, are respectively equivalent to 40,20,10, and 9.5 feet per second forward velocity (Figure 11). Between a CT,FS,S of 4 and 0, the velocity varies between 40 fps and infinity. Also, in Figure 10, the 60° Princeton data has a value of CX,FS,S equal to zero (trim) at a CT,FS,S of 12 compared to about 9 for the 60° NASA data. Referring to Figure 11, a difference of 3 fps in measuring velocity could account for the disparity in the data. Depending on the region of interest, small errors in measuring velocity can easily result in large percentage changes in CT,FS,S.

Another objection that could be raised against plotting the data on this basis for comparison purposes is that the wind-axes forces, lift and horizontal force coefficient, will contain large components of propeller thrust as angle of attack is varied. Because the thrust was held constant, the component of propeller thrust (for certain flight conditions) may account for a large portion of the magnitude of the lift and drag coefficients, leaving only a small remaining portion to be the aerodynamic characteristic data measured and compared.

COMPARISON OF BASIC POWER-ON LIFT, HORIZONTAL FORCE, AND PITCHING MOMENT DATA USING WIND-AXES COEFFICIENTS AND DRAG POLARS

The basic uncorrected 30-by-60 power-on lift, horizontal force, and pitching moment data are presented for a number of nearly constant thrust coefficient conditions in Appendix B of Reference 1. Because of the lay-out of the measuring transducers (Figure 12), it was possible to read propeller thrust independent of the main six-component strain gauge. As mentioned, tests were accomplished with thrust maintained constant during

the course of the run for each test condition simply by monitoring a readout system and adjusting propeller rpm accordingly. Although this is a fairly standard technique used at some facilities and probably desirable for the purposes of the research conducted in Reference 1, it does result in effectively eliminating any propeller aerodynamic characteristics from the data. An exception to this would be that any propeller normal force generated in non-axial flight would be included in the total measured force. In reality, if one considers the normal force of the propeller/rotor to be negligible, then only the aerodynamic effects on the wing (immersed in a slipstream and a free-stream flow field) are measured with this technique during the course of a run. The effect of holding the thrust constant on the measured data and the resulting plots is shown graphically and pictorially for a typical slow flight case in Figure 13. Figure 13a shows graphs of CL,FS,S and CX,FS,S versus angle of attack. Since the lift and horizontal force are defined as wind-axes forces, a component of propeller thrust will appear in these forces as angle of attack is varied from 0 - 90 degrees. If thrust can be maintained exactly constant during the angle-of-attack variation, the propeller force envelope will appear, for an ideal case, as a sine wave on the lift curve and a cosine wave on the horizontal force (drag) curve (shaded area on Figure 13a). If a different test technique is used, that of holding rpm constant during the course of a run, then thrust will vary and the aerodynamic characteristics of the propeller (in combination with the wing) will be measured. Then the values of CL,FS,S and CX,FS,S as a function of α and due to varying propeller thrust can simply be calculated by the expressions:

$$CL,FS,S = (CT,FS,S)\ (\sin \alpha) \tag{11}$$

$$CX,FS,S = (CT,FS,S)\ (\cos \alpha) \tag{12}$$

The propeller thrust contribution to CL,FS,S and CX,FS,S as a function of α is displayed pictorially below the curves in Figure 13a.

If the propeller thrust is subtracted from the total measured force (resultant), the remaining force is due to the wing immersed in the free stream and slipstream. Again, because of the instrumentation layout, this is only approximately true if there is any measurable propeller normal force due to the non-axial flow field. For the experiments discussed in this report, the propeller normal force is considered to be negligible compared to the force measured on the wing. This was checked on a few cases during the course of experiments conducted in Reference 2 and showed that the propeller normal force strain gauge revealed less than a pound of force perpendicular to the thrust axis when the total lift was equal to about 40 to 50 pounds. However, depending on the design of the propellers and/or rotors, this force often may become significant; in this case, the notation (WING* FORCE) is used to denote a wing force that excludes all propeller axial force but includes any existing propeller normal force. For the purposes of this report, it is considered reasonably correct and greatly beneficial to understanding the comparison data if WING* FORCE is regarded as the force resulting primarily from the

wing alone, immersed in a slipstream and subjected to a free-stream flow field. This force is depicted in Figure 13b for a typical case of powered flight (presence of a slipstream) and a slow forward speed ($C_{T,SS,S} \approx 0.94$). The total measured force or resultant force is shown in Figure 13c as the sum of propeller thrust force and WING* FORCE.

A more comprehensive representation of the relationship between lift, drag, and angle of attack may sometimes be obtained by studying drag polars. Reference 1 has made extensive use of displaying the basic data in terms of a series of polar plots for various thrust levels. However, unless one has studied "power-on polars", interpretation of the plots for the separate details shown in Figure 13 may be somewhat difficult. First, the polar is shifted into both quadrants (as opposed to the common polars of wing data) and the magnitude of the scales is vastly larger (because of the power added to the system). The radius vector, connecting every point on the curve with the origin, still represents the resultant aerodynamic force acting on the model (total measured force). However, now the grid is "square" (equal scale on the ordinate and abscissa as opposed to the normally expanded abscissa for unpowered wing data) and the direction of the resultant force vector (experienced by a model flying from right to left) is shown geometrically correct. Similarly, all angles of attack may be properly depicted and are shown on all Princeton polar data. Also, it should be noted that the wind-axes force polar of the propeller thrust may be plotted separately on the same graph. If propeller thrust is constant, the thrust polar will appear as a portion of a circle (center at the origin) whose radius is the magnitude of the thrust coefficient; the angles are easily plotted from 0° to 90° in the second quadrant and 90° to 180° in the first quadrant. If thrust is not constant, the circle becomes slightly distorted and is defined by equations (11) and (12).

If one desires to analyze the drag polars and separate the forces as shown in Figure 13, all that is necessary is the construction of the appropriate vector diagram for the angle of attack and condition of interest. This is shown for a typical "trim" case of $C_{T,SS,S} \approx 0.95$ for <u>both</u> the NASA and Princeton data in Figure 14. Three "polars" are shown:

1. Propeller thrust polar, NASA and Princeton (dashed line)

2. Resultant force polar, NASA (broken line)

3. Resultant force polar, Princeton (solid line)

Similarly, a typical "out-of-trim" case is shown in Figure 15 for $C_{T,SS,S} \approx 0.92$ with all the pertinent force components labeled for the Princeton data.

Sets of lift, horizontal force, pitching moment, and propeller thrust coefficients versus angle of attack graphs are presented for seven slipstream thrust coefficient values. Drag polars are shown and

matching data from References 1 and 2 are plotted for comparison purposes on these seven graphs (Figures 16 through 22). Note that in the plot of propeller thrust force, CT,FS,S versus α, the Princeton data are exactly the same as the NASA data. This is because the NASA data were "matched" by Princeton by searching the crossplots from Reference 2 for exactly the same angle and thrust condition and recording the measured values of the forces and moments. The small variation of CT,FS,S versus α in these curves is not aerodynamic characteristic data but occurs just because of the practical difficulty of maintaining thrust precisely constant at the time of the run. One graph is included to check a "Flaps On" test point and is shown in Figure 23.

When an effort is made to determine the degree of correlation or to evaluate the comparison of the data on the basis of the drag polars shown in Figures 16 through 22, several general statements on the trends and conclusions may seem appropriate. First, it appears that similar trends are visible in the polar plots and that all Princeton data fall close to but slightly below the NASA data. Furthermore, comparing Figure 16a (CT,SS,S $\approx$ 0.80, the fastest speed shown in the graphs) and Figure 22a (CT,SS,S $\approx$ 0.95, the slowest speed), the curves show about the same trends, and the magnitudes of the lift coefficients of the Princeton data (say a trim, where the horizontal force is equal to zero) are within about 5% (good ?) agreement of the absolute magnitudes of the NASA data. On the other hand, if one considers the thrust polars (dashed lines) as the lower limit of the measured data and the NASA polar as the other limit, then the Princeton lift coefficient trim data are within about 15% (fair?) agreement of the NASA data for CT,SS,S $\approx$ 0.80 and about midway between or 50% (poor?) agreement of the NASA data for CT,SS,S $\approx$ 0.95.

Actually, if one analyzes the details of these drag polars or studies Figures 13, 14 and 15, it should be apparent that the utility and validity of the above general statements is questionable and that in reality, not very much can be stated positively by any of the previous reasoning. In order to compare the data on wind-axes drag polars, it appears that the angle-of-attack relationship must be noted and the vector diagrams constructed (as shown in Figures 14 and 15) for each condition of interest. Although separate drag polars with angle-of-attack points are provided for each thrust condition (Figures b of 16 through 22) for plotting any desired vector diagram, the rewards and meaningful conclusions gained probably are still not justified by the amount of effort required.

After reviewing much of the data, it appears to the author that plots using a wind-axes resolution of the measured forces may not be the best way of analyzing and comparing aerodynamic characteristic data for the slow-speed envelope of these types of vehicles. First, from the standpoint that as slower and slower speed data are analyzed, the dependence or importance of the direction of the free stream becomes less and less until at hover the wind-axes system loses definition and meaning entirely. Secondly, at the slower speeds of these vehicles,

most of the "lift" and "drag" of the vehicle is being provided primarily by a body-axis oriented force, namely, propeller thrust and components thereof. Noting this and also realizing that there is a great deal of familiarity and vast aerodynamic characteristic data on airfoils compiled on a wind-axes basis, it is still suggested that another system of viewing the data may reveal more beneficial results.

Also, the standard wind-axes plots and polars are already somewhat more unfamiliar with the addition of "power-added" effects.

In this instance, it would seem worthwhile to attempt to view all the data on a body-axes basis. This would be especially beneficial if the separate effects of the propeller alone and the wing alone could be analyzed. Because of the methodology used in Reference 1 for running the tests, it should be evident that the only aerodynamic characteristic data presented in that research is the Wing* Force. Propeller thrust was held constant and is known and may be subtracted from the total measured force (resultant force) to yield the Wing* Force. The relationships between the Wing* Force components in a wind-axis system and the Wing* Force components in a body-axis system may be obtained by the following expressions:

WING* FORCE (WIND-AXIS SYSTEM)

$$C_L = CL,FS,S - CT,FS,S \ (\sin \alpha) \qquad (+ \text{upward}) \qquad (13)$$

$$C_D = -CX,FS,S + CT,FS,S \ (\cos \alpha) \qquad (+ \text{aft}) \qquad (14)$$

WING* FORCE (BODY-AXIS SYSTEM)

$$C_{X_{BODY}} = C_L \sin \alpha - C_D \cos \alpha \qquad (+ \text{forward}) \qquad (15)$$

$$C_{Z_{BODY}} = -C_L \cos \alpha - C_D \sin \alpha \qquad (+ \text{downward}) \qquad (16)$$

Referring once again to Figure 15 and the above equations, it can be seen on the graph that the Wing* Force vector may be resolved into two body-axes components, one parallel to the chord line and thrust axis ($C_{X_{BODY}}$) and one normal to the thrust axis ($C_{Z_{BODY}}$). The origin of the body-axis system is not defined. On the typical example shown, the Wing* Forces disagree both in magnitude and direction; the NASA vector tilts forward of the perpendicular and the Princeton vector tilts aft.

COMPARISON OF WING* FORCE DATA USING BODY-AXES COEFFICIENTS AND FORCE POLARS

Before proceeding directly into a comparison of the "power-on" aerodynamic characteristic WING* Force data in body-axes coefficient form, it may be useful to become familiar with the character of the plot for "power-off" wing data plotted in body-axes form.

In Figure 24, aerodynamic characteristic data were plotted as obtained from References 1 and 7. In Reference 1, Figure 6 presents power-off, three-dimensional aerodynamic characteristic data (airfoil section 0015) of the general research VTOL model with propellers removed. Reference 7 presents power-off aerodynamic characteristic data on a two-dimensional, 0015 airfoil section. In Figure 24, the lower plot presents these data in standard wind-axes drag polar form with the scale "square" and for angles of attack up to 28° for Reference 1 and 90° for Reference 7. In the upper plot of Figure 24, the same data are shown in a body-axis system "force polar". This second type of force polar (Reference 8) is sometimes used in strength, stability, and dynamics problems of aircraft and reveals the magnitude and direction of the resultant force in relation to a body-axis system fixed in the wing as shown. It is interesting to note in the plot of the two-dimensional data of the 0015 airfoil section on the body-axis force polar between the angles of 30° and 90°, that the $C_{x_{BODY}}$ axial force tends to be small and both positive and negative, crossing the ordinate at about 48°.

In Figure 25, seven sets of Wing* Force aerodynamic data are plotted on a body-axis system using the data from References 1 and 2. In these plots, the actual measured aerodynamic data obtained from the two different facilities are shown and may be studied for comparison purposes and analyzed. Both the magnitude and direction (with respect to reference lines parallel and perpendicular to the wing chord) are reflected in the graphs. The axial coefficient $C_{x_{BODY}}$ may be either positive or negative (pointing forward or aft). The plotted Princeton points (taken from Reference 2), denoted by circle symbols, represent actual experimental values and have not been faired; this accounts for some of the data scatter shown in these graphs and elsewhere in the report.

The comparison of the $C_{z_{BODY}}$ force or normal force component of the WING* FORCE for the different values of CT,SS,S indicates several trends. For the fastest speeds where CT,SS,S $\approx$ 0.80 and 0.86, agreement is quite good and is within a few percent of the Reference 1 data. As forward speed decreases (CT,SS,S $\approx$ 0.90 and larger), the Princeton normal force shows approximately the same trends with angle of attack, but the magnitude of the normal force tends to be greater as compared to the NASA data. As forward velocity is decreased to the slowest speeds shown (CT,SS,S $\approx$ 0.94 and 0.95), the NASA normal force is approximately 85 to 90 percent of the magnitude of the Princeton data.

The comparison of the $C_{a_{BODY}}$ force or axial force component of the WING* FORCE (along the thrust line or chord line) for the different values of CT,SS,S is more difficult to evaluate. First, the component of WING* FORCE along the chord of the wing is much smaller in magnitude than the normal force. The comparison is further compounded by the fact that the strain-gauge layout and measurement technique requires that the magnitude be evaluated by finding the difference between two quantities that are very close to the same value (the propeller axial force and the total axial force, Figure 12). All the problems associated with strain-gauge layout, sensitivity, calibration accuracy, etc., must be carefully attended to in order to obtain confident and accurate measurements. The difficulty in doing this with the measurement techniques used in this research may account for some discrepancy in the values of the axial force shown. In general, the only statement that can be made about the comparison of the $C_{a_{BODY}}$ axial force shown is that the Princeton values are smaller than the NASA values. The NASA axial forces tend to be positive and remain so for the values of CT,SS,S shown. The Princeton axial forces are closer to zero and tend to be both positive and negative depending on the angle of attack and CT,SS,S analyzed. Referring to Figure 15, this means that the NASA WING* FORCE vector always is tilted forward of a line perpendicular to the wing chord line, whereas the Princeton data tend to align more with the perpendicular and tilt slightly forward and aft depending on the test condition studied. As a general point, one is tempted to suggest that, as opposed to the normal force component, the absolute magnitude of the axial component of the WING* FORCE seems to be relatively small (as compared to the axial thrust force of the propeller) and may not have a significant influence on the aerodynamic characteristics of the total tilt-wing configuration in the slow-speed range.

CONCLUSIONS

A comparison of the aerodynamic characteristic data obtained from a large wind tunnel and a moving-model/track facility on a general research tilt-wing/propeller VTOL configuration was studied and the following conclusions are made. Because of the methodology used for conducting the wind tunnel tests (propeller thrust set and held constant during the course of a run) and the method of plotting the results, the aerodynamic characteristics of the propeller were not measured or presented. However, the known thrust of the propeller may be subtracted from the total measured force to obtain the aerodynamic data on the wing immersed in a slipstream and subjected to a free-stream flow field.

The usefulness of the comparison of the total force and moment coefficient data plotted versus free-stream thrust coefficient is questionable. The total forces measured contained large components of propeller thrust (which was set), and little can be said about the degree of correlation of the measured wing forces plotted versus free-stream thrust coefficient.

A study of the comparison of the wind-axes forces and moments (lift, horizontal force, and pitching moment coefficient data plotted versus angle of attack) and the use of drag polars presents the same difficulties. The known propeller thrust should be separated from the total measured data before a useful comparison can be made. One method of making this comparison is to plot the wing force on a body-axis basis. Analysis of these data reveals the degree of correlation of the normal and axial force acting on the wing. In general, the wing normal force obtained from the wind tunnel experiments is approximately 85% to 90% of the magnitude of the wing normal force measured in the track data. The wing axial force was small and difficult to measure, and the plotted data generally did not correlate.

RECOMMENDATIONS

Further analysis of the data obtained in the moving-model/track facility on the general research tilt-wing/propeller model is recommended. Additional study should be made on the presentation of the propeller aerodynamic characteristics (in combination with the wing) and on more meaningful methods of plotting these data for the flight conditions of slow speed and high angles of attack.

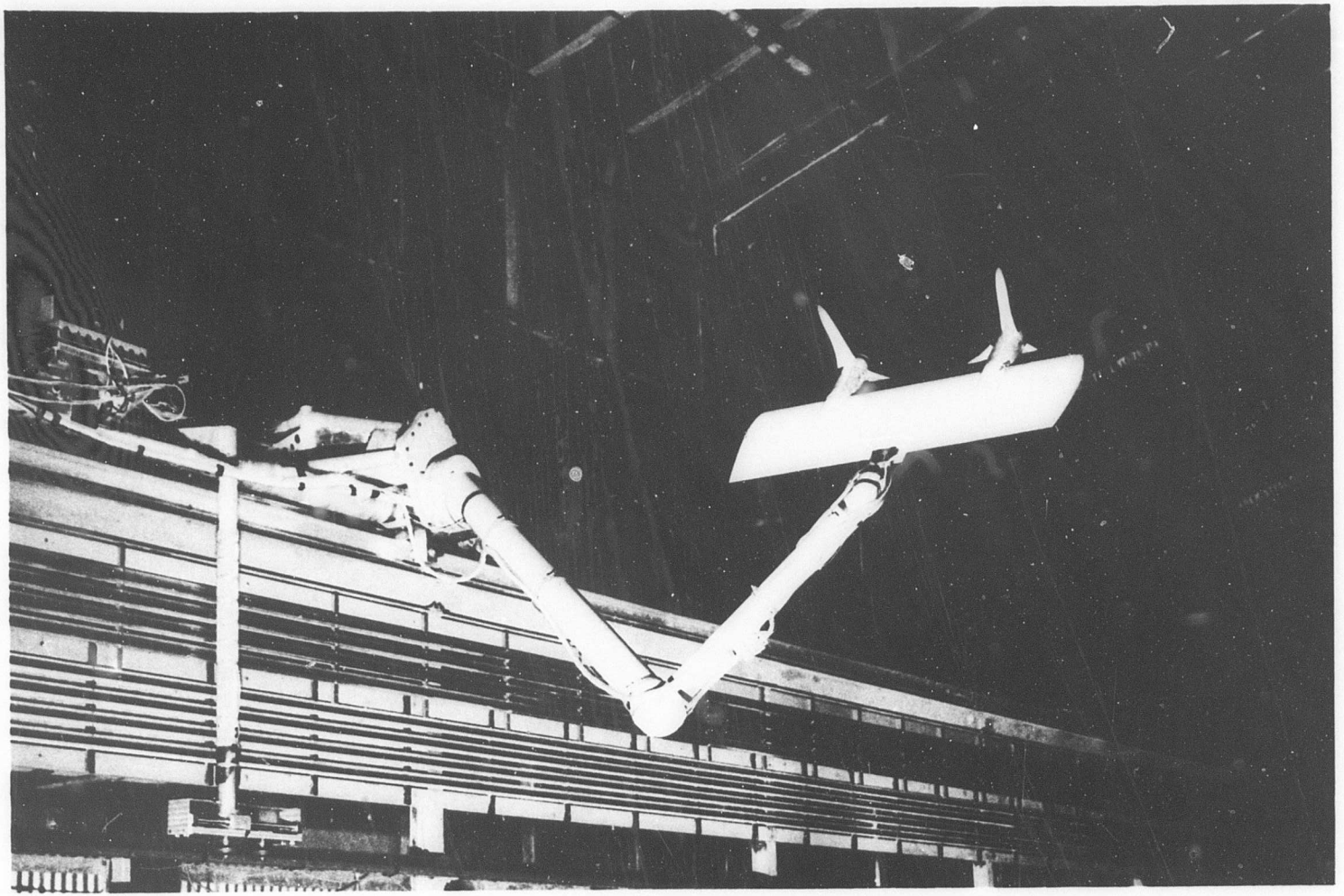

Figure 1. Model Installed on Sting-Mount/Carriage Assembly in Track Facility.

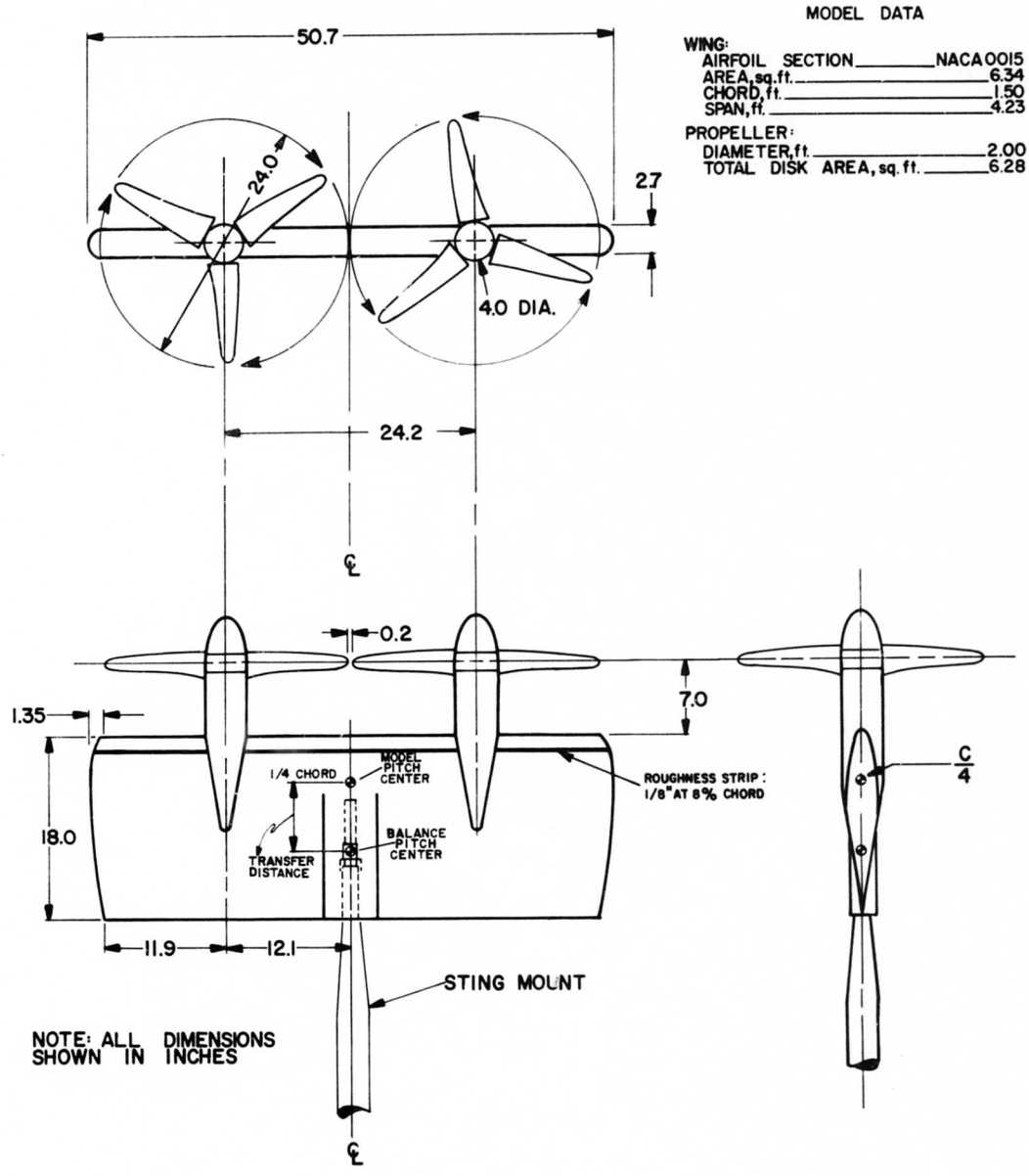

Figure 2. General Research Tilt-Wing/Propeller Model Configuration.

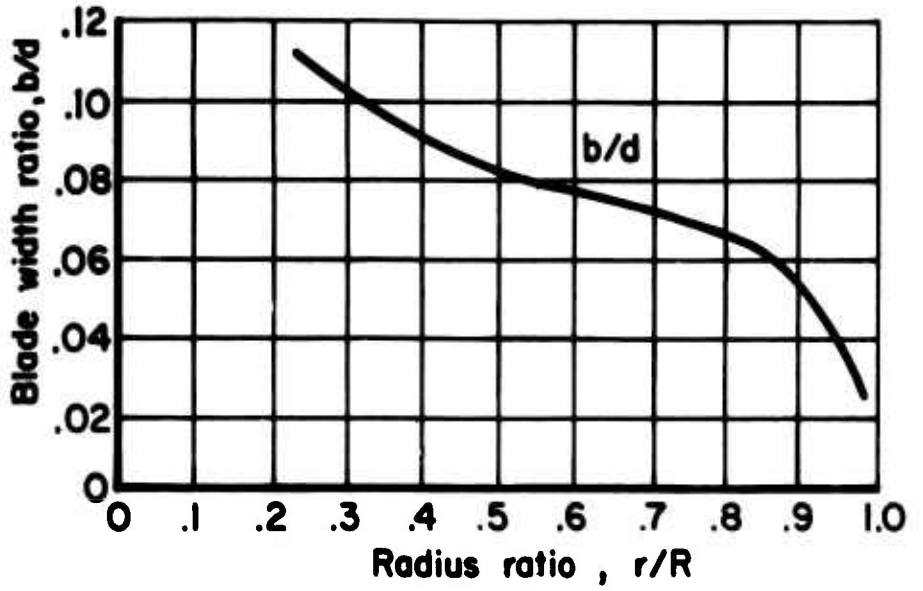

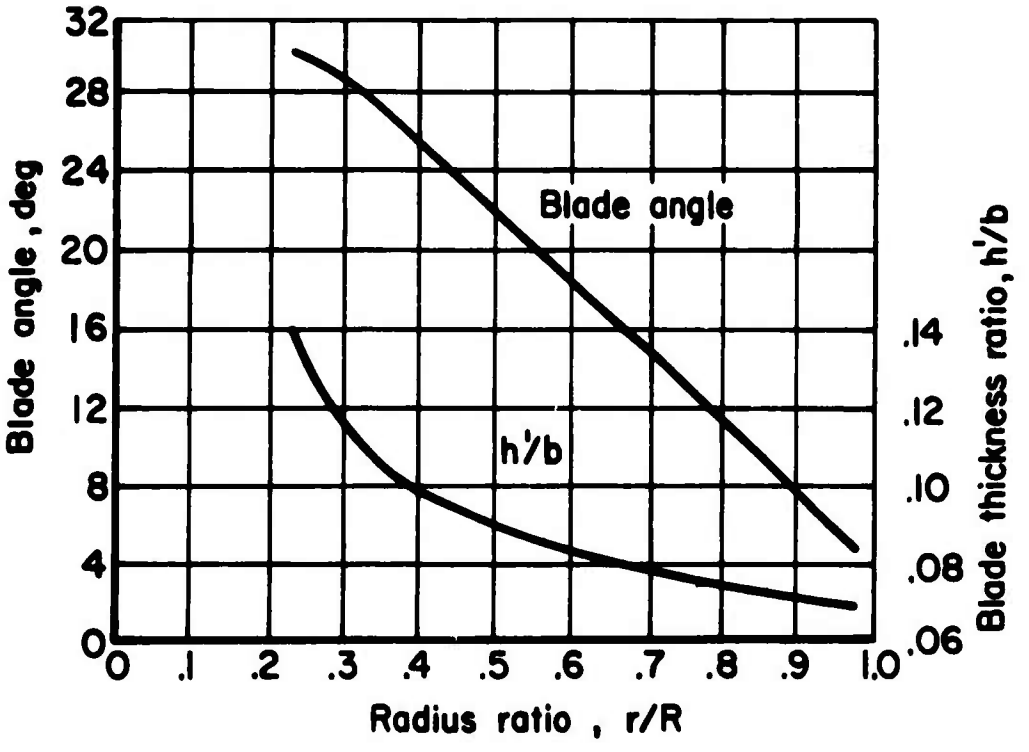

Figure 3. Propeller Blade Form Curves.

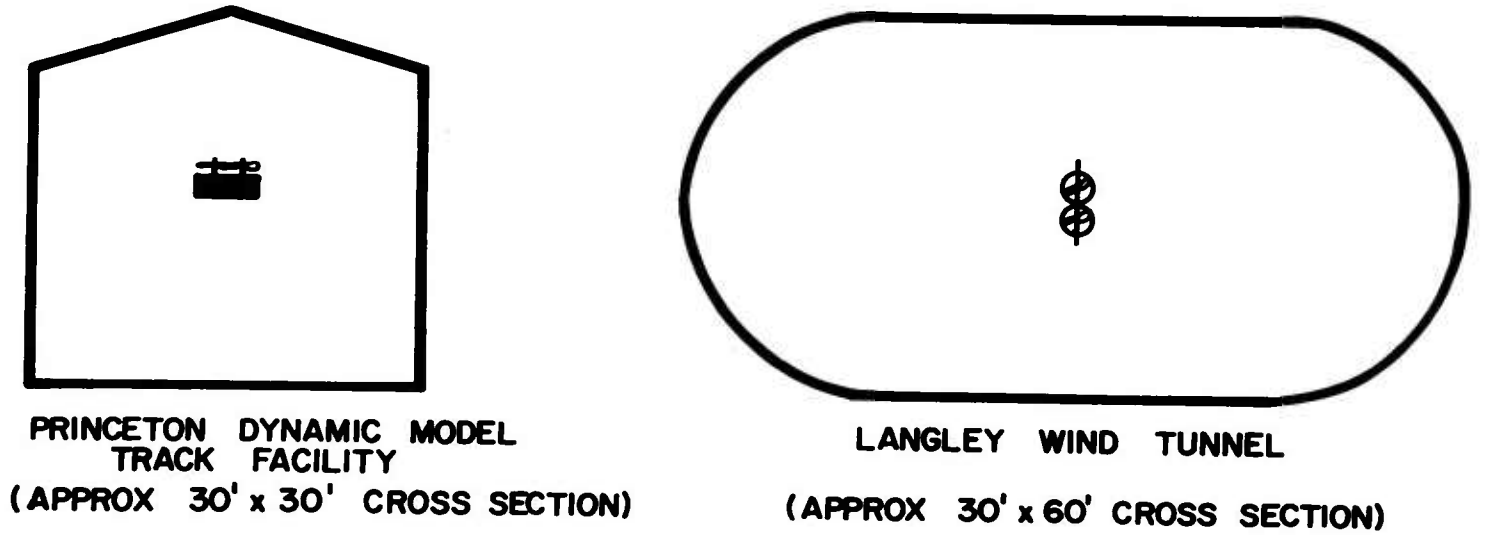

Figure 4. Scale Drawing Indicating Relative Size and Position of Model in Two Facilities.

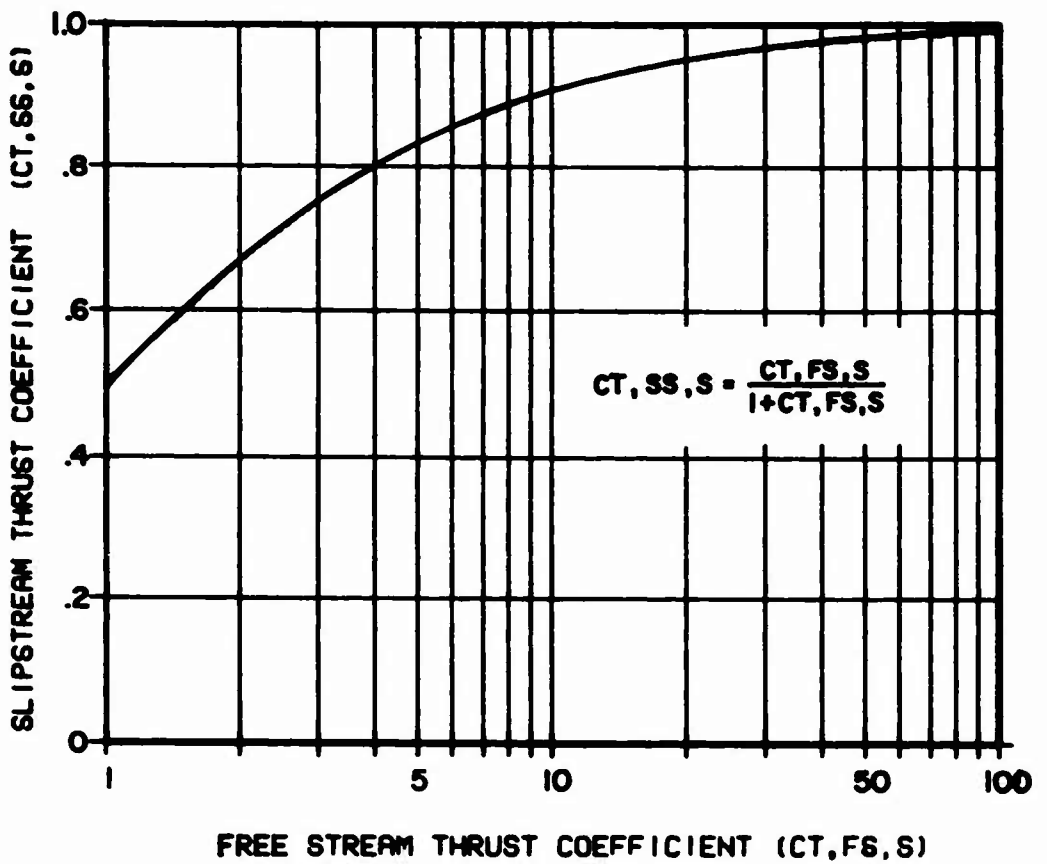

Figure 5. Plot Showing Relationship of Thrust Coefficients Based on Free-Stream Dynamic Pressure and Slipstream Dynamic Pressure.

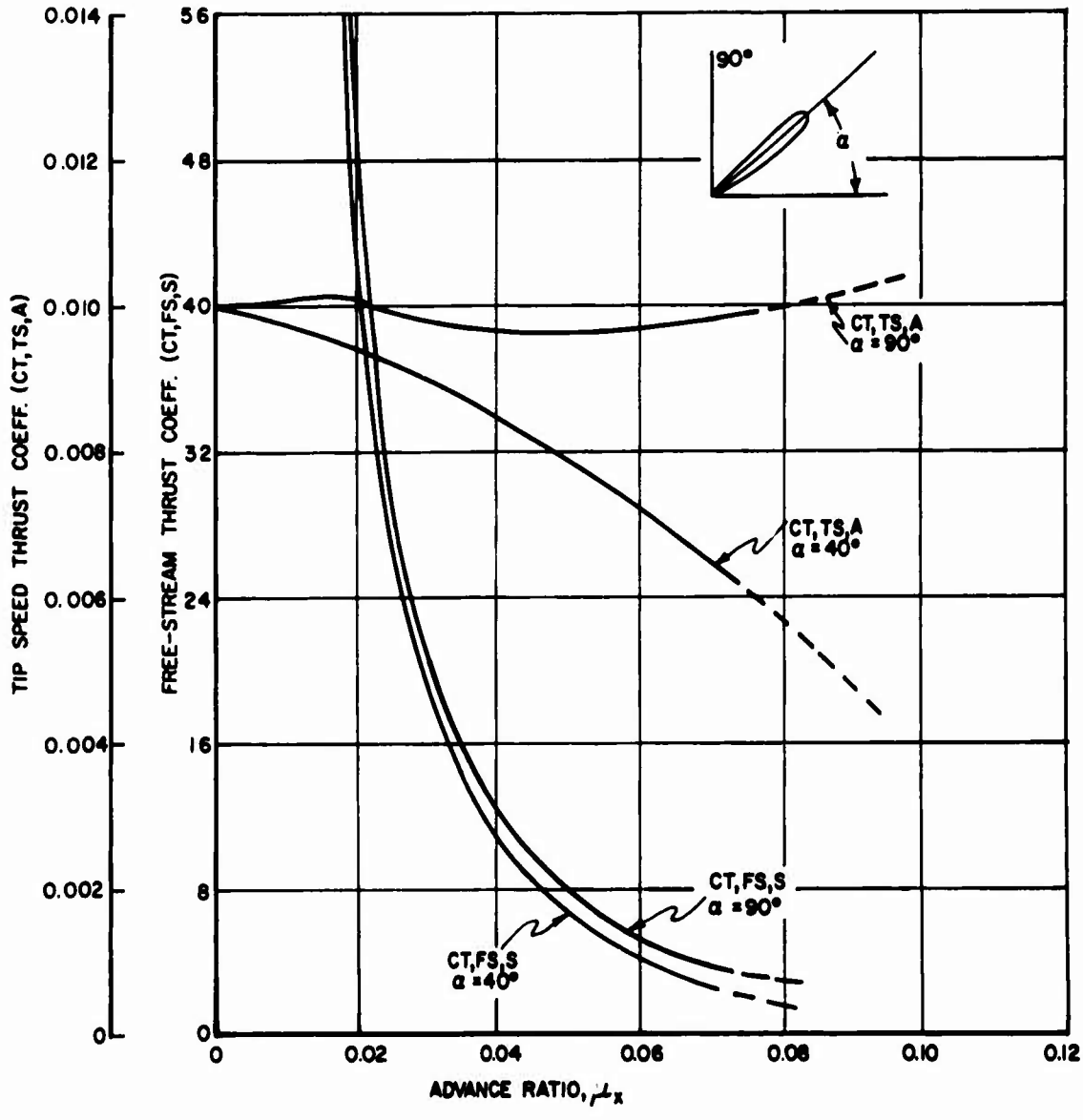

Figure 6. Typical Plot Showing Free-Stream and Tip Speed Thrust Coefficients Versus Advance Ratio at Fixed Blade Angle.

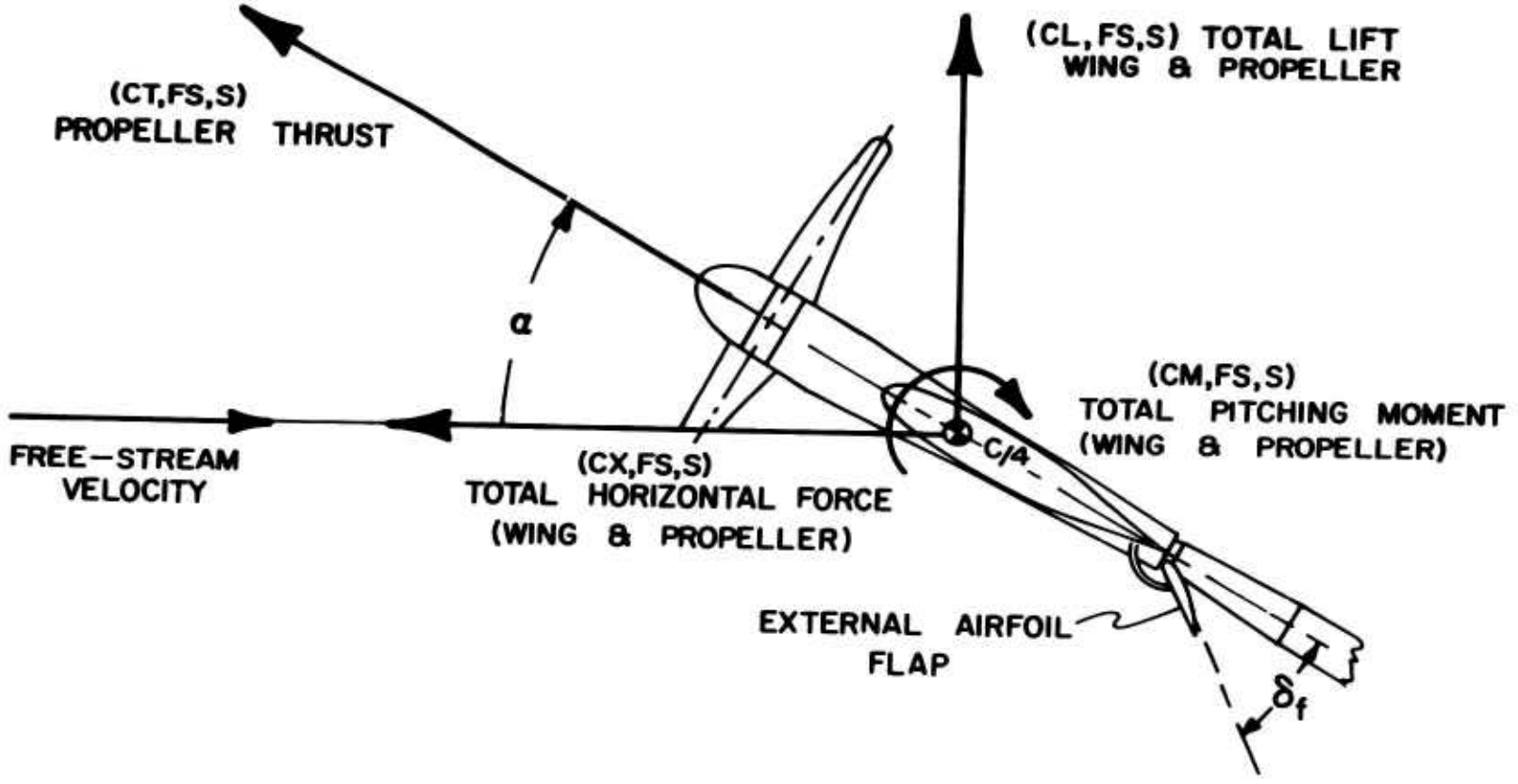

Figure 7. General Notation Showing Positive Direction of Forces, Moments and Angles.

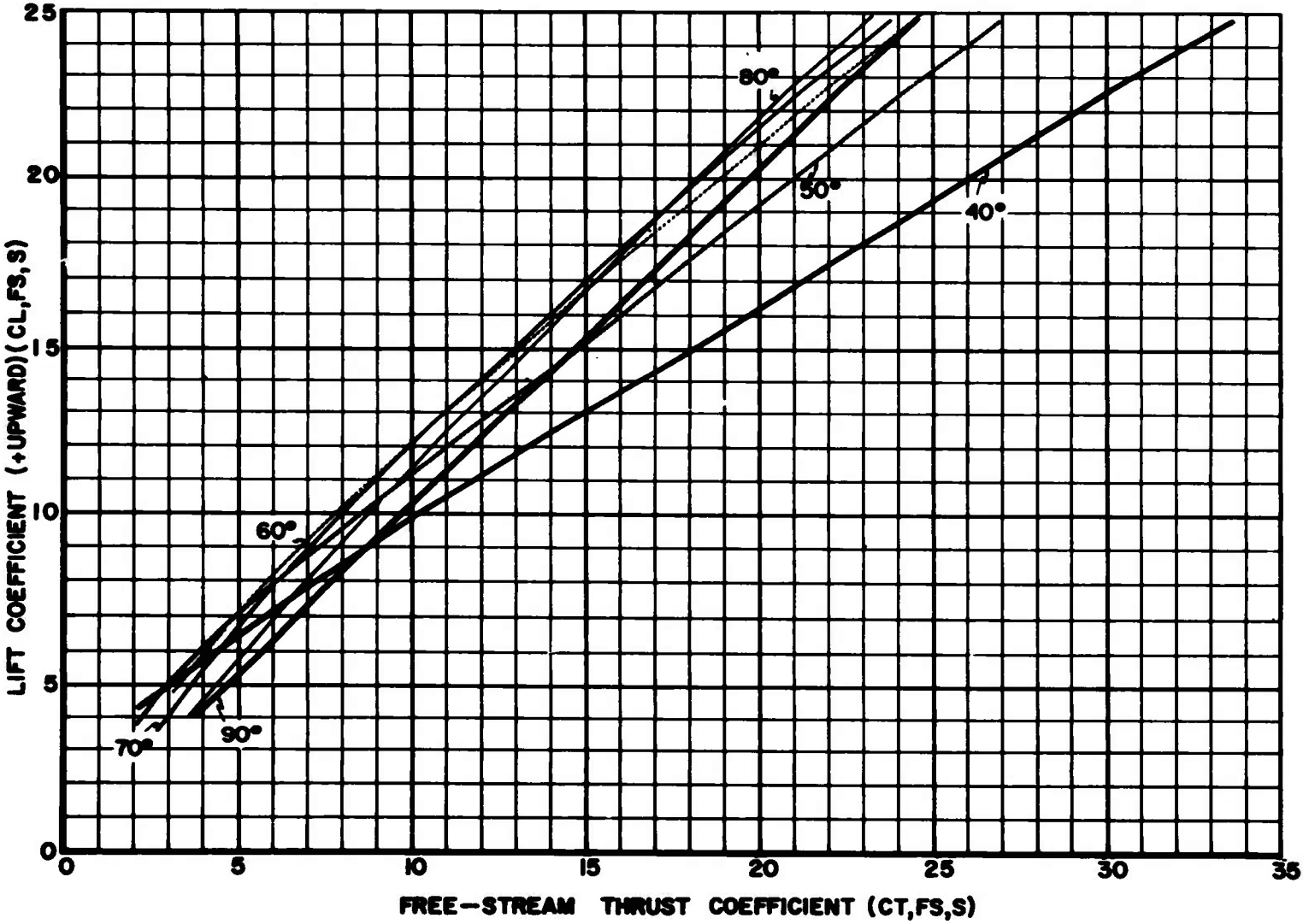

Figure 8a. Lift Coefficient as a Function of Free-Stream Thrust Coefficient (Data From Reference 2).

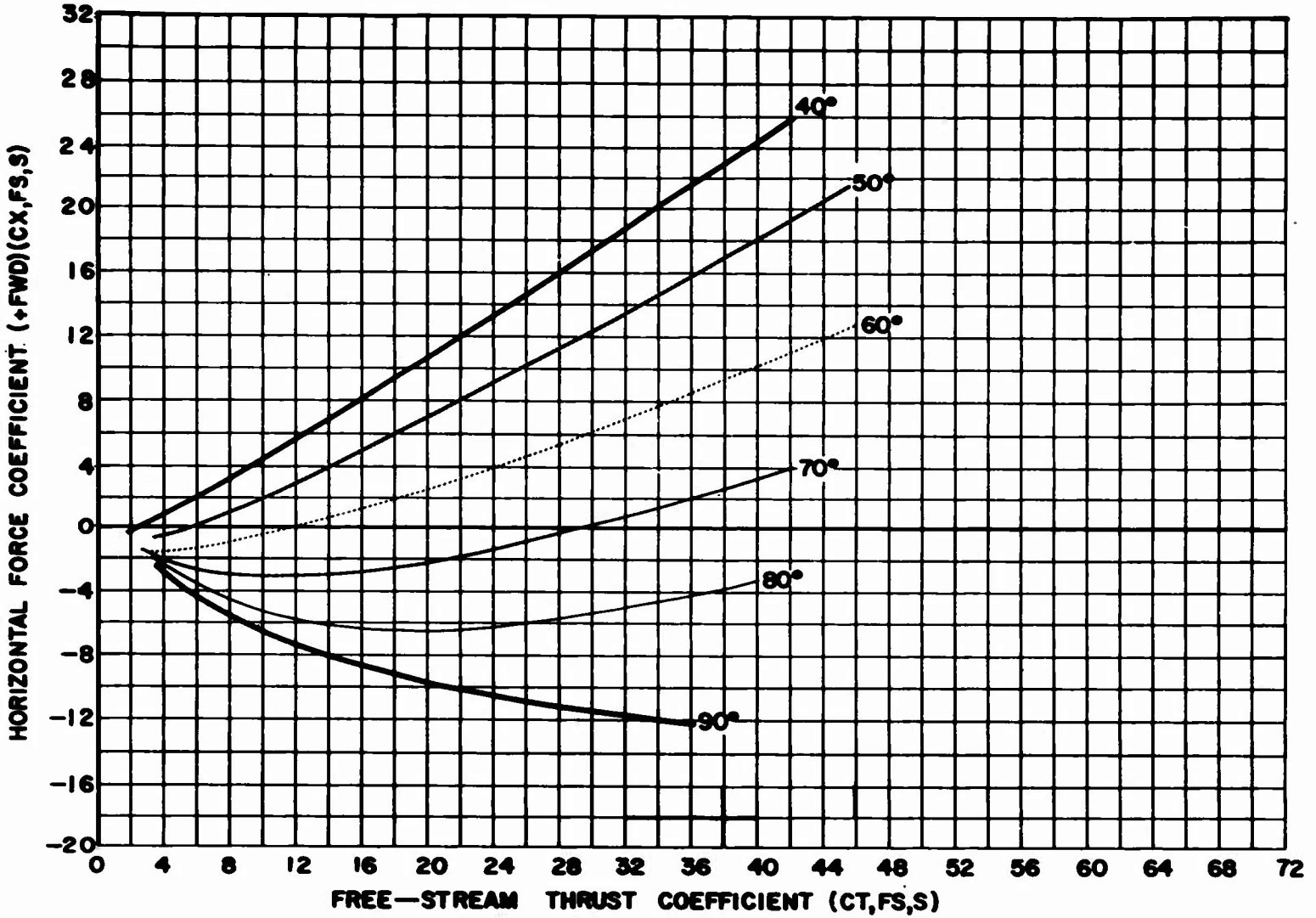

Figure 8b. Horizontal Force Coefficient as a Function of Free-Stream Thrust Coefficient (Data From Reference 2).

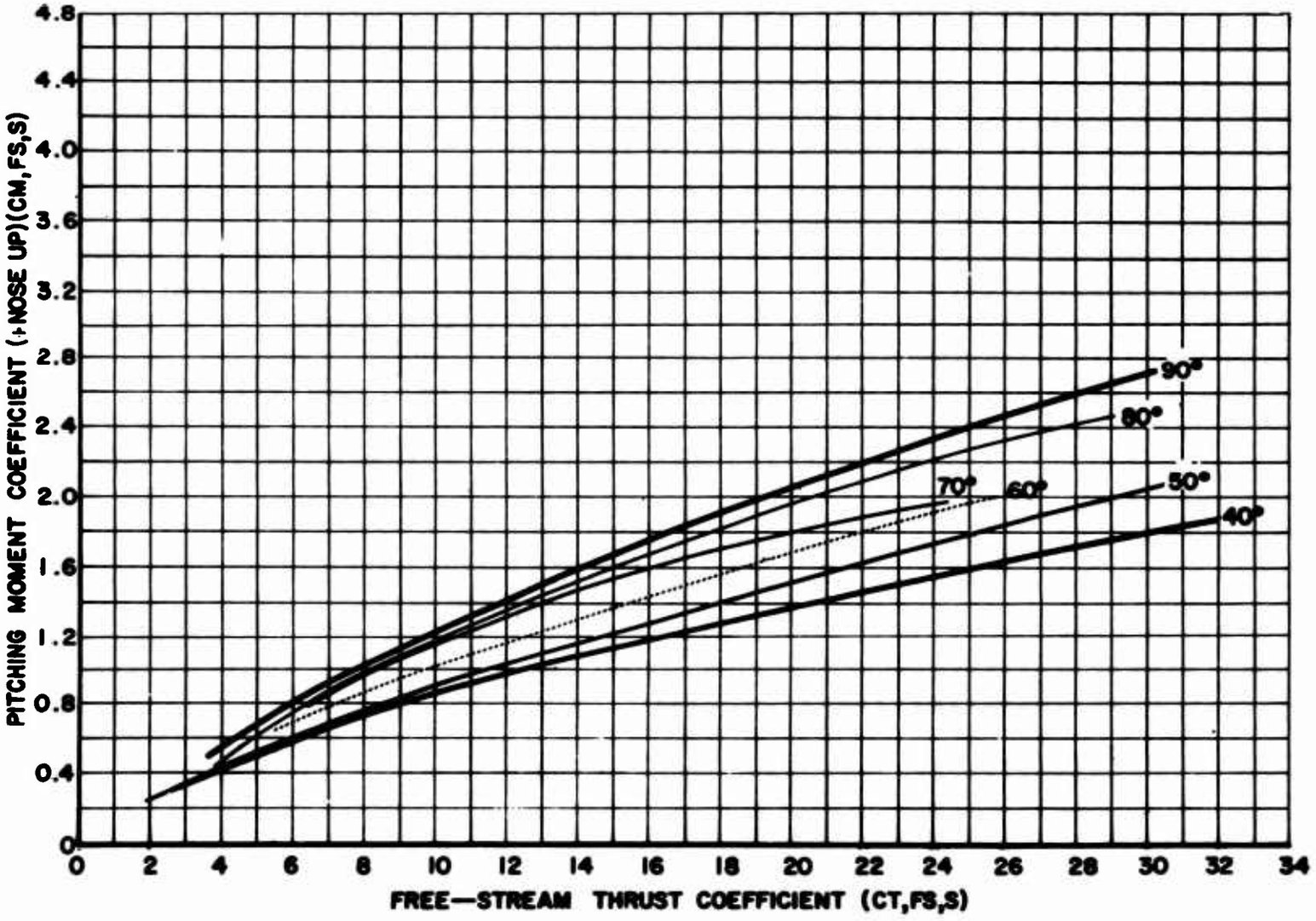

Figure 8c. Pitching Moment Coefficient as a Function of Free-Stream Thrust Coefficient (Data From Reference 2).

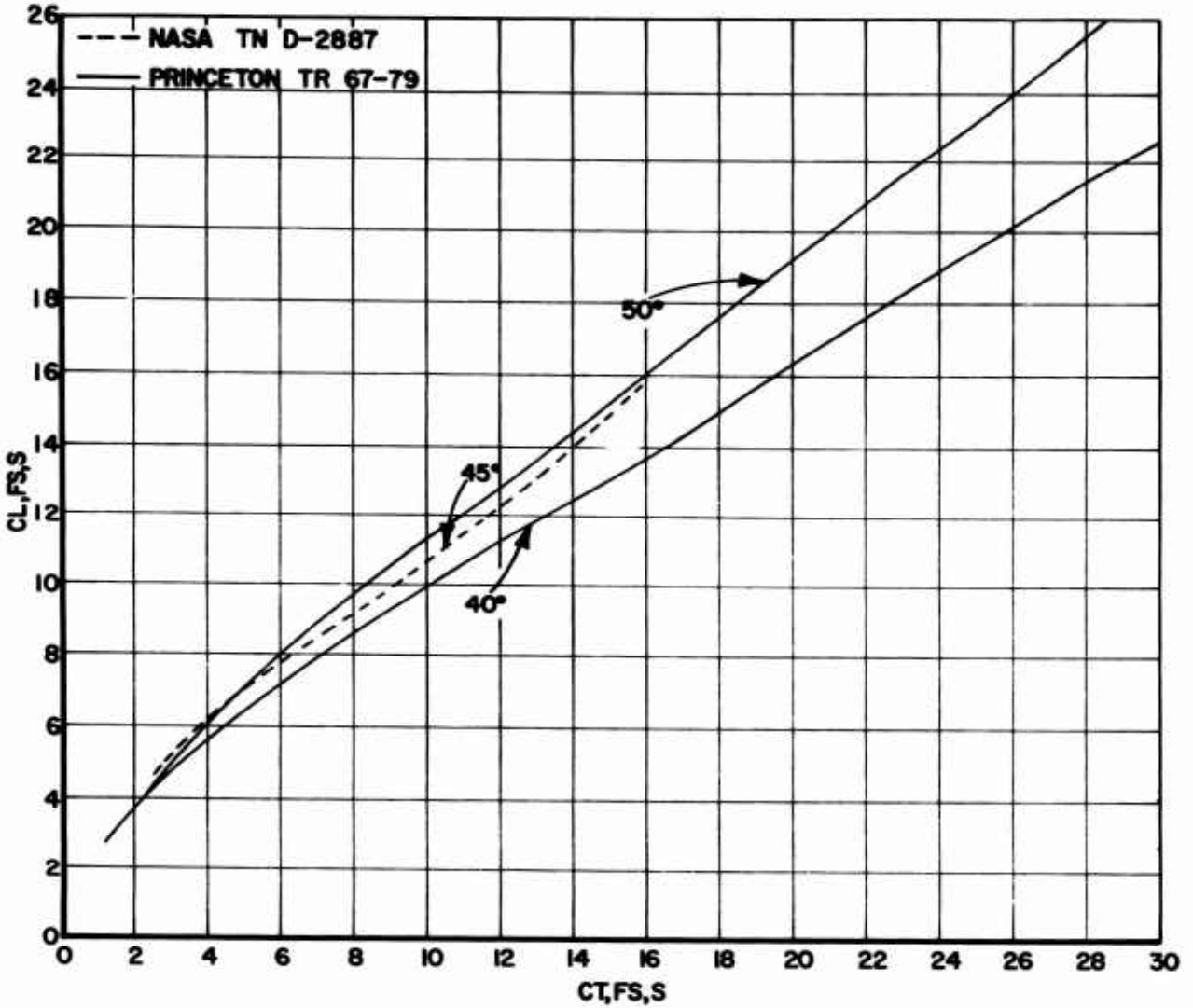

Figure 9. Comparison of Lift Coefficient Versus Free-Stream Coefficient Data as Obtained From References 1 and 2.

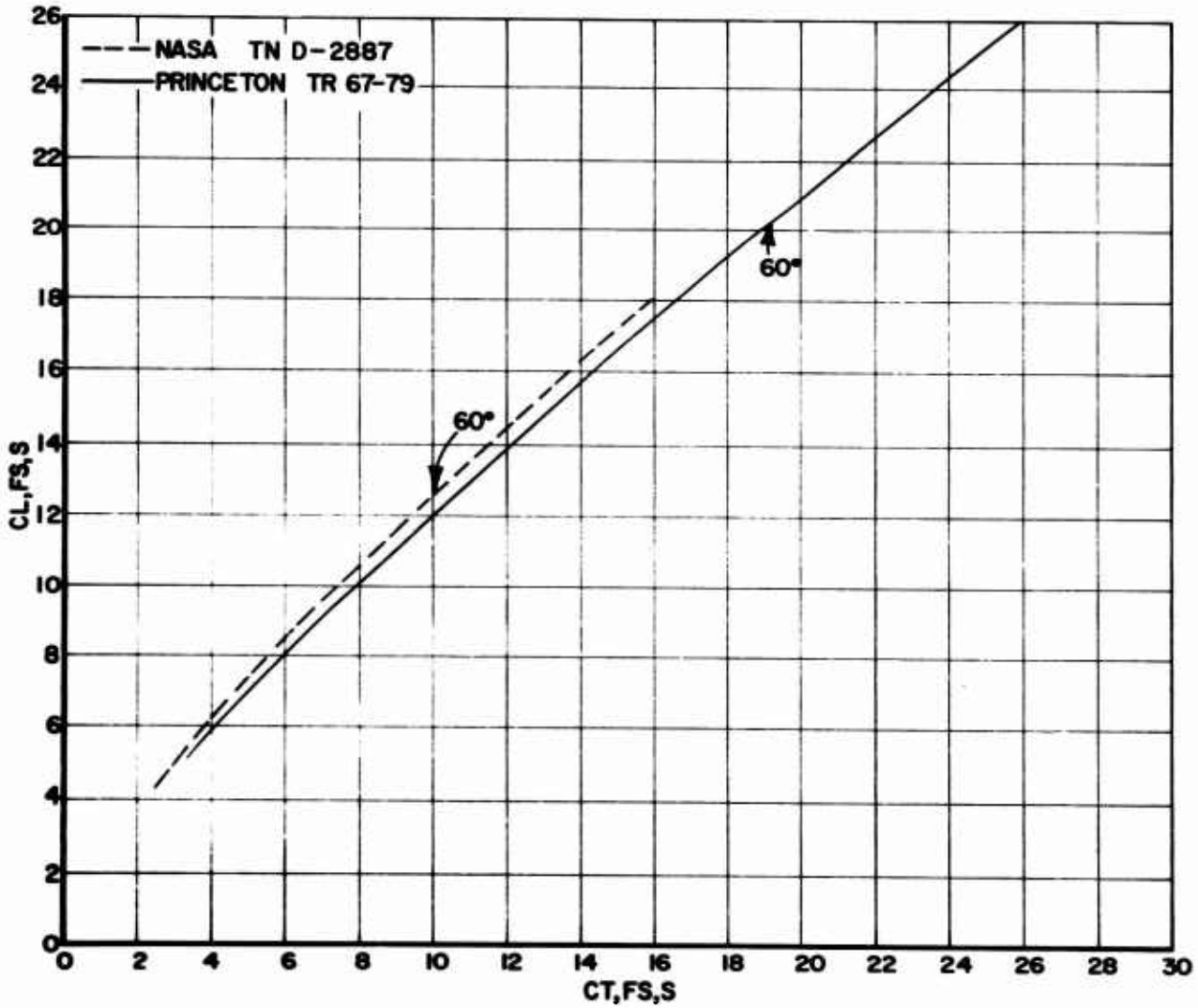

Figure 9. (Continued).

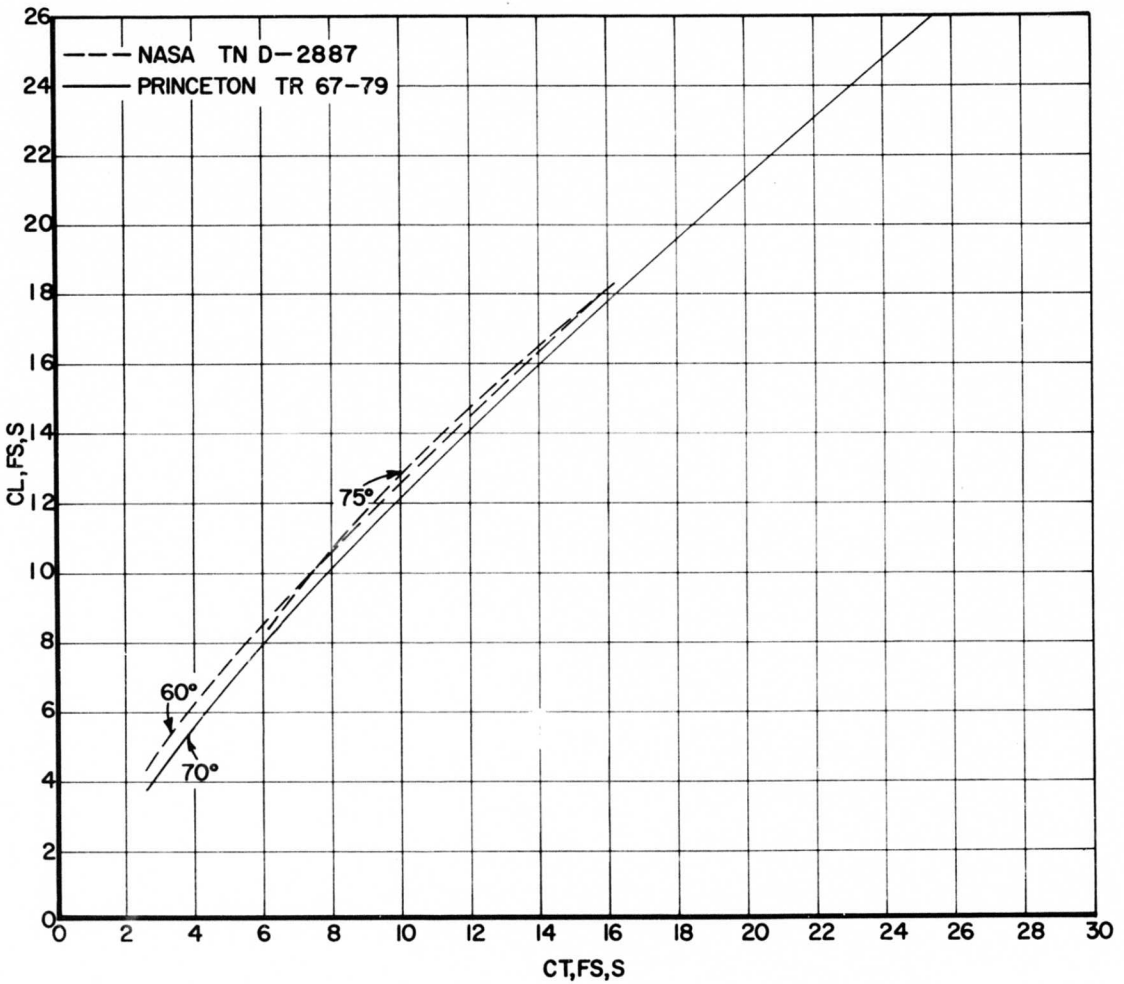

Figure 9. (Continued).

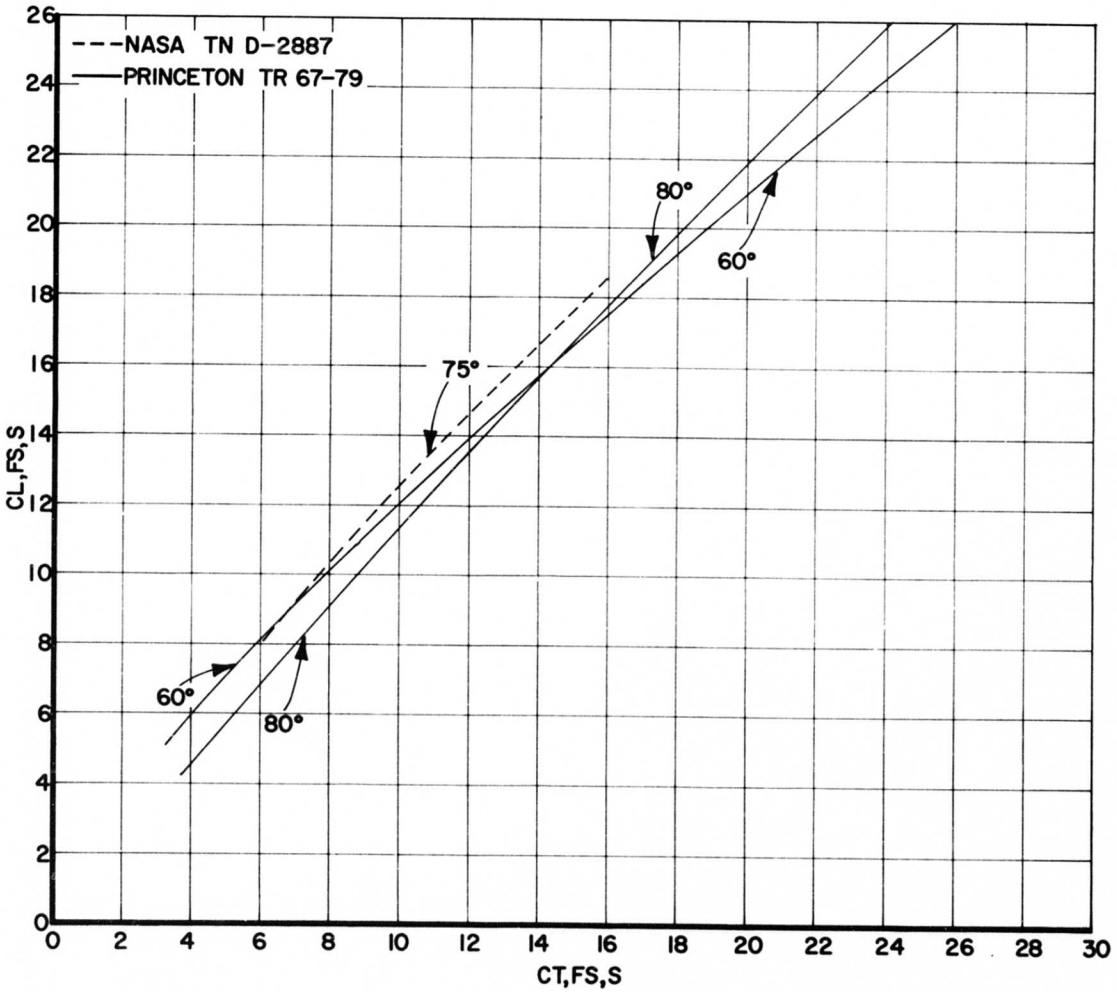

Figure 9. (Continued).

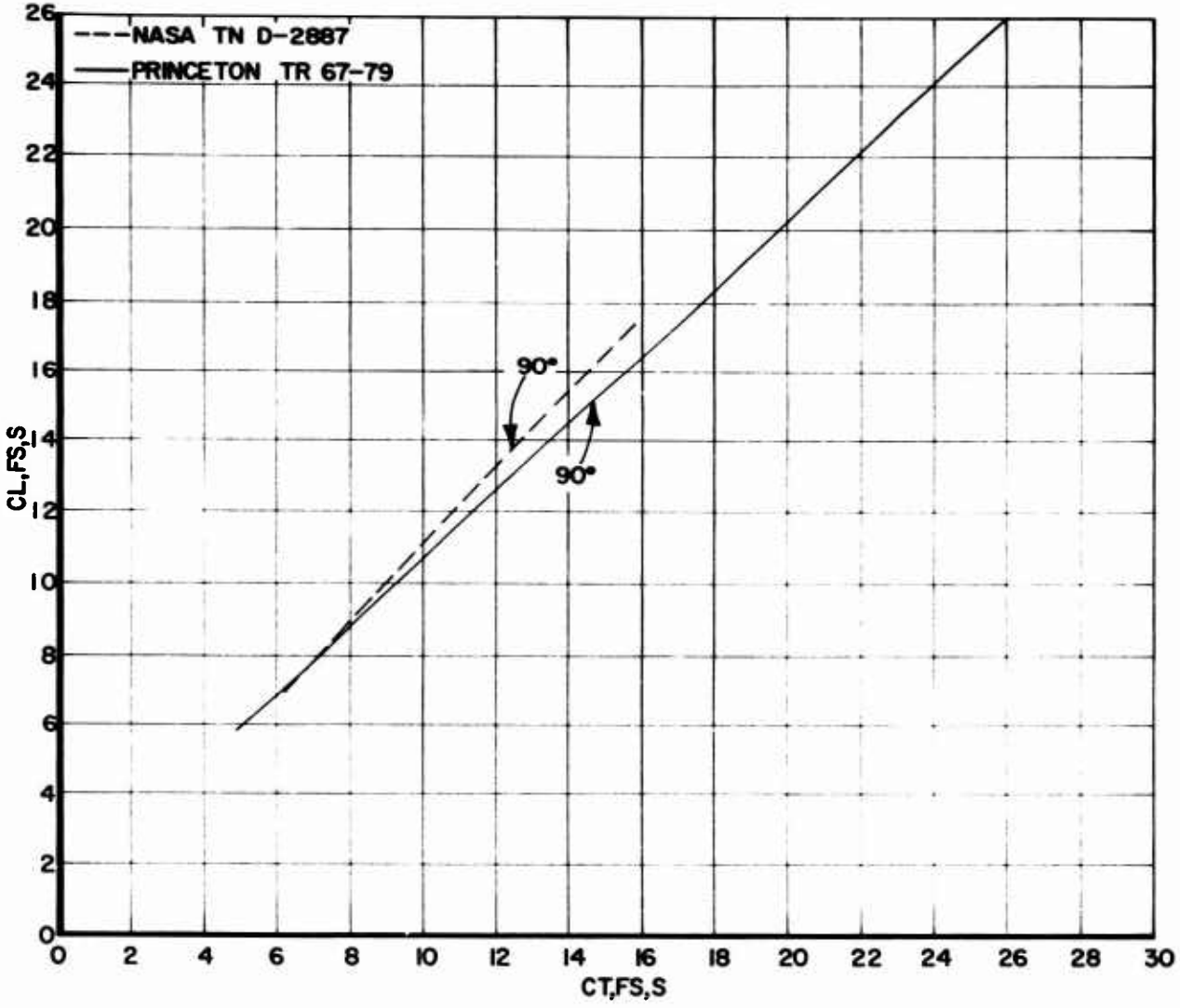

Figure 9. (Concluded).

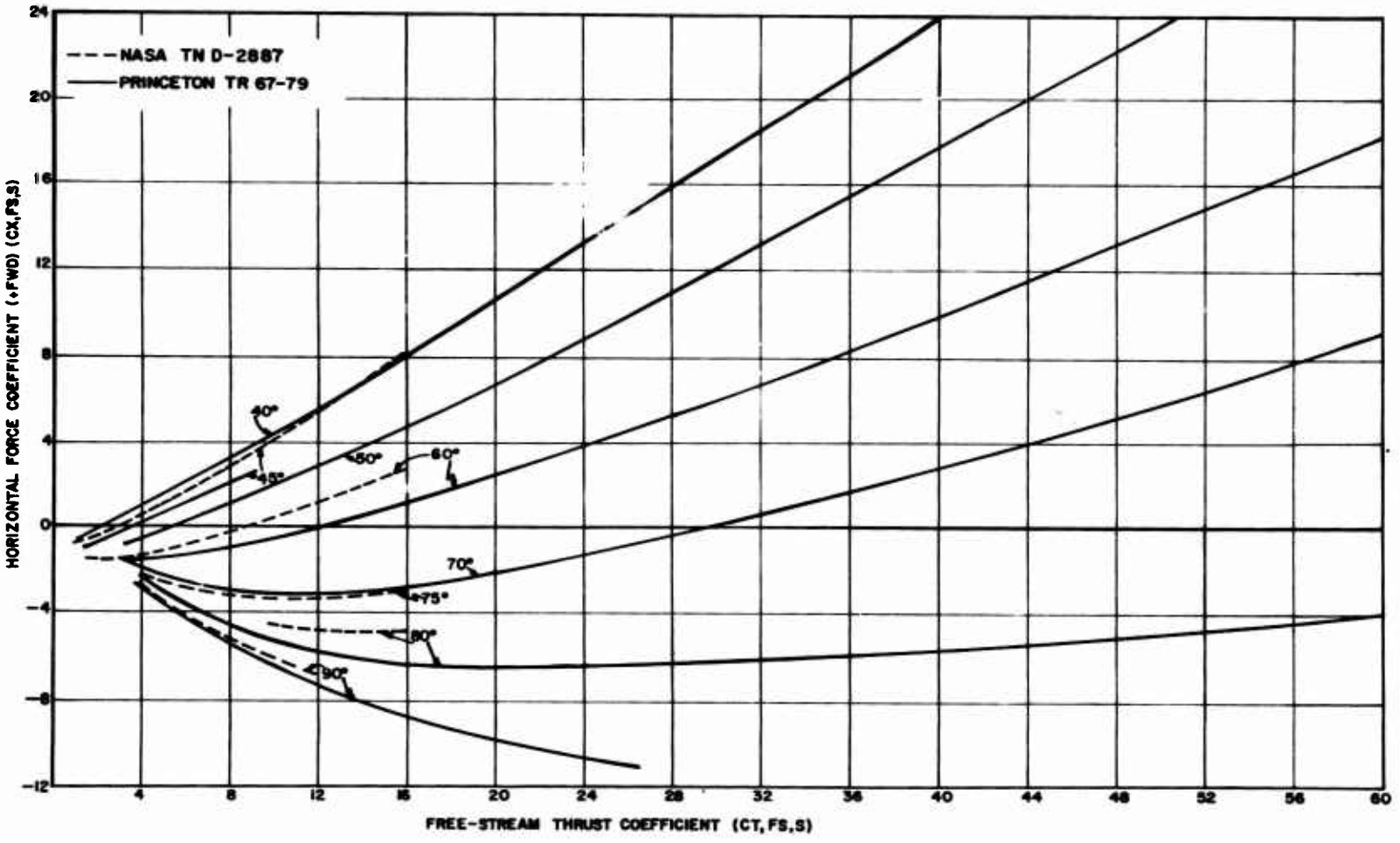

Figure 10. Comparison of Horizontal Force Coefficient With Free-Stream Coefficient Data as Obtained From References 1 and 2.

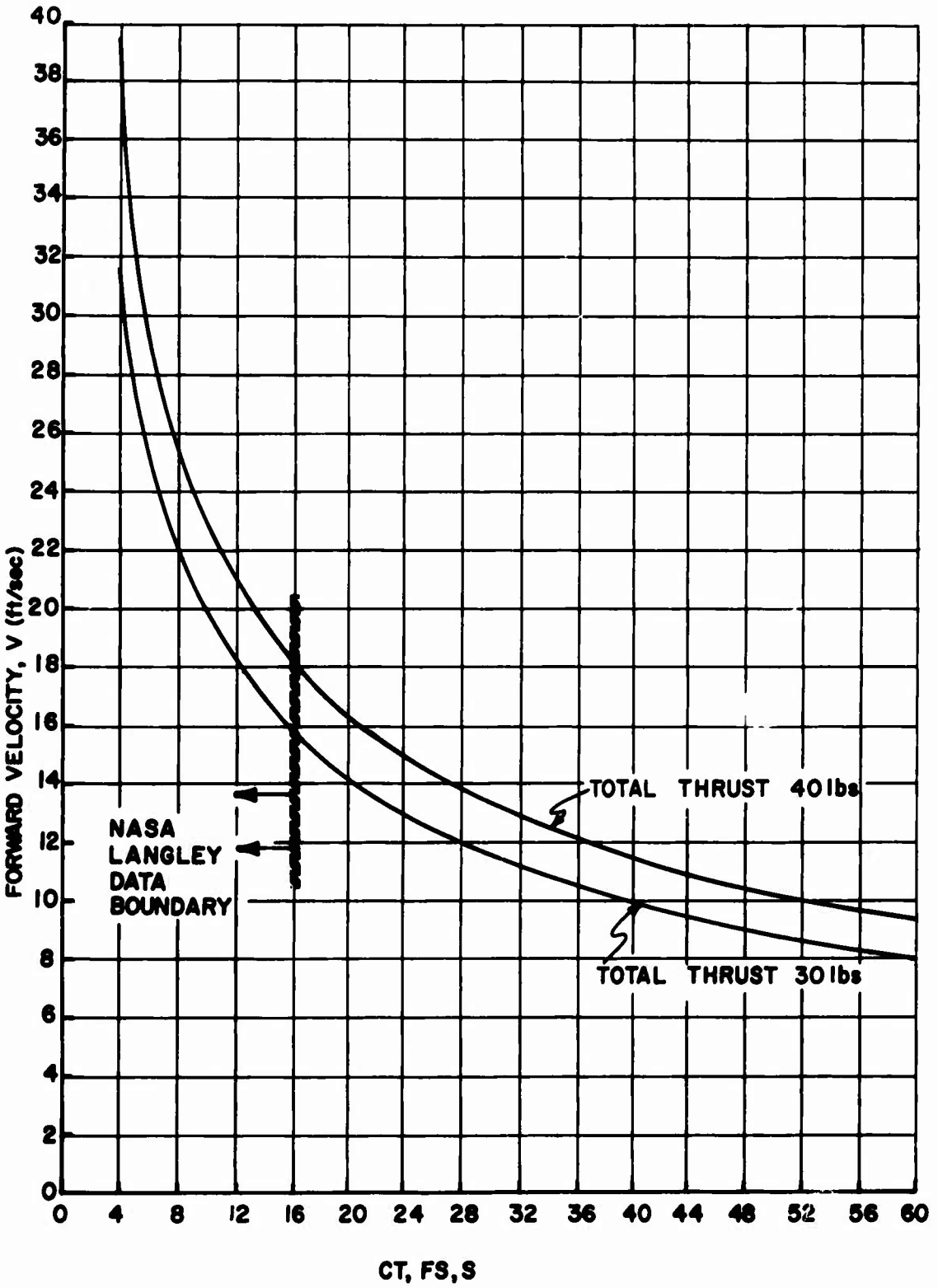

Figure 11. Typical Plot of Forward Velocity Versus Free-Stream Thrust Coefficient for Two Thrust Levels.

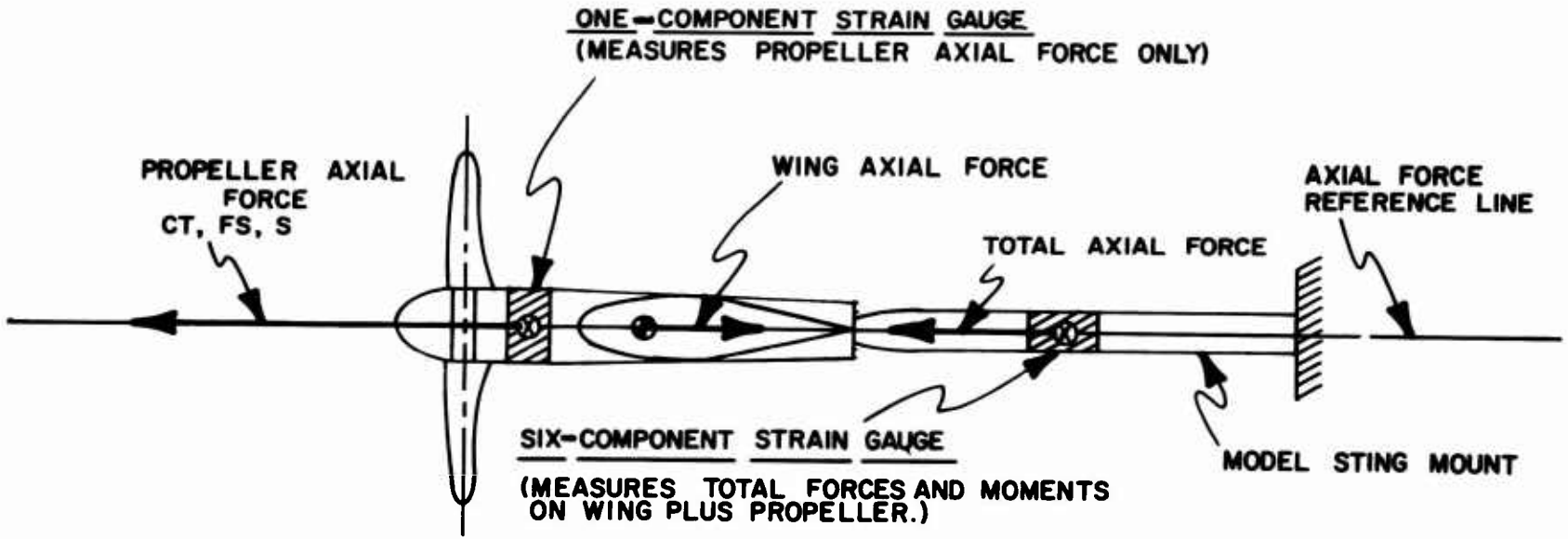

Figure 12. Schematic of Strain-Gauge Layout.

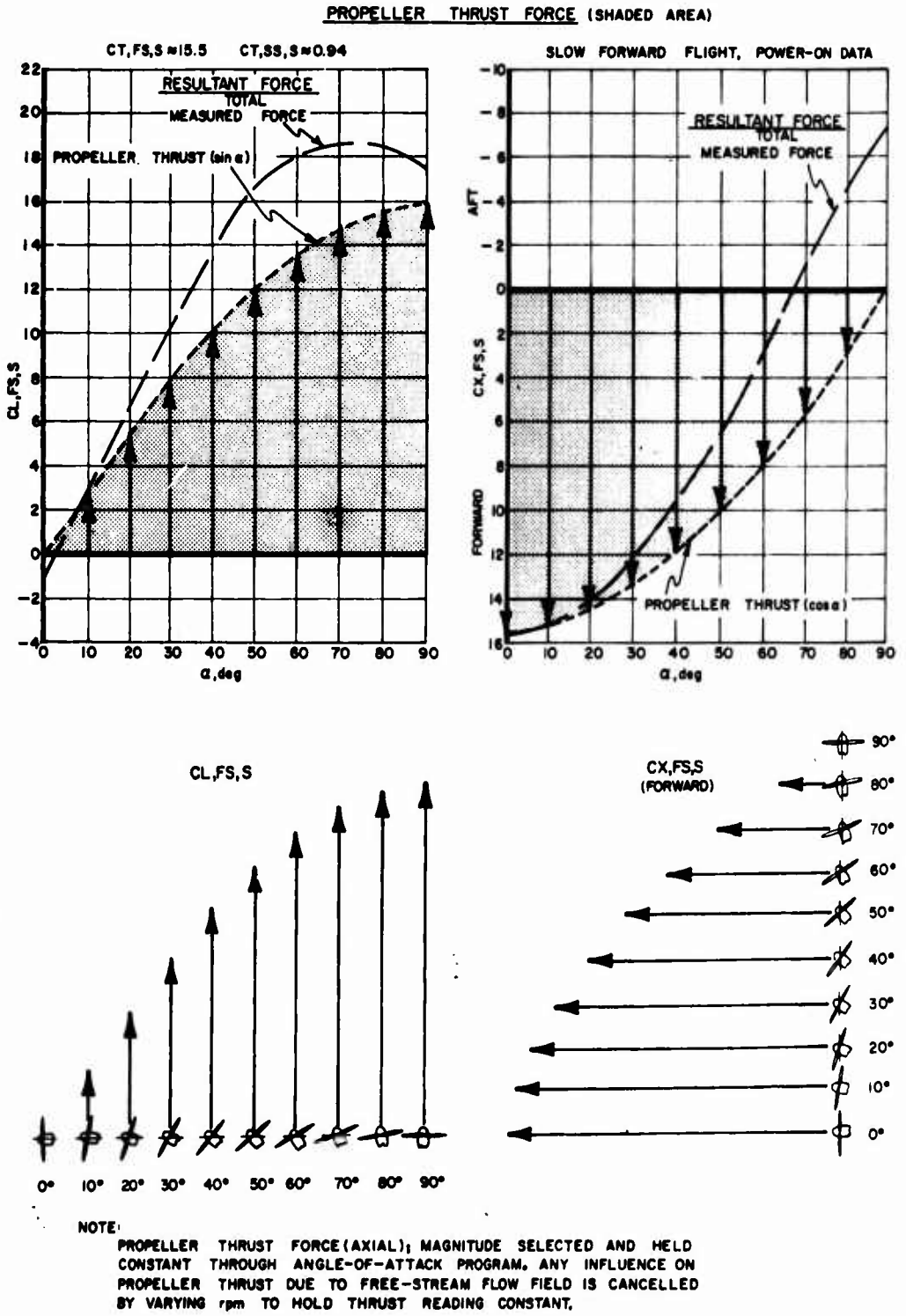

Figure 13a. Depiction of Typical Slow Flight, Lift and Horizontal Force Coefficients due to a Given Propeller Thrust.

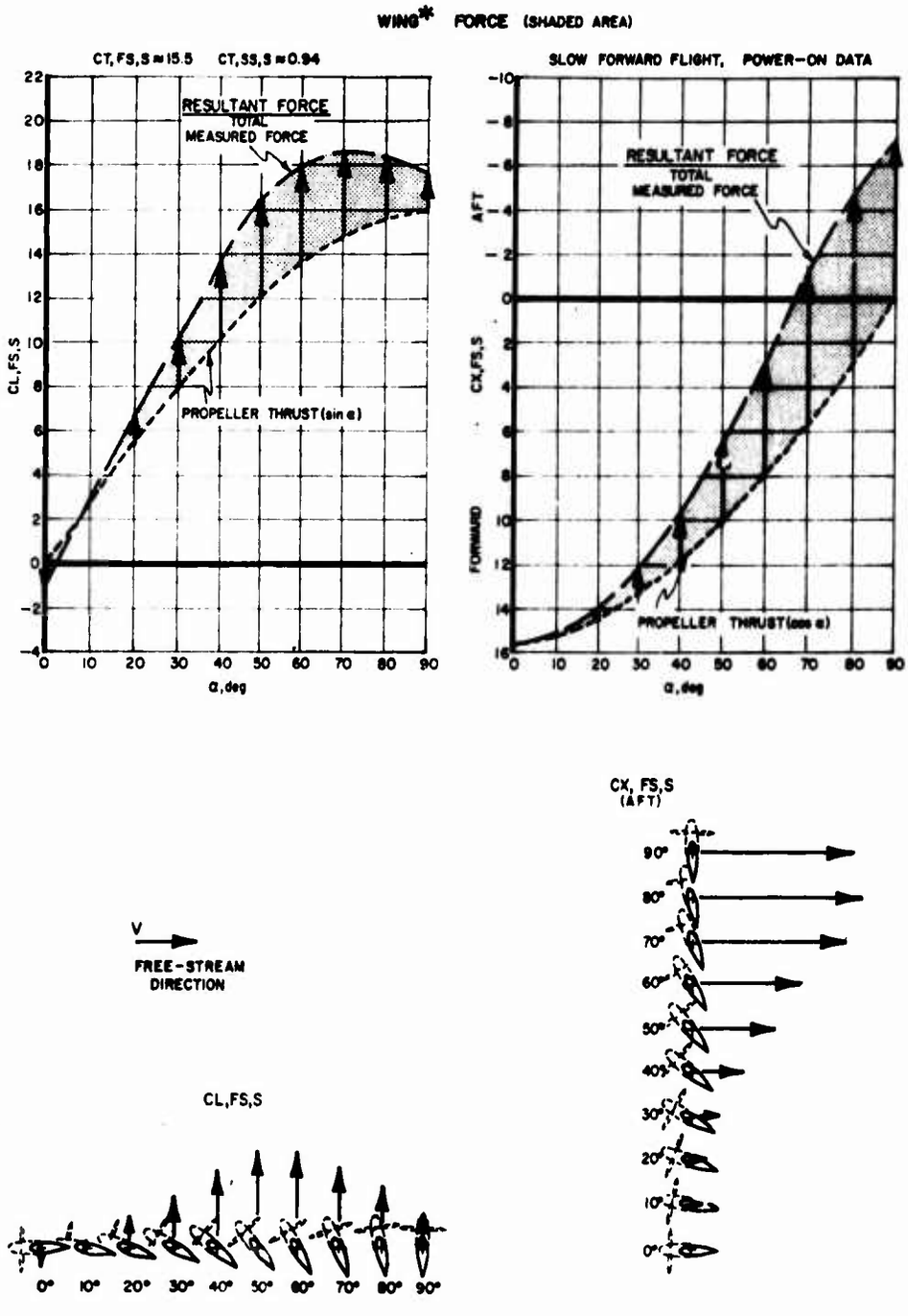

NOTE:
WING* FORCE = RESULTANT FORCE − PROPELLER THRUST FORCE.
WHERE WING* FORCE EXCLUDES ALL PROPELLER THRUST (AXIAL FORCE) BUT INCLUDES ANY EXISTING PROPELLER NORMAL FORCE. WING IS IMMERSED IN A SLIPSTREAM AND SUBJECTED TO A FREE-STREAM FLOW FIELD.

Figure 13b. Depiction of Typical Slow Flight, Lift and Horizontal Force Coefficients Due to Wing* Force.

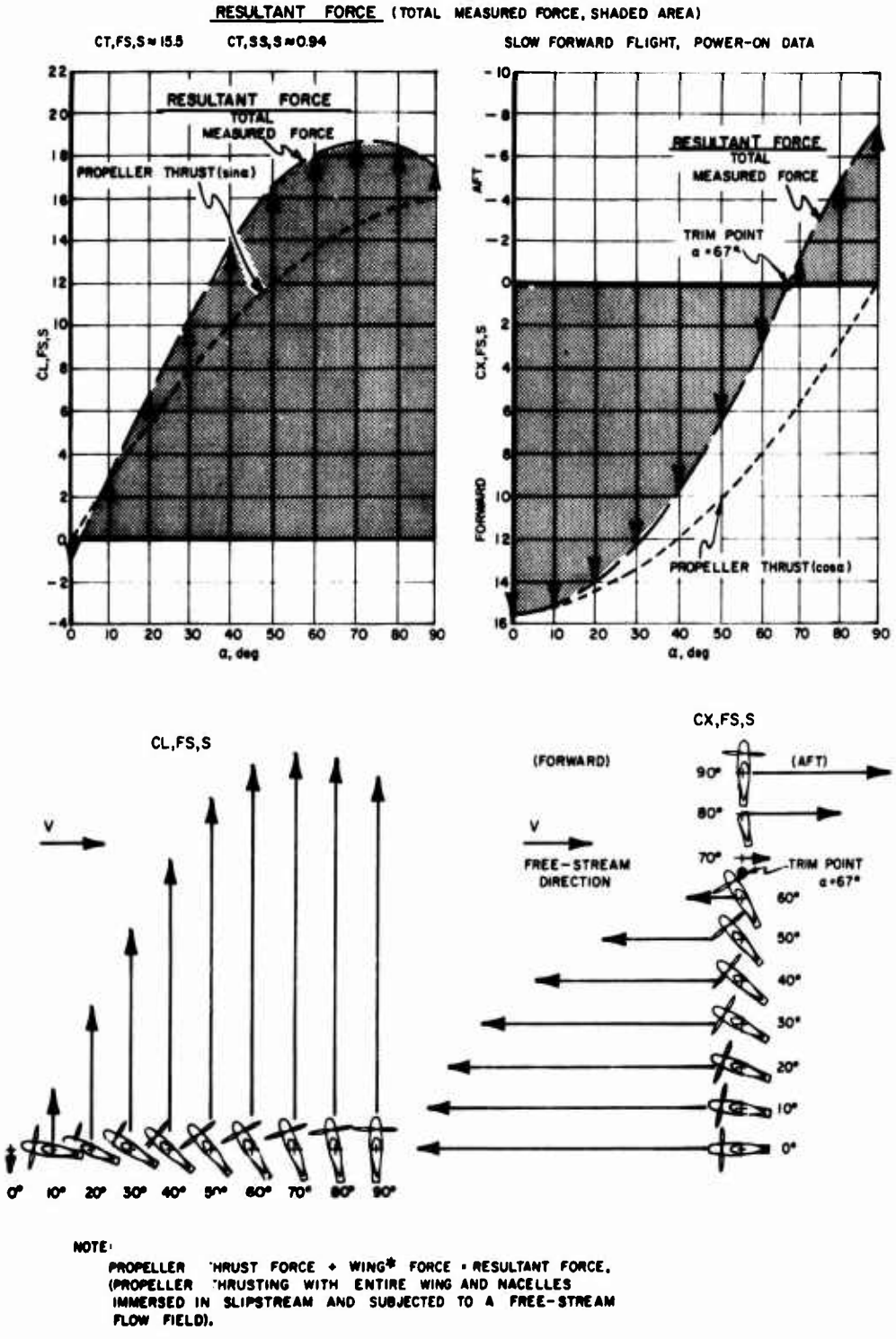

Figure 13c. Depiction of Typical Slow Flight, Lift and Horizontal Force Coefficients due to Resultant Force.

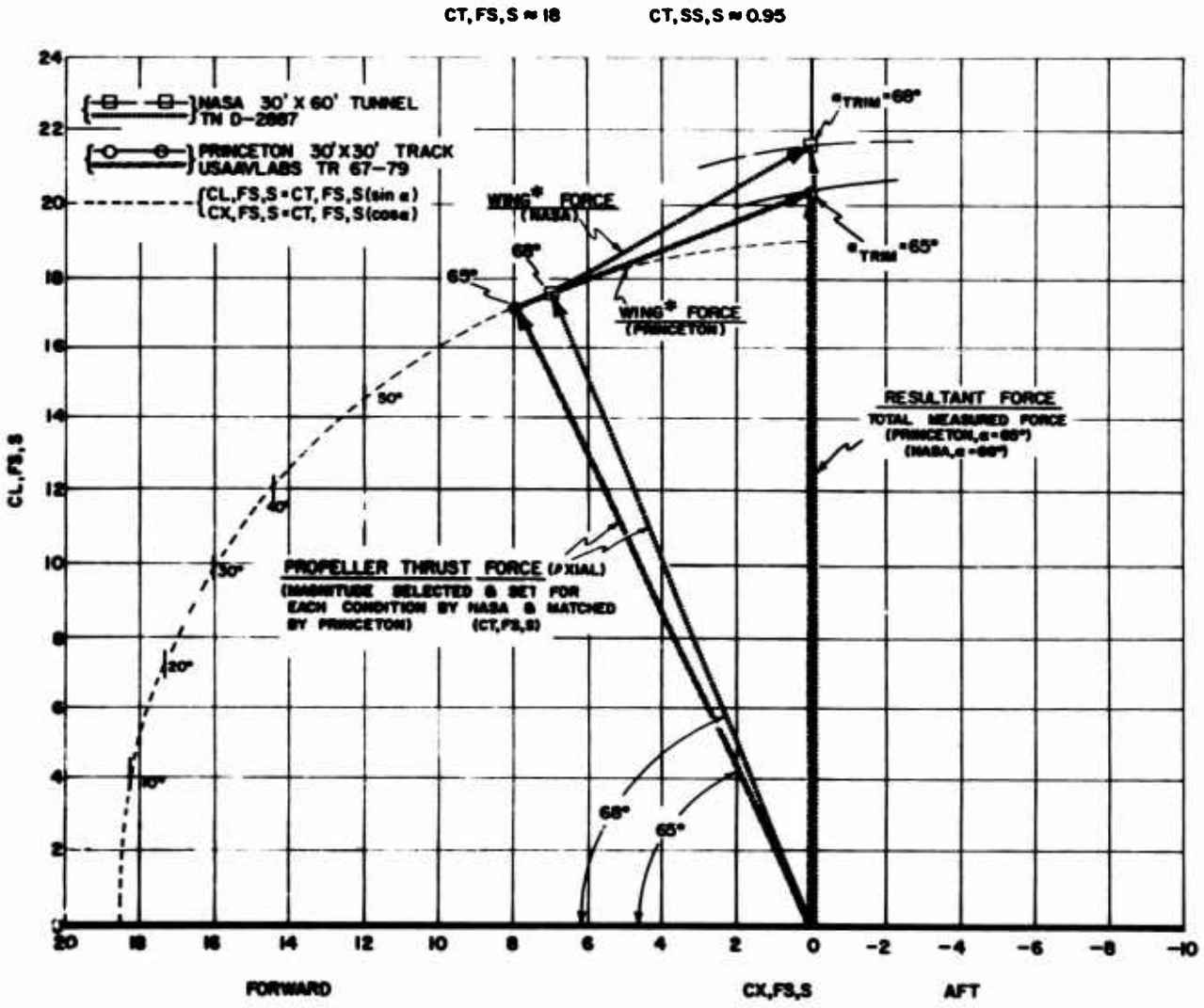

Figure 14. Typical Drag Polar With Force Vector Diagram Showing Trim Conditions.

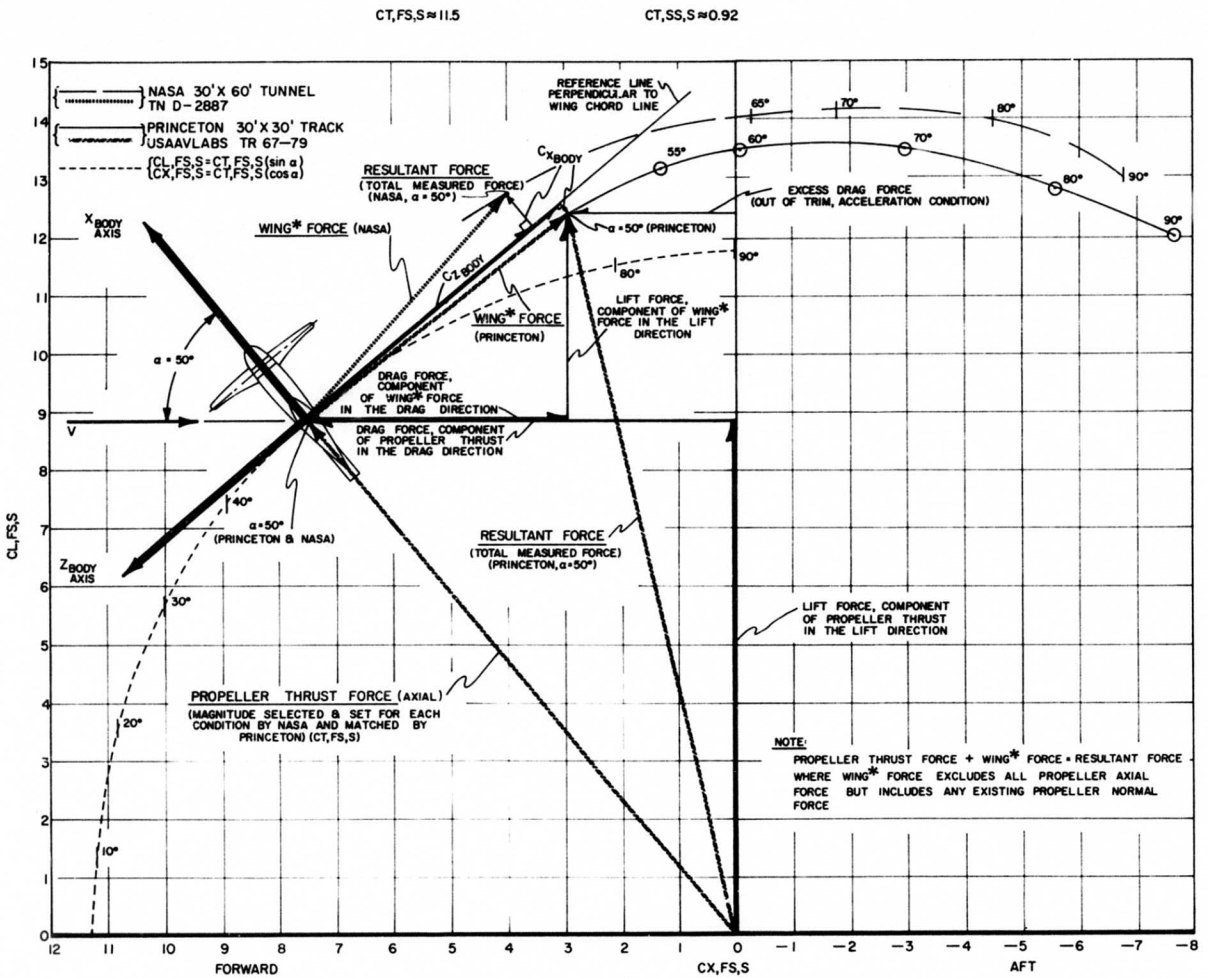

Figure 15. Typical Drag Polar With Force Vector Diagram Showing Out-of-Trim Conditions.

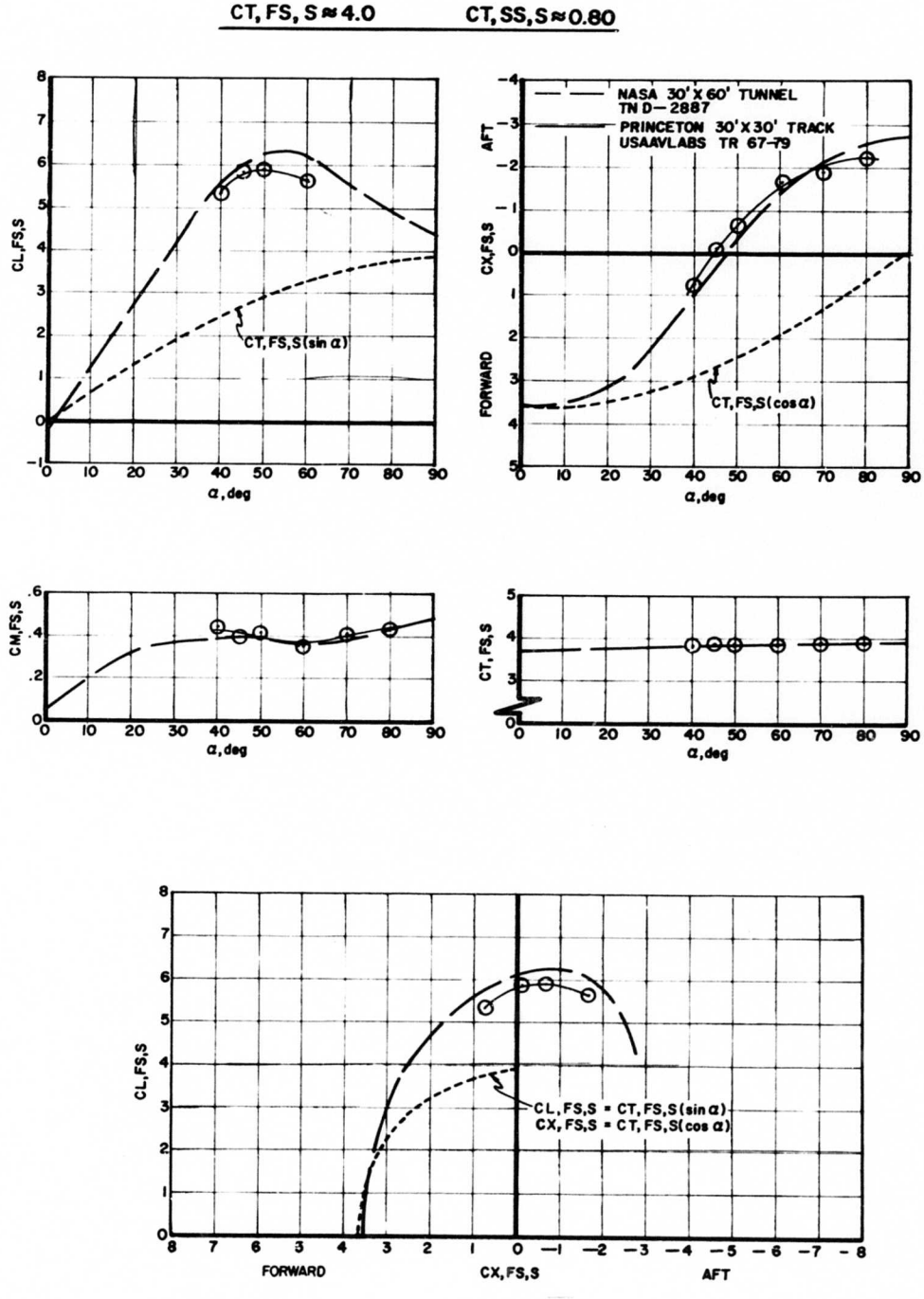

Figure 16a. Comparison of Data From References 1 and 2 for CT,SS,S ≈ 0.8.

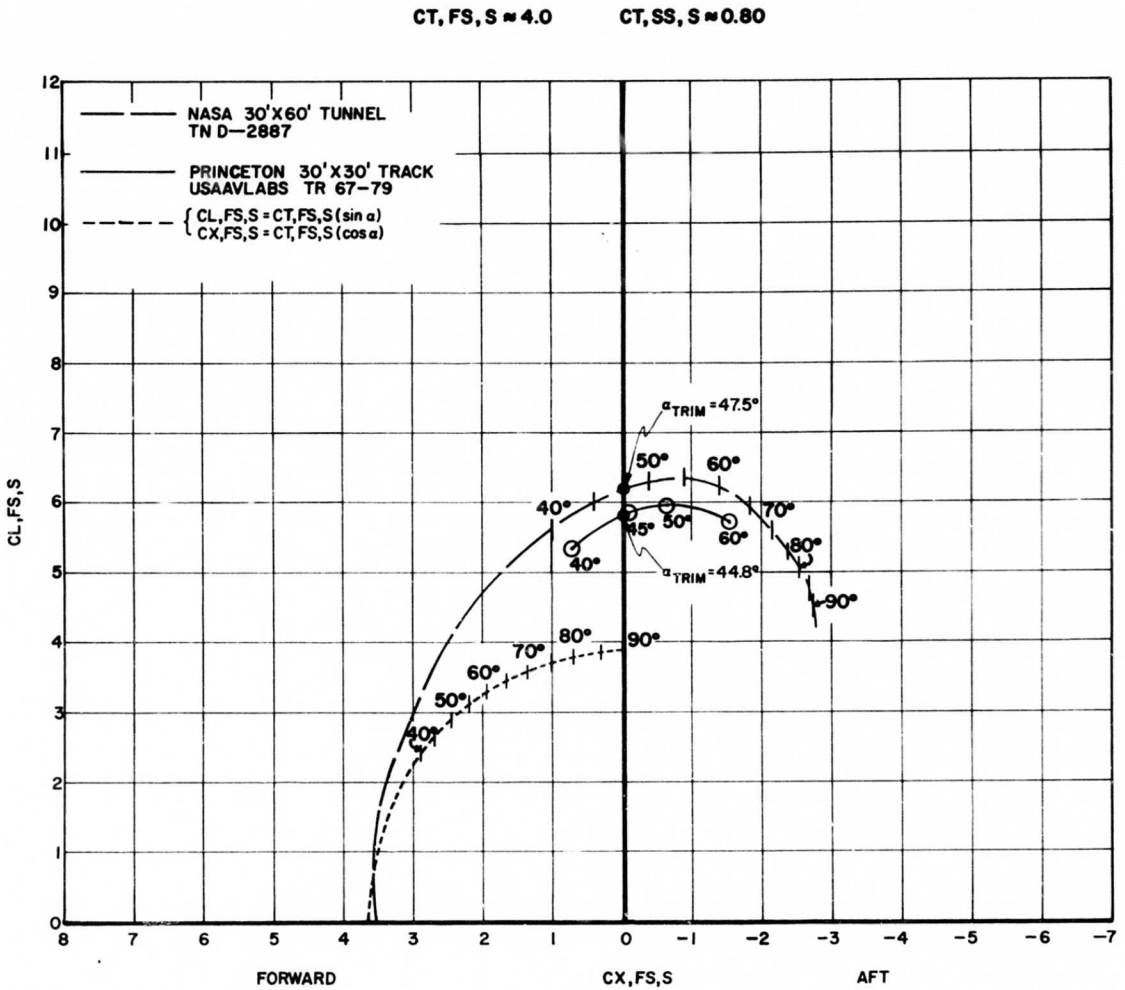

Figure 16b. Drag Polar Comparison of Data From References 1 and 2 for CT,SS,S ≈ 0.8.

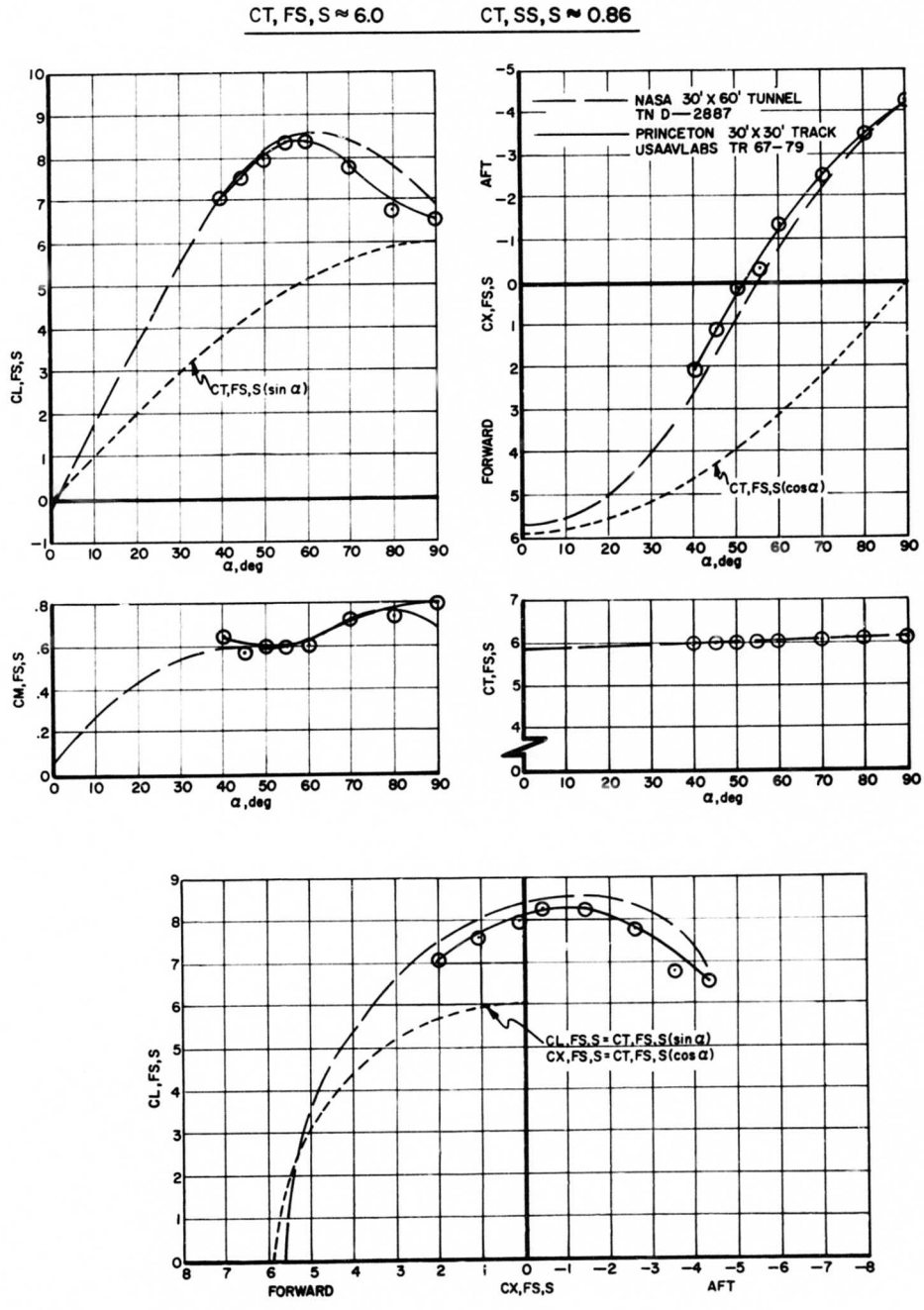

Figure 17a. Comparison of Data From References 1 and 2 for CT,SS,S ≈ 0.86.

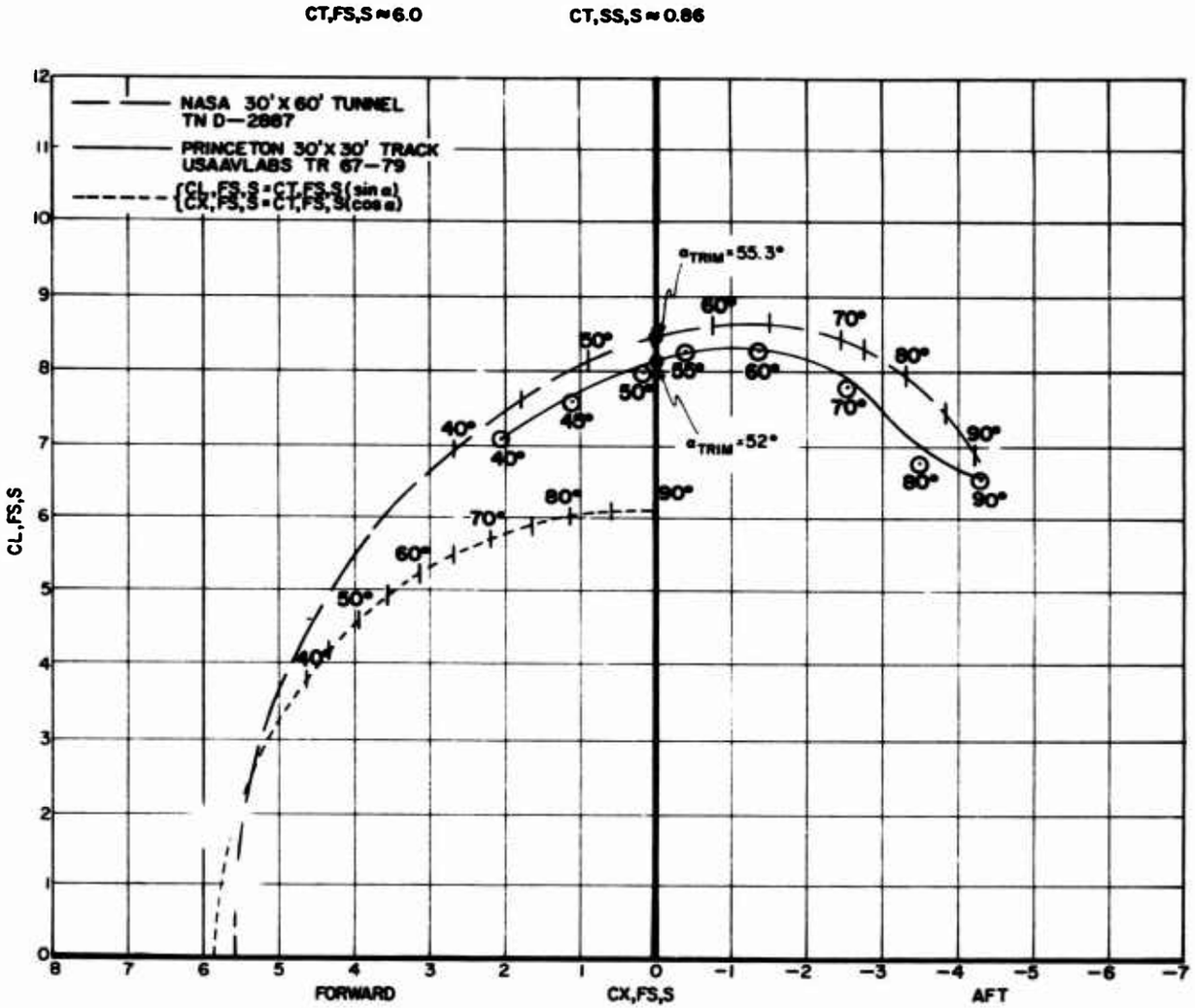

Figure 17b. Drag Polar Comparison of Data From References 1 and 2 for CT,SS,S ≈ 0.86.

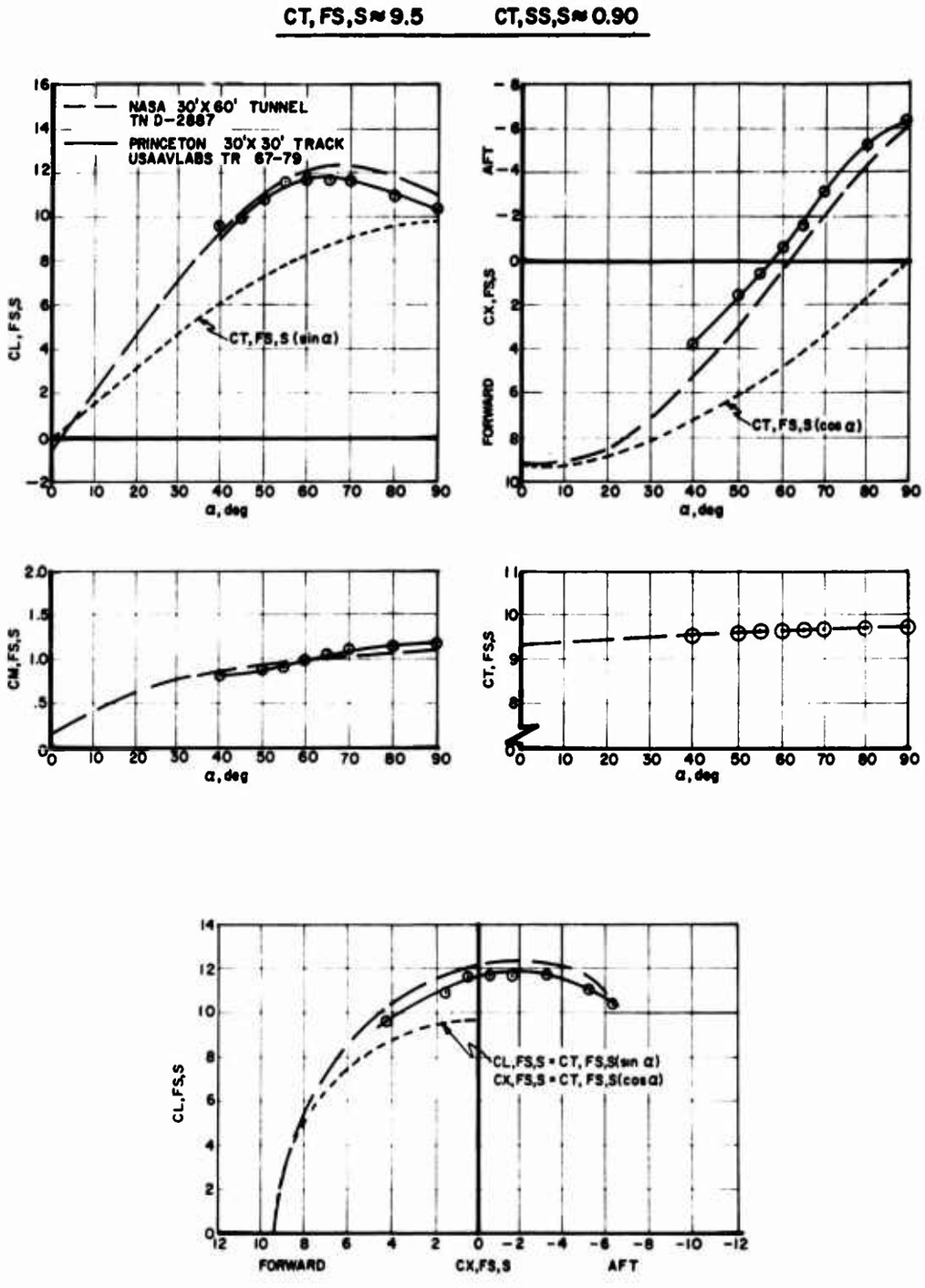

Figure 18a. Comparison of Data From References 1 and 2 for CT,SS,S ≈ 0.90.

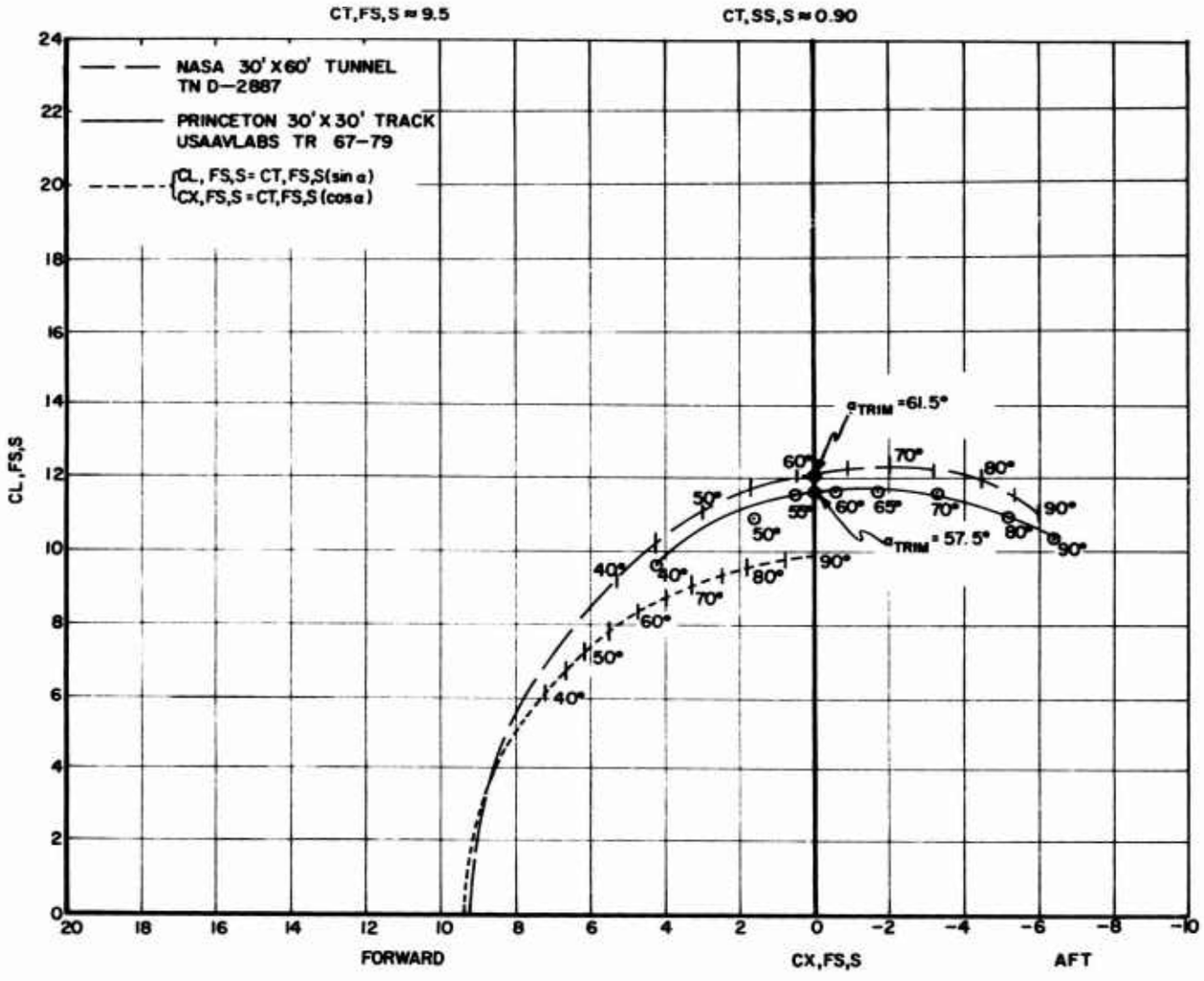

Figure 18b. Drag Polar Comparison of Data From References 1 and 2 for CT,SS,S ≈ 0.90.

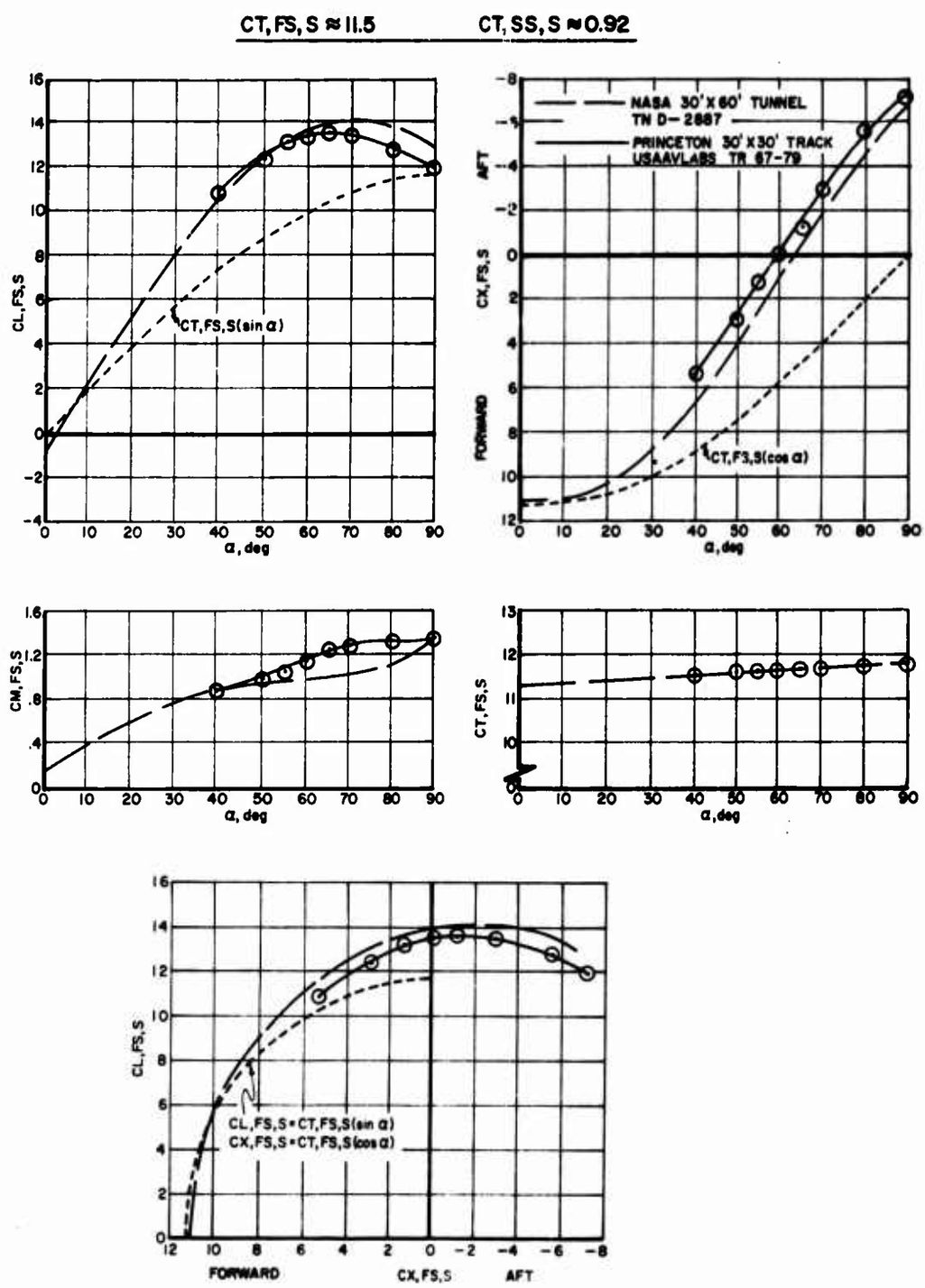

Figure 19a. Comparison of Data From References 1 and 2 for CT, SS, S ≈ 0.92.

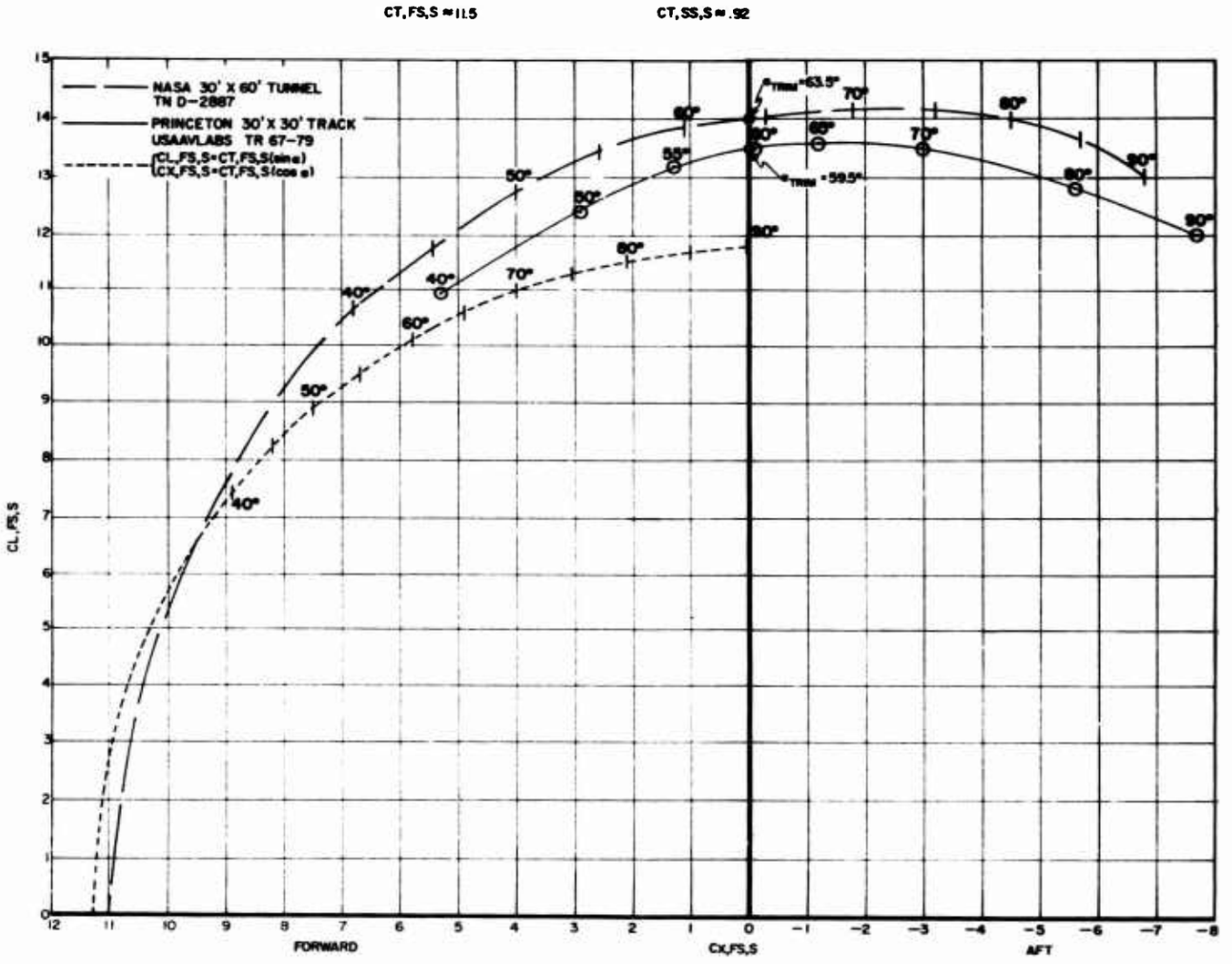

Figure 19b. Drag Polar Comparison of Data From References 1 and 2 for CT.SS,S ≈ 0.92.

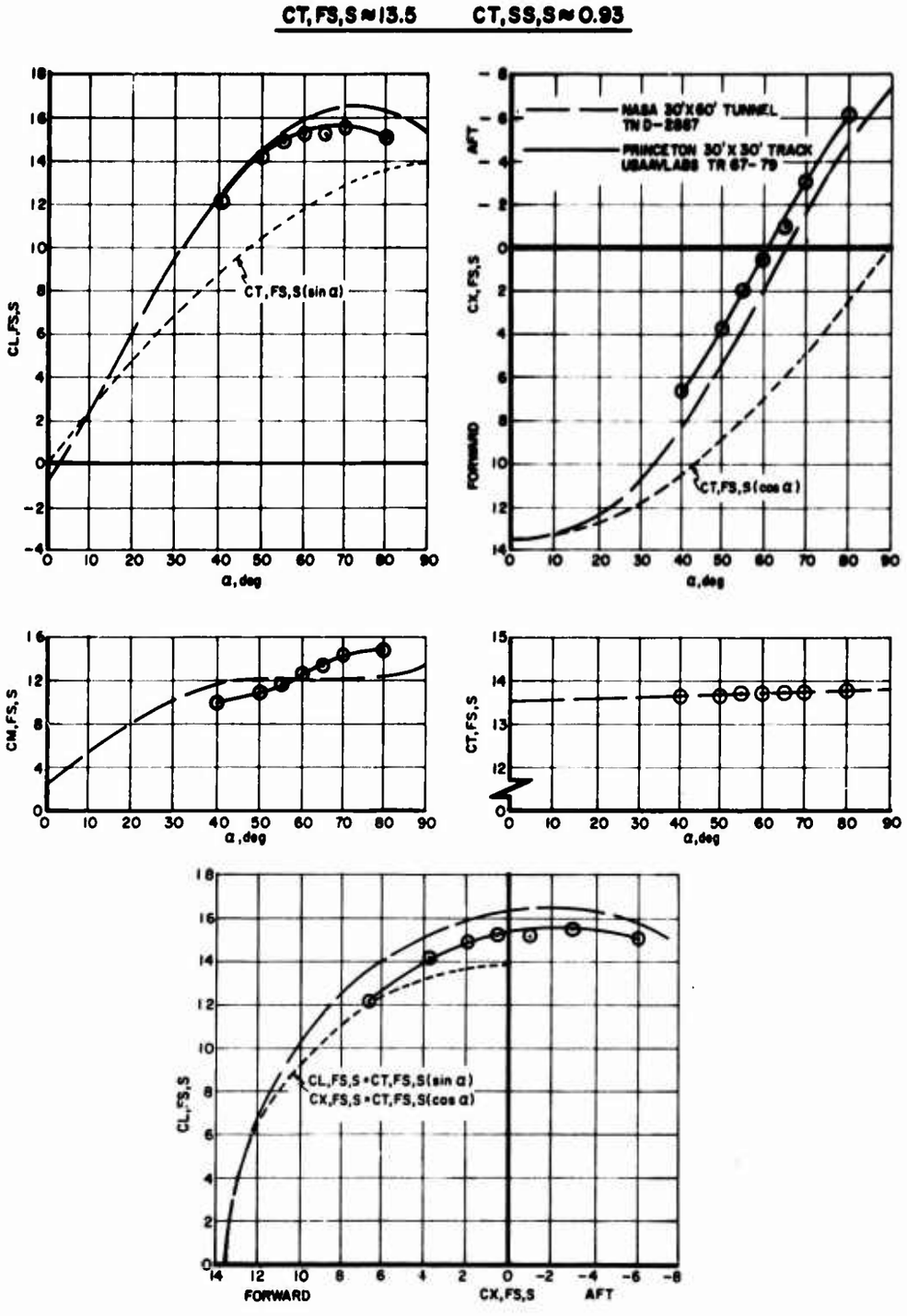

Figure 20a. Comparison of Data From References 1 and 2 for CT,SS,S ≈ 0.93.

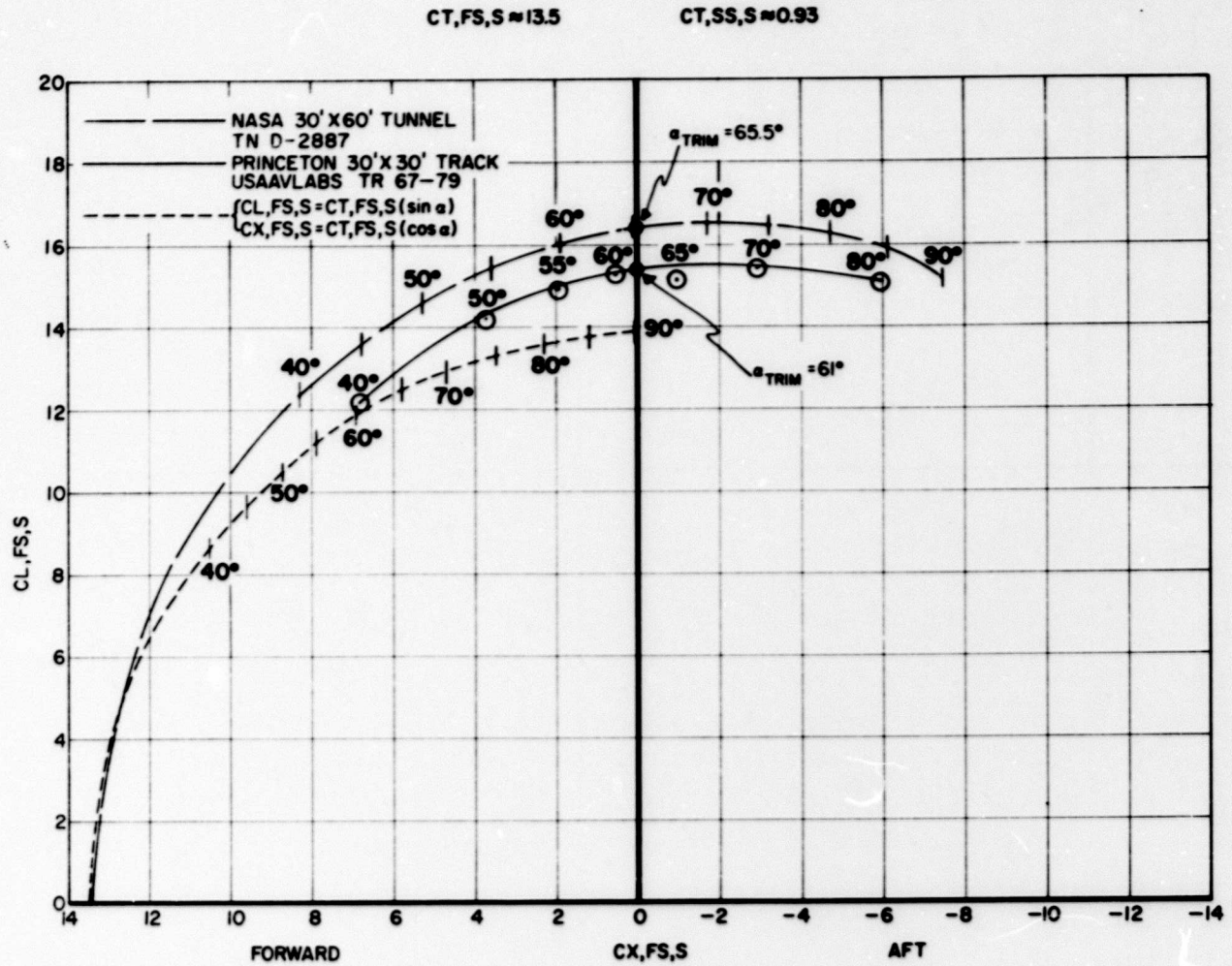

Figure 20b. Drag Polar Comparison of Data From References 1 and 2 for CT,SS,S ≈ 0.93.

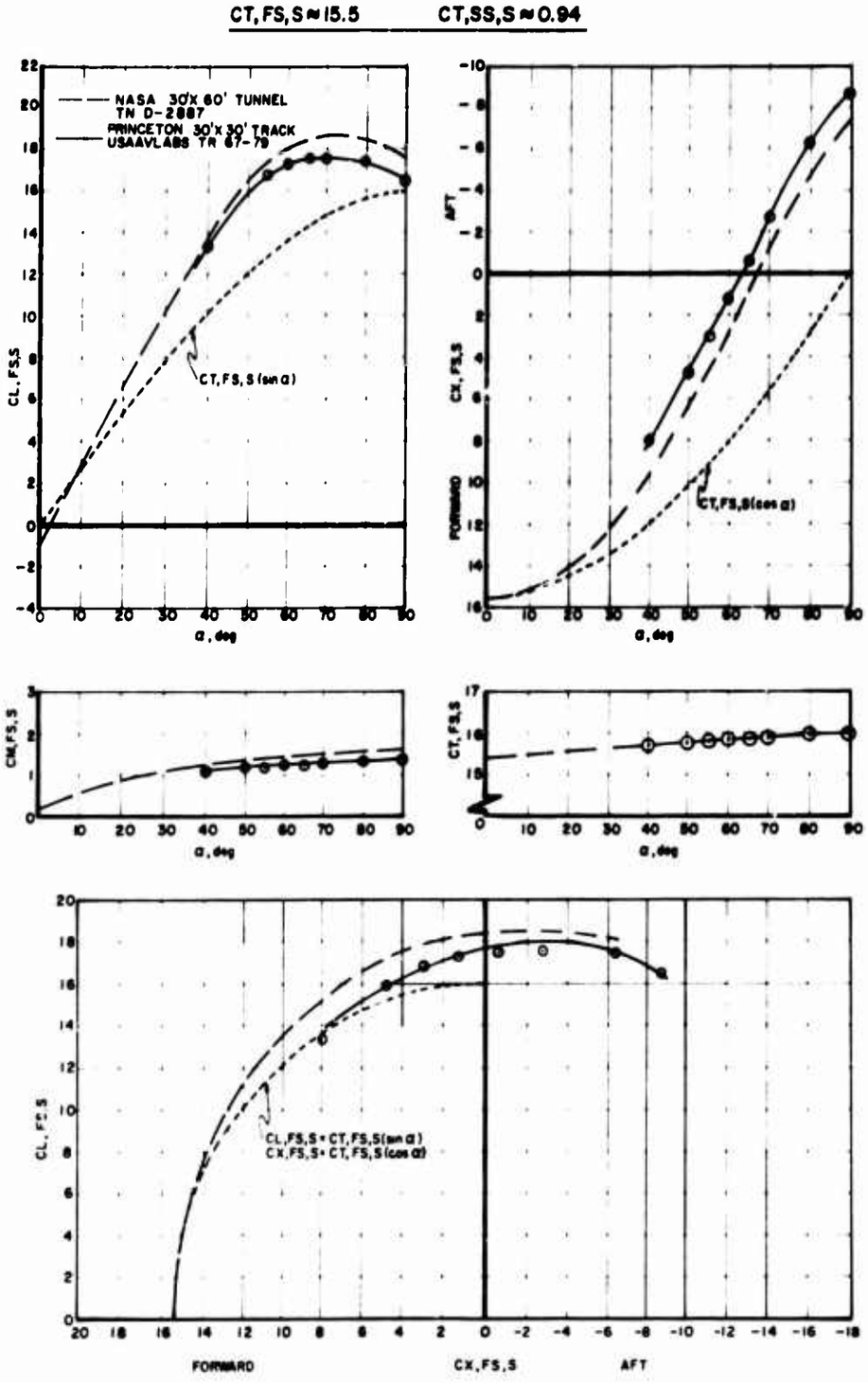

Figure 21a. Comparison of Data From References 1 and 2 for CT,SS,S ≈ 0.94.

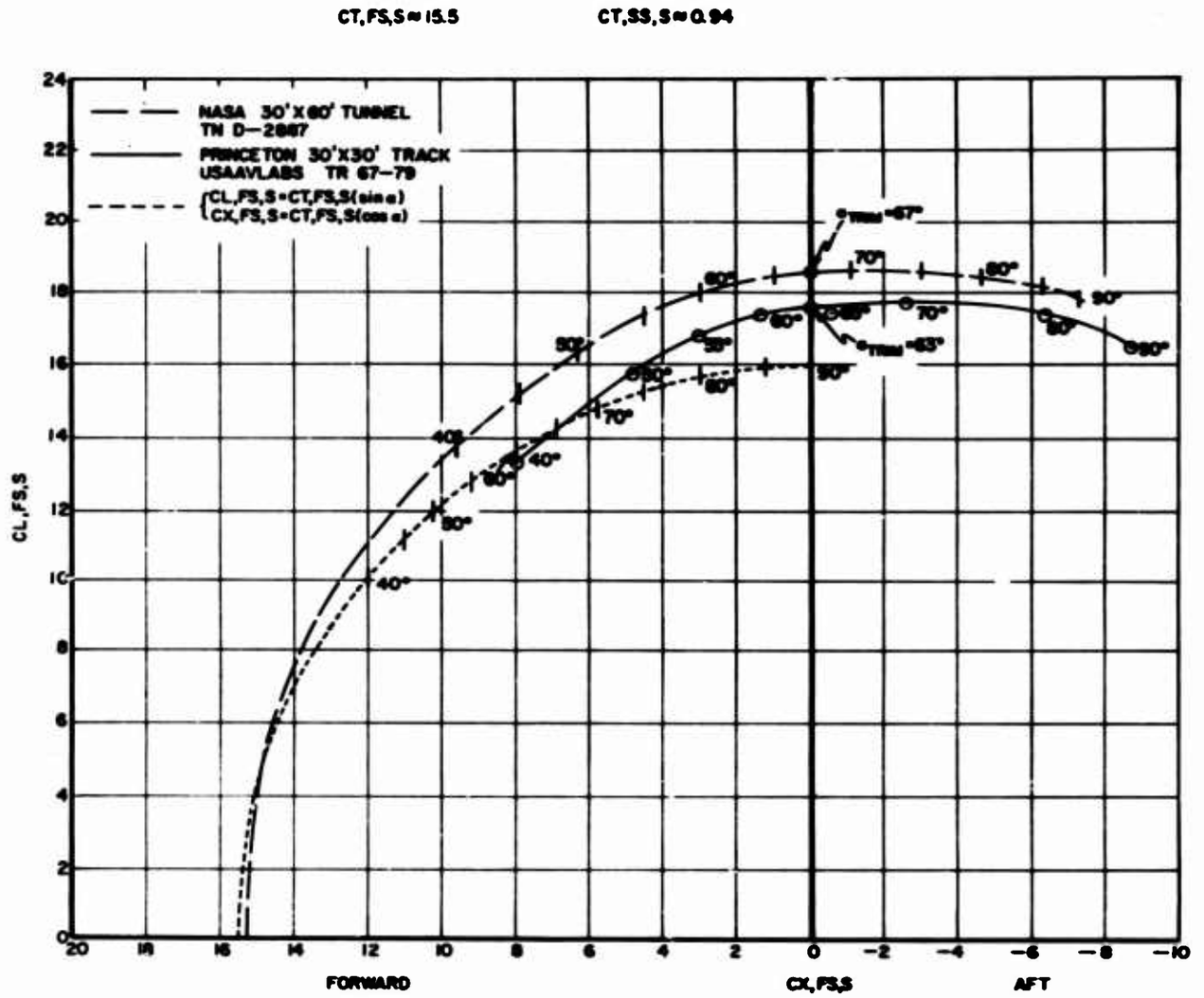

Figure 21b. Drag Polar Comparison of Data From References 1 and 2 for CT,SS.S ≈ 0.94.

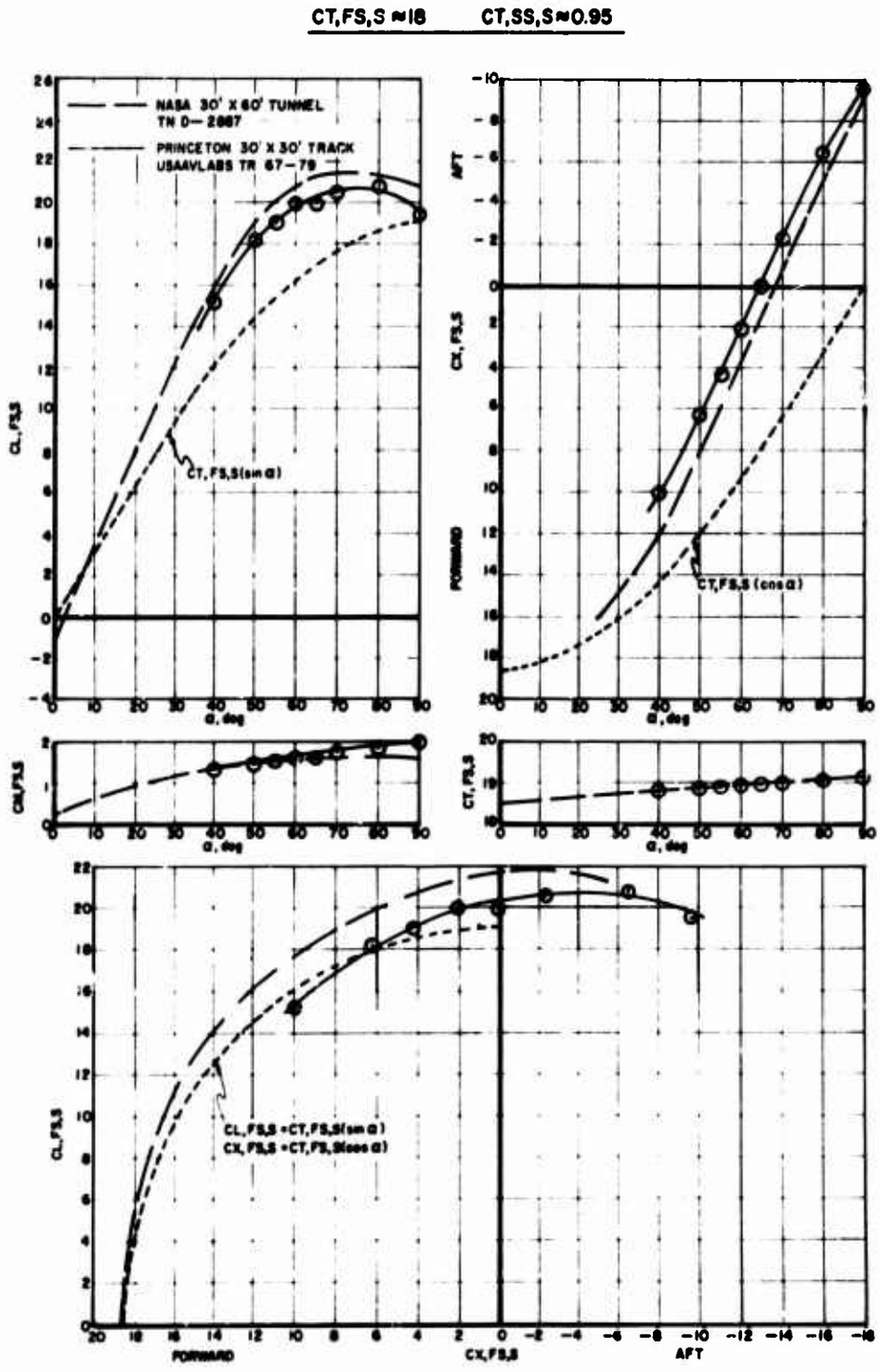

Figure 22a. Comparison of Data From References 1 and 2 for CT,SS,S ≈ 0.95.

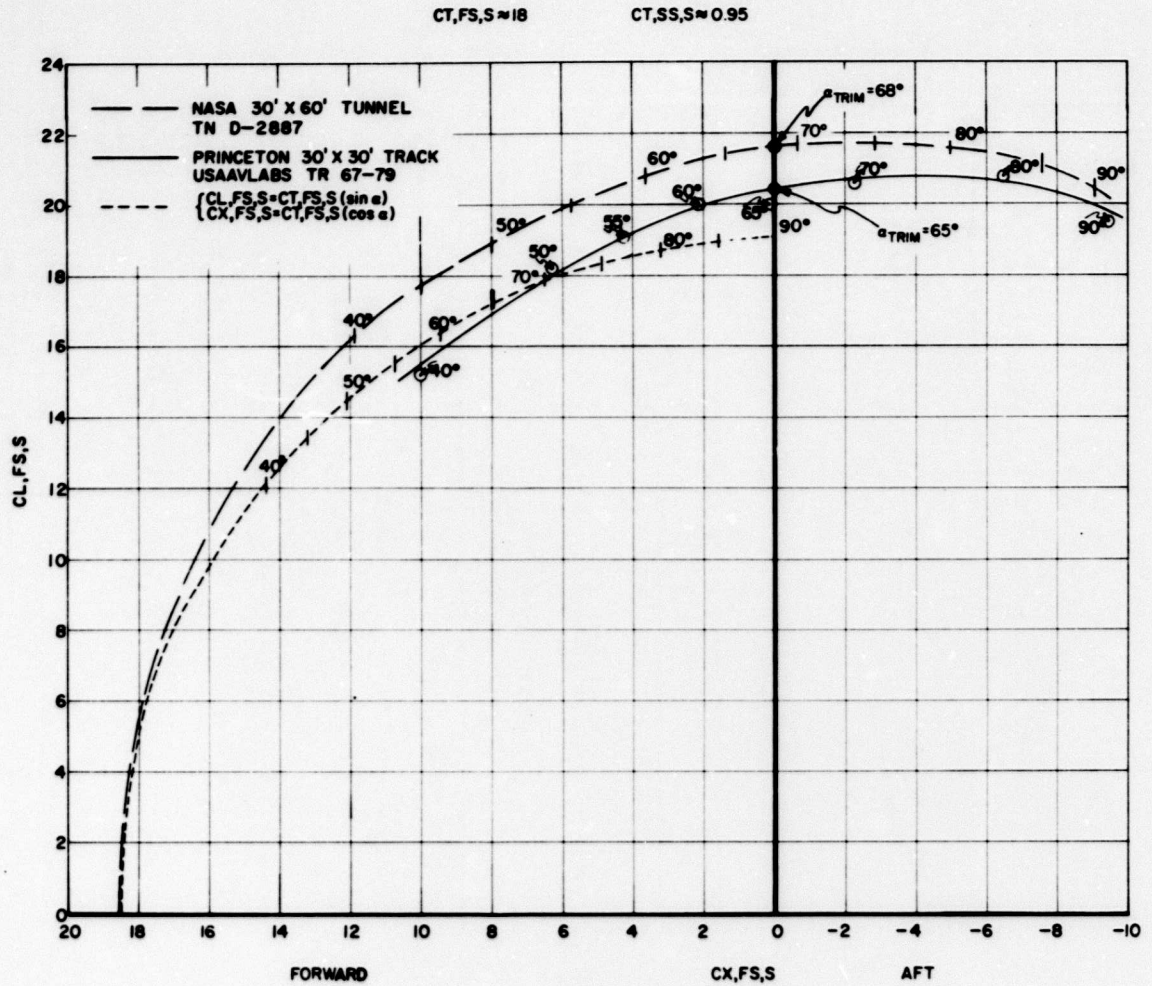

Figure 22b. Drag Polar Comparison of Data From References 1 and 2 for CT,SS,S ≈ 0.95.

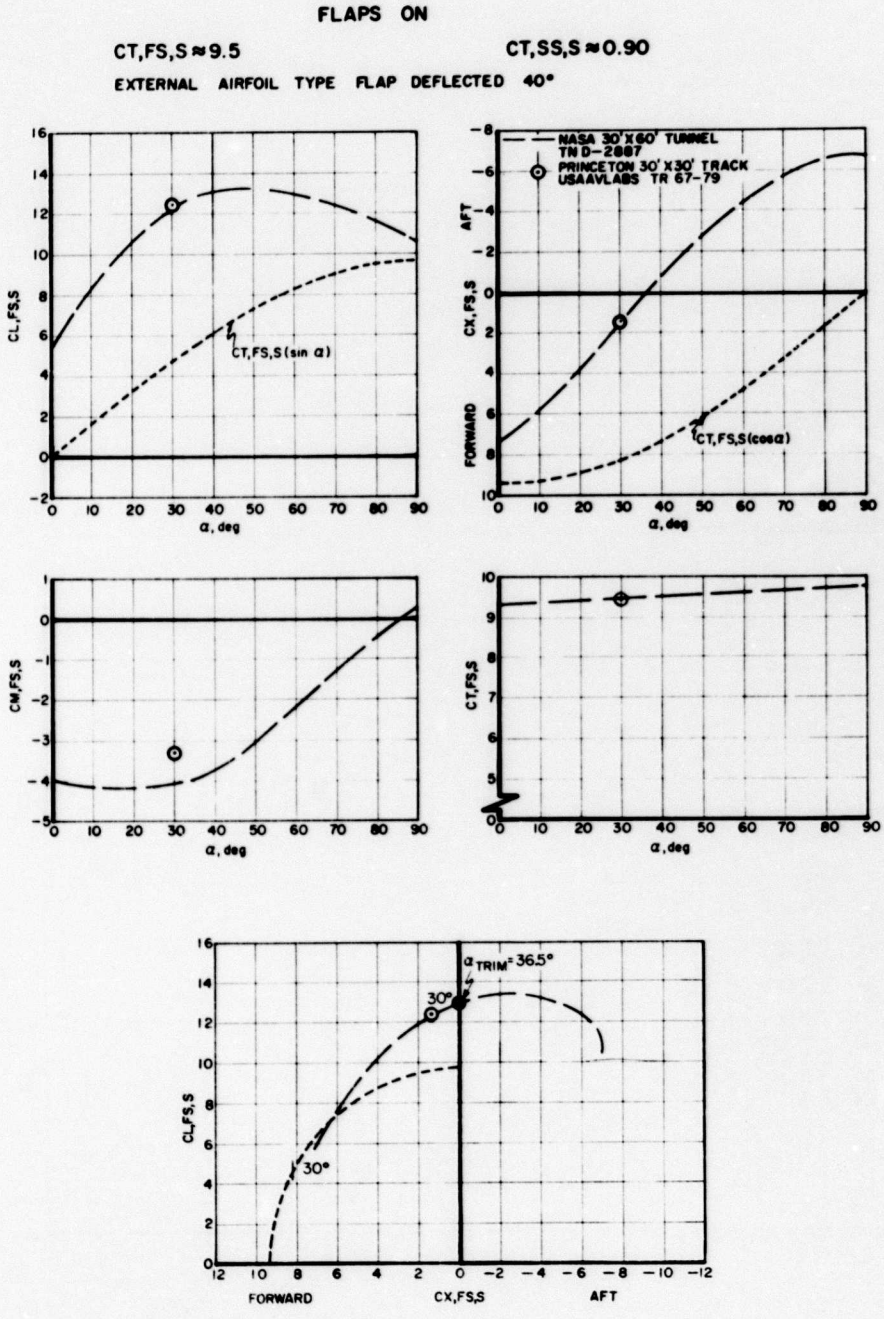

Figure 23a. Comparison of Data From References 1 and 2 for CT,SS,S ≈ 0.90. Flaps on.

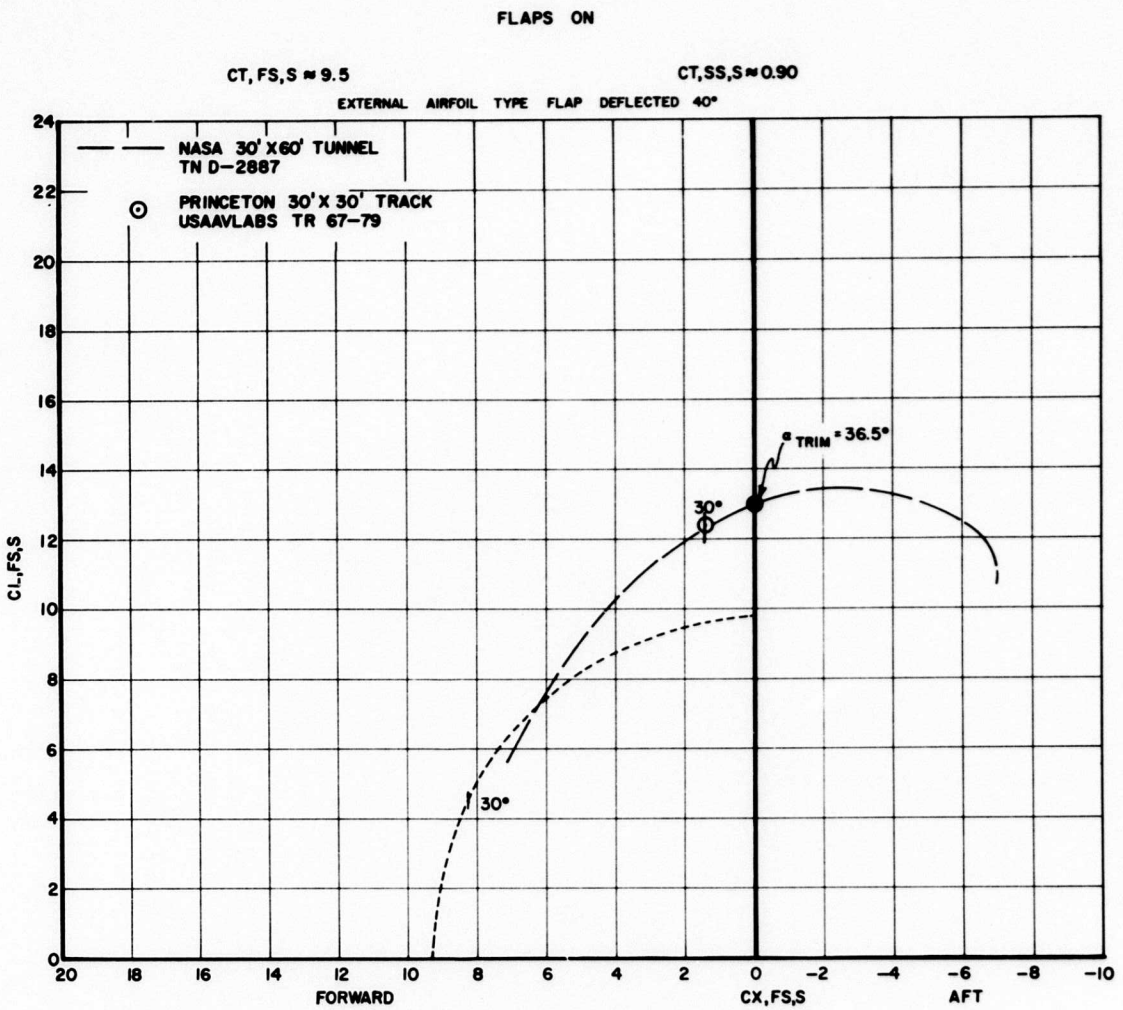

Figure 23b. Drag Polar Comparison of Data From References 1 and 2 for CT,SS,S ≈ 0.90. Flaps on.

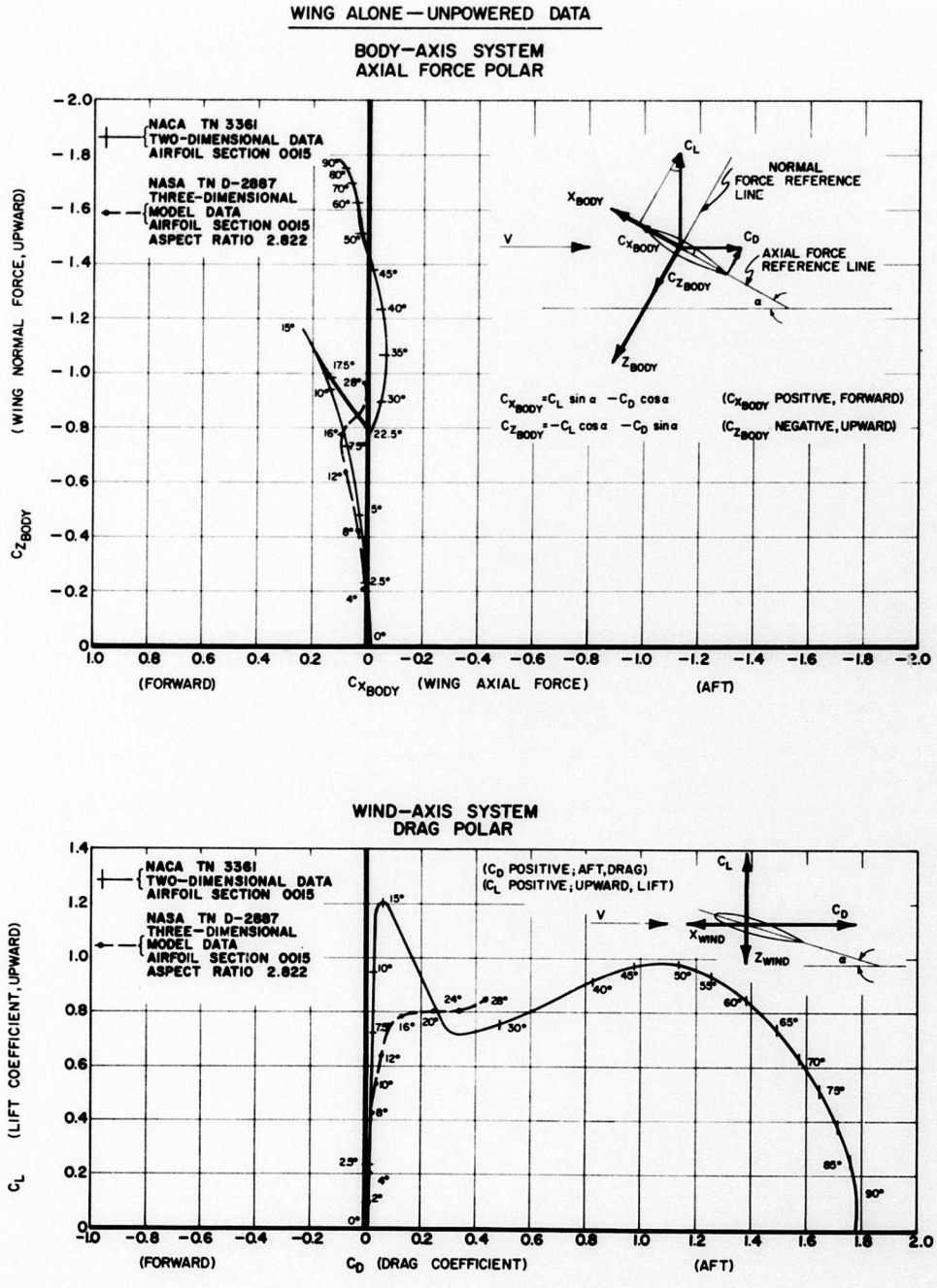

Figure 24. Comparison of Wing Alone (Unpowered) Aerodynamic Data Plotted in Wind-Axes and Body-Axes Polar Diagrams.

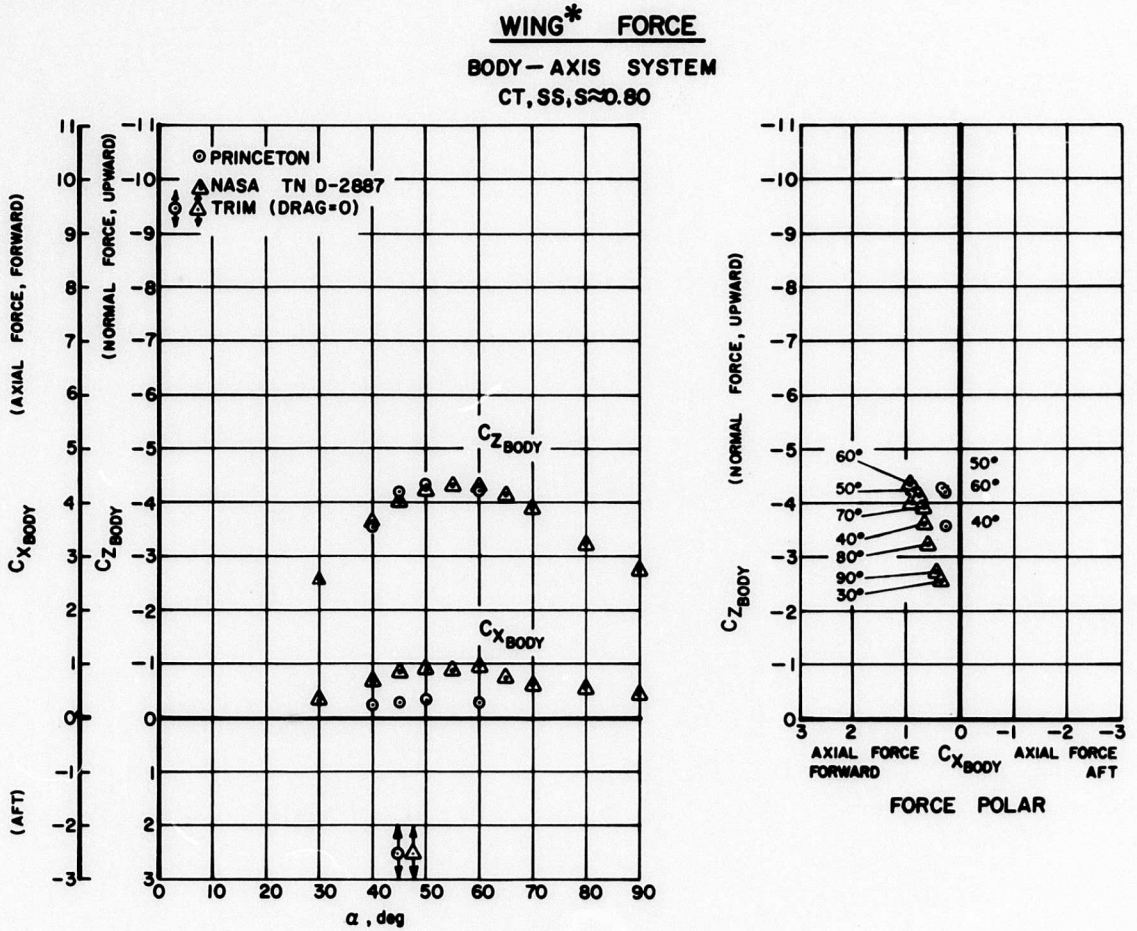

Figure 25a. Comparison of Wing* Data Plotted in Body-Axis System Force Coefficients CT,SS,S ≈ 0.80.

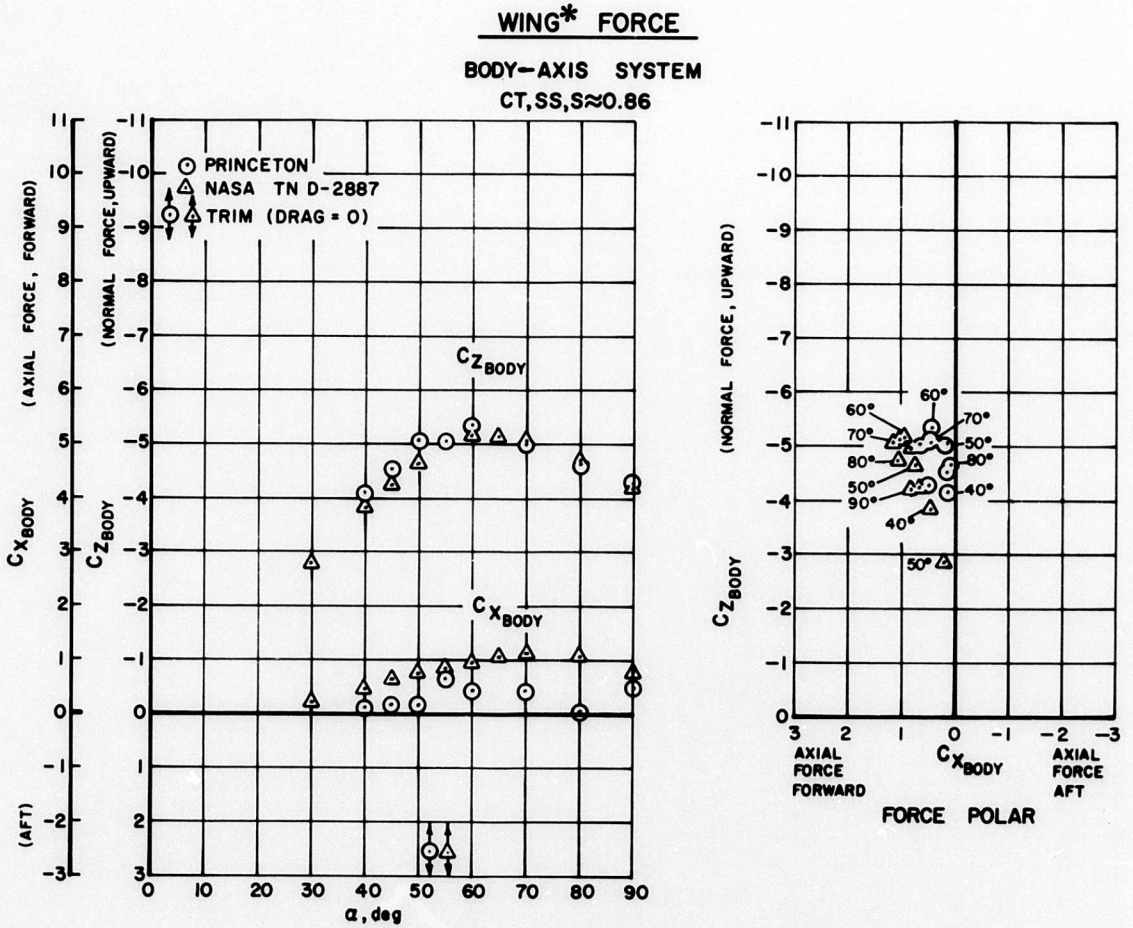

Figure 25b. Comparison of Wing* Data Plotted in Body-Axis System Force Coefficients CT,SS,S ≈ 0.86.

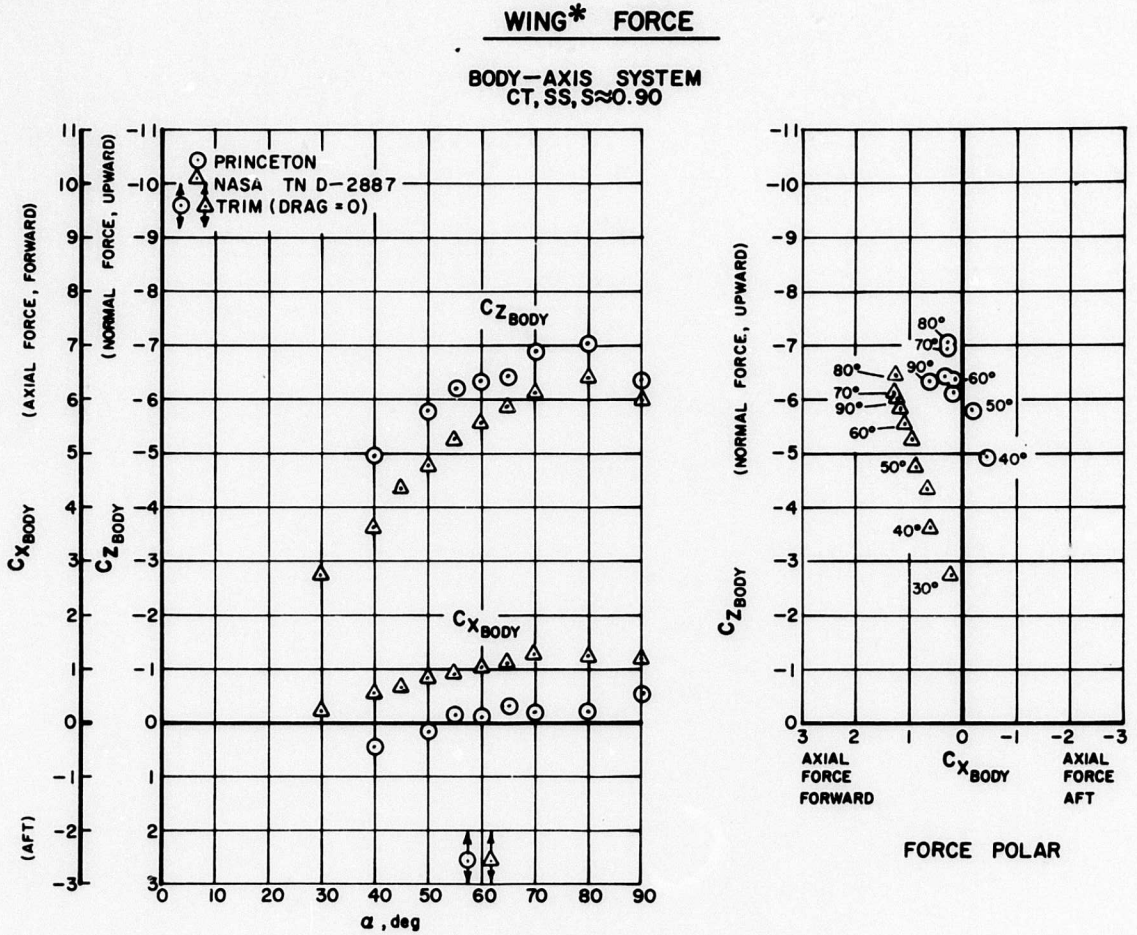

Figure 25c. Comparison of Wing* Data Plotted in Body-Axis System Force Coefficients CT,SS,S ≈ 0.90.

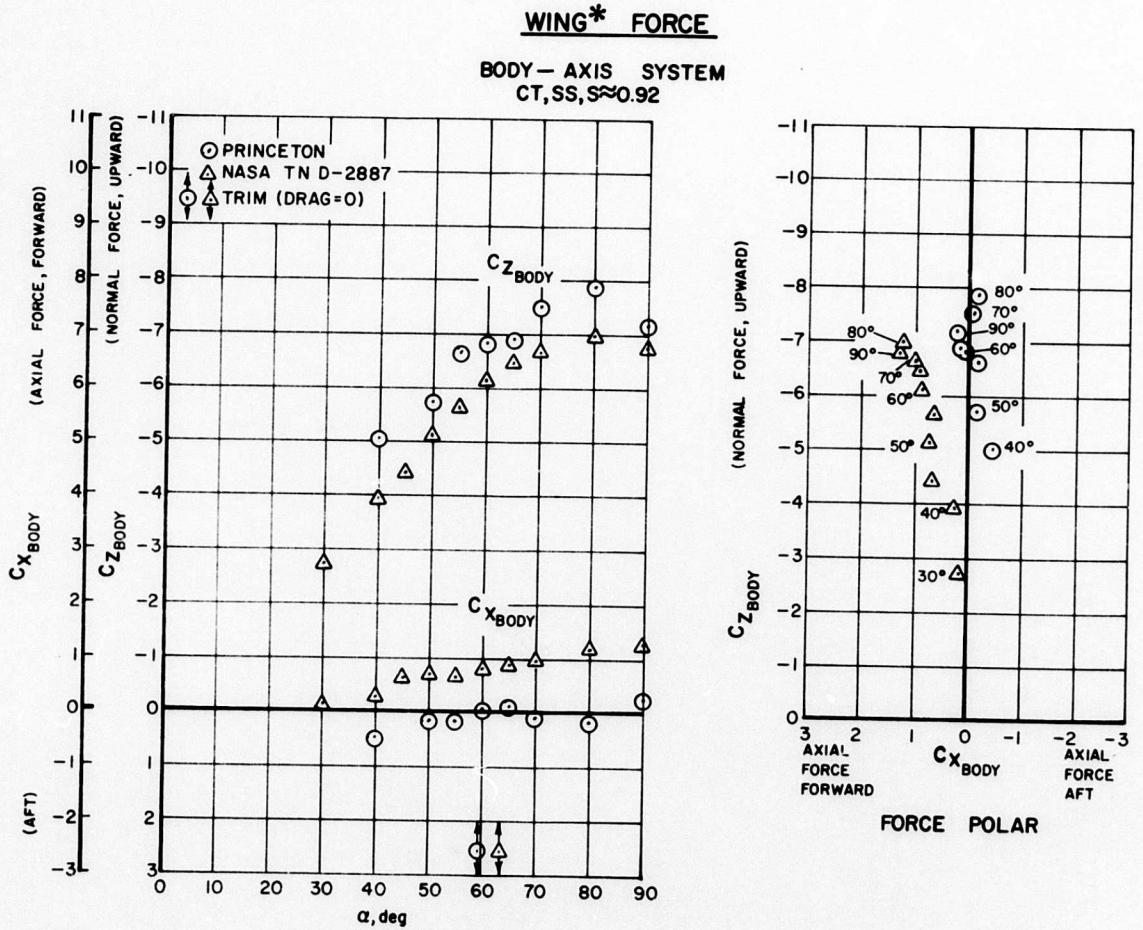

Figure 25d. Comparison of Wing* Data Plotted in Body-Axis System Force Coefficients CT,SS,S ≈ 0.92.

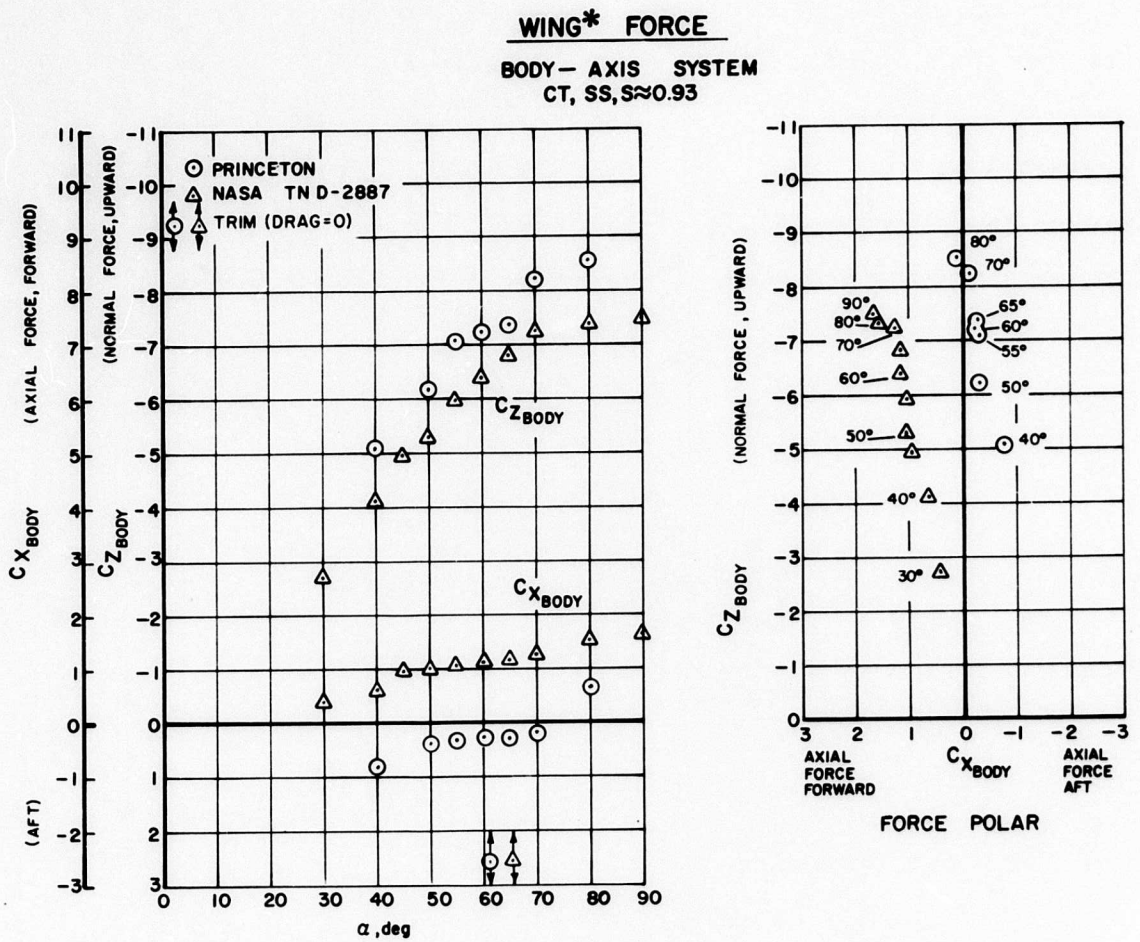

Figure 25e. Comparison of Wing* Data Plotted in Body-Axis System Force Coefficients CT,SS,S ≈ 0.93.

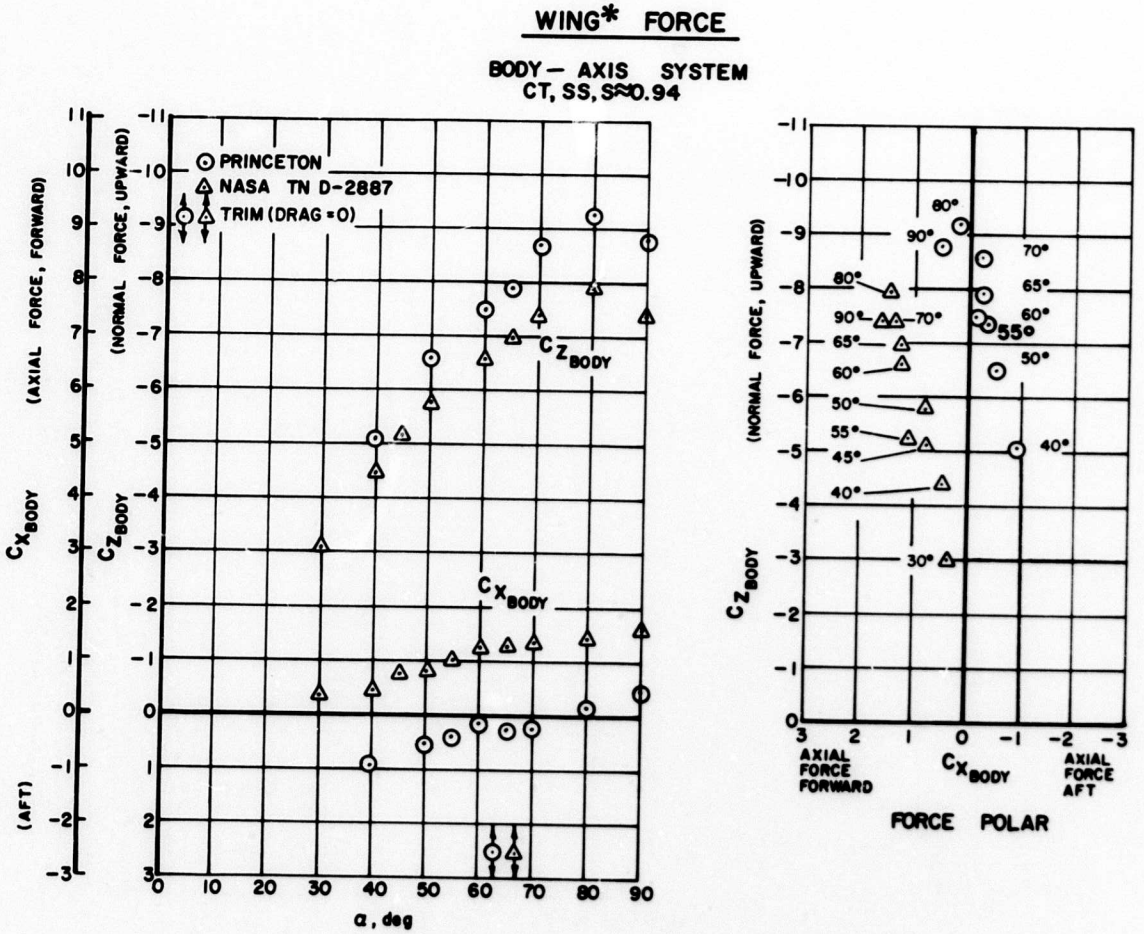

Figure 25f. Comparison of Wing* Data Plotted in Body-Axis System Force Coefficients CT,SS,S ≈ 0.94.

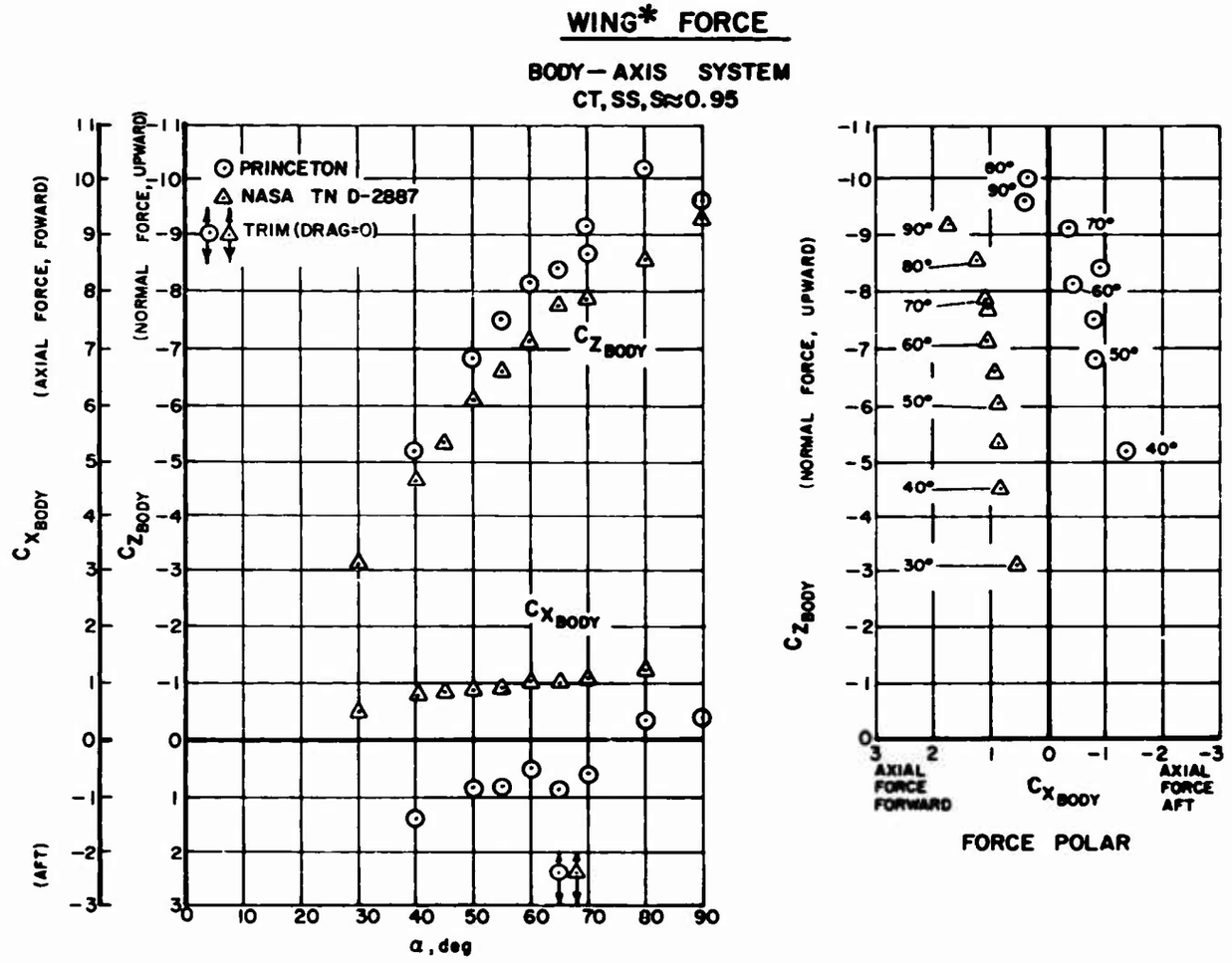

Figure 25g. Comparison of Wing* Data Plotted in Body-Axis System Force Coefficients CT,SS,S ≈ 0.95.

LITERATURE CITED

1. Grunwald, Kalman J., EXPERIMENTAL STUDY OF WIND-TUNNEL WALL EFFECTS AND WALL CORRECTIONS FOR A GENERAL-RESEARCH V/STOL TILT-WING MODEL WITH FLAP; NASA TN D-2887, Washington, D. C., July 1965.

2. Traybar, Joseph J., AERODYNAMIC CHARACTERISTICS OF A GENERAL TILT-WING/PROPELLER MODEL TESTED AT SLOW SPEEDS AND HIGH ANGLES OF ATTACK; USAAVLABS Technical Report 67-79, U. S. Army Aviation Materiel Laboratories, Fort Eustis, Virginia, February 1968, AD 671666.

3. Kuhn, Richard E., and Draper, John W., INVESTIGATION OF THE AERODYNAMIC CHARACTERISTICS OF A MODEL WING-PROPELLER COMBINATION AND OF THE WING AND PROPELLER SEPARATELY AT ANGLES OF ATTACK UP TO 90°; NACA Report No. 1263, Washington, D. C., 1956.

4. Abbott, Ira H., and Von Doenhoff, Albert E., THEORY OF WING SECTIONS - INCLUDING A SUMMARY OF AIRFOIL DATA; Dover Publications, Inc., New York, June 1958.

5. DeFrance, Smith J., THE NACA FULL-SCALE WIND TUNNEL; NACA Report No. 459, Langley Memorial Aeronautical Laboratory, National Advisory Committee for Aeronautics, Langley Field, Virginia, March 13, 1933.

6. Curtiss, H. C., Jr., Putman, W. F., and Traybar, J. J., GENERAL DESCRIPTION OF THE PRINCETON DYNAMIC MODEL TRACK; USAAVLABS Technical Report 66-73, U. S. Army Aviation Materiel Laboratories, Fort Eustis, Virginia, November 1966, AD 645883.

7. Critzos, Chris C., Heyson, Harry H., and Boswinkle, Robert W., Jr., AERODYNAMIC CHARACTERISTICS OF NACA 0012 AIRFOIL SECTION AT ANGLES OF ATTACK FROM 0° TO 180°; NACA TN 3361, Langley Aeronautical Laboratory, Langley Field, Virginia, January 1955.

8. Martinov, A. K., PRACTICAL AERODYNAMICS, New York, The MacMillan Company, 1965.

BLANK PAGE

Unclassified

Security Classification

DOCUMENT CONTROL DATA - R & D

(Security classification of title, body of abstract and indexing annotation must be entered when the overall report is classified)

1. ORIGINATING ACTIVITY (Corporate author) Department of Aerospace and Mechanical Sciences Princeton University Princeton, New Jersey	2a. REPORT SECURITY CLASSIFICATION Unclassified 2b. GROUP

3. REPORT TITLE

Analysis and Comparison of Aerodynamic Data Obtained in a Large Wind Tunnel and a Moving-Model/Track Facility for a General Tilt-Wing/Propeller VTOL Configuration

4. DESCRIPTIVE NOTES (Type of report and inclusive dates)

Final Data Report

5. AUTHOR(S) (First name, middle initial, last name)

Joseph J. Traybar

6. REPORT DATE September 1969	7a. TOTAL NO. OF PAGES 77	7b. NO. OF REFS 8
8a. CONTRACT OR GRANT NO. DAAJ02-67-C-0025 b. PROJECT NO. Task 1F162204A14233 c. d.	9a. ORIGINATOR'S REPORT NUMBER(S) USAAVLABS Technical Report 69-74 9b. OTHER REPORT NO(S) (Any other numbers that may be assigned this report) Aerospace Sciences Report 872	

10. DISTRIBUTION STATEMENT

This document is subject to special export controls, and each transmittal to foreign governments or foreign nationals may be made only with prior approval of US Army Aviation Materiel Laboratories, Fort Eustis, Virginia 23604.

11. SUPPLEMENTARY NOTES	12. SPONSORING MILITARY ACTIVITY US Army Aviation Materiel Laboratories Fort Eustis, Virginia 23604

13. ABSTRACT

A comparison and analysis was conducted of the aerodynamic characteristic data obtained in a large wind tunnel and a moving-model/track facility for a general research tilt-wing/propeller VTOL configuration. The two facilities were the Langley 30-by-60 Full-Scale Wind Tunnel and the Princeton Dynamic Model Track. The experiments included test conditions corresponding to free-stream velocities from transition flight to hovering and wing angles of attack up to 90 degrees. The experimental data obtained from both facilities are compared in several ways in a series of graphs plotted in coefficient form for the range of slipstream thrust coefficients of 0.80 to 0.95. The comparisons and analyses first are made on the basis of wind-axes force and moment coefficients and drag polars. An additional comparison is made of the wing forces by using body-axes force coefficients and polars.

DD FORM 1 NOV 68 1473 REPLACES DD FORM 1473, 1 JAN 64, WHICH IS OBSOLETE FOR ARMY USE.

Unclassified

Security Classification

Unclassified

Security Classification

14. KEY WORDS	LINK A		LINK B		LINK C	
	ROLE	WT	ROLE	WT	ROLE	WT
Airplanes, VTOL Airplanes, Tilt-Wing Airplanes - Aerodynamic Characteristics Princeton Dynamic Model Track Wind Tunnels (NASA 30-foot by 60-foot)						

Unclassified

Security Classification

9696-69